**Diana Alves Moita**

Licenciatura em Bioquímica

# New insights into interferon-mediated immune responses elicited by *Plasmodium* liver stage infection

## Unravelling the role of Viperin induction

Dissertação para obtenção do Grau de Mestre em
Bioquímica para a Saúde

Orientador: António M. Mendes, PhD, Prudêncio Lab, Instituto de Medicina Molecular João Lobo Antunes, Faculdade de Medicina da Universidade de Lisboa

Co-orientador: Miguel Prudêncio, PhD, Prudêncio Lab, Instituto de Medicina Molecular João Lobo Antunes, Faculdade de Medicina da Universidade de Lisboa

**Setembro de 2018**

**Diana Alves Moita**

Licenciatura em Bioquímica

# New insights into interferon-mediated immune responses elicited by *Plasmodium* liver stage infection

## Unravelling the role of Viperin induction

Dissertação para obtenção do Grau de Mestre em
Bioquímica para a Saúde

Orientador: António M. Mendes, PhD, Prudêncio Lab, Instituto de Medicina Molecular João Lobo Antunes, Faculdade de Medicina da Universidade de Lisboa

Co-orientador: Miguel Prudêncio, PhD, Prudêncio Lab, Instituto de Medicina Molecular João Lobo Antunes, Faculdade de Medicina da Universidade de Lisboa

Júri:

Presidente: Profª. Doutora Maria Teresa Nunes Mangas Catarino

Arguente: Doutora Birte Blankenhaus

Vogal: Doutor António Manuel Barbeiro Mendes

**Faculdade de Ciências e Tecnologia da Universidade Nova de Lisboa**

**Setembro de 2018**

**New insights into interferon-mediated immune response elicited by *Plasmodium* liver stage infection.** Unravelling the role of Viperin induction.

## Acknowledgements/ Agradecimentos

"Rodeia-te de pessoas que te inspiram, que te motivam, que te desafiam, que te tornam melhor."

Em primeiro lugar, quero agradecer-te a ti, **Miguel**, por teres tornado este sonho possível. O voto de confiança que me deste ao me aceitares no teu grupo deu-me asas para agarrar este sonho e ir mais longe. Tenho a certeza que és uma fonte de inspiração para todos nós e, sob a tua liderança, vamos de certeza mais longe.

A ti, **António**, devo-te o maior dos agradecimentos por me teres permitido voar. Desde cedo deste-me a liberdade de conquistar o meu espaço, ganhar a minha independência, pensar por mim própria, deste-me uma voz no meio de um grupo tão grande como o nosso. Neste último ano, fizeste-me crescer com cada desafio que me colocavas e com todas as vezes que me ajudaste a ir mais longe. És uma inspiração pelo empenho que colocas em tudo o que fazes, por seres a força motriz de muitas coisas que acontecem no laboratório e por nunca negares ajuda a ninguém. O esforço que empregas, e que muitas vezes ninguém vê, não será esquecido.

Não posso deixar de agradecer à **Profª. Drª. Teresa Catarino** por me ter aceite no mestrado e por se encontrar sempre disponível para nos receber. Ao **Instituto de Medicina Molecular**, agradeço por me ter recebido tão bem e sempre proporcionar um ambiente de excelência científica.

Aos restantes membros do laboratório que me acompanharam todos os dias ao longo deste percurso tenho muito a agradecer. **Patrícia**, obrigada por me teres ajudado a dar os primeiros passos no laboratório. A enorme disponibilidade que sempre demonstraste, tudo o que me ensinaste sem nunca hesitar, todas as vezes que me apoiaste e me fizeste ver que estava tudo bem. Não tenho palavras para te agradecer. És uma pessoa extraordinária e espero, um dia, conseguir transmitir a alguém tudo o que me ensinaste a mim sempre de forma tão paciente. **Helena**, confesso que é difícil arranjar palavras para ti. És aquela pessoa que aparece sempre nas alturas em que precisamos de alguém. Obrigada por teres sempre a palavra certa no momento certo, por apareceres simplesmente para perguntar se está tudo bem e por não haver um dia em que não estejas com um sorriso. E é claro que não podia deixar de te agradecer por toda a ajuda que me deste no laboratório. Foste, sem dúvida, essencial! **Francisca**, apesar de já não pertenceres ao laboratório, tens um lugar muito especial no meu coração. Pela pessoa querida e divertida que és, por nunca me teres faltado com uma palavra de apoio e por, simplesmente, seres como és. **Denise**, obrigada por seres sempre tão querida e atenciosa. **Fontinha**, obrigada pela disponibilidade e toda a ajuda com as células. **Margarida**, uma pessoa que gosta tanto do Natal quanto eu, obrigada pela simpatia e boa disposição. À pessoa que fala com a maior paixão sobre a sua terra, a **Filipa**, não posso deixar de agradecer por todo o esforço que colocas em tudo o que fazes, principalmente em manteres o insectário de pé. **Raquel**, obrigada por me teres recebido tão bem no dia em que fui à entrevista e estava, literalmente, uma pilha de nervos. **Teresa**, chegaste há pouco tempo mas não posso deixar

de te agradecer por toda a ajuda que me tens dado desde que chegaste. **Adriana**, obrigada pela tua simpatia e gargalhadas que já partilhámos à custa do Rafael. A vocês as duas, desejo-vos a maior sorte do mundo neste vosso percurso que tenho a certeza que tem tudo para correr bem.

Um agradecimento muito especial ao meu trio fantástico, **Daniela**, **Rafael L.** e **Rafael S.**. Sem vocês, este percurso não teria sido o mesmo. Obrigada por todo o apoio, por todas as gargalhadas e momentos partilhados, por estarem sempre presentes nos bons e maus momentos nem que fosse à distância de uma mensagem. Tenho também que agradecer por toda a disponibilidade que sempre demonstraram nem que fosse só para me ouvir. Foram uma parte essencial e especial deste percurso e eu tenho a certeza que nunca vos irei esquecer.

Quero também agradecer ao pessoal do **Figueiredo Lab** por serem uns excelentes companheiros de laboratório, sempre prestáveis e muito acolhedores e ao **Mota Lab** por me terem recebido tão bem nos meus primeiros dias no iMM. Obrigada também à **Ana Rita** da Unidade de Histologia e Patologia Comparada pela disponibilidade que sempre demonstrou e toda a ajuda dada.

Um grande obrigado aos meus amigos por estarem sempre presentes em todas as fases da minha vida e por me darem certezas de que estarão sempre disponíveis nem que seja à distância de um telefonema.

O meu maior obrigado à minha **família**, em especial aos meus **pais** e **irmã**. Obrigada por apoiarem todos os meus sonhos, por vibrarem tanto ou mais do que eu com as minhas conquistas, por me ampararem nos meus momentos menos bons e, acima de tudo, por estarem sempre presentes e me verem crescer. São parte de mim e, sem vocês, não chegaria onde cheguei e não seria quem sou.

Para ti, **Luís**, as palavras faltam-me e apenas um turbilhão de coisas surge na minha cabeça, coisas pelas quais tenho que te agradecer. Todo o apoio, todas as vezes que me ajudaste a ultrapassar obstáculos, a ver (e não só a olhar) com mais clareza, por acreditares em mim mais do que eu acredito em mim mesma, por estares sempre ao meu lado e nunca me deixares ir abaixo. Acima de tudo, obrigada por seres a pessoa que és, para mim e para todos os que te rodeiam. És uma pessoa muito especial e tens muito, mesmo muito, para dar. Obrigada.

A **todos** os que não mencionei mas que de algum modo me ajudaram a chegar onde estou hoje, obrigada.

## Abstract

Malaria is a mosquito-borne infectious disease caused by *Plasmodium* parasites. Despite the efforts being put into the malaria control, the development of efficient therapies has been hindered by the lack of knowledge on the parasite-elicited immune responses. Recent work showed that *Plasmodium* triggers an innate type I IFN response in the liver, resulting in the induction of interferon-stimulated genes (ISGs). Viperin, an antiviral molecule, is one of the most induced ISGs in the host's antiplasmodial response.

This thesis aims at characterizing the interferon-mediated immune responses triggered by *Plasmodium* liver stage infection, providing an integrated view of the potential cellular effectors of intrahepatic parasite control. A time course analysis throughout *P. berghei* infection revealed that type I and type II interferons-regulated expression of ISGs present two waves of induction coincident with different stages of the parasite's life cycle. A first peak occurs at 42 hours post-infection (hpi) and is followed by a higher peak of induction at 84 hpi, which was identified as potentially being mediated by innate lymphoid cells, whose functionality is yet to be explored.

Furthermore, we proposed to unravel the role of Viperin induction during *Plasmodium* liver infection. *In vivo* bioluminescence measurements revealed that mice lacking Viperin exhibited a higher liver stage burden compared with wild type mice at 42 hpi. The investigation of the cellular mediators of Viperin's expression in the liver was also performed through qRT-PCR and flow cytometry, identifying the hepatocytes and monocytes as the major sources of Viperin at 42 and 84 hpi, respectively.

This thesis reveals a cell population exhibiting the type I interferon signature that may act as effectors on controlling either a primary or secondary infection. Moreover, knowledge on the role of Viperin can significantly contribute to the design of new antiplasmodial strategies by increasing the knowledge on the host-parasite interactions.



**Keywords:** Malaria, *Plasmodium*, Innate immune system, Interferon, Innate Lymphoid cells, Viperin

## Resumo

A malária é uma doença transmitida por mosquito causada pelo parasita *Plasmodium*. Apesar dos esforços empregues no controlo da malária, o desenvolvimento de terapias eficazes tem sido desafiado pela falta de conhecimento acerca das respostas imunitárias desencadeadas pelo parasita. Recentemente, foi demonstrado que o *Plasmodium* aciona uma resposta inata de interferão tipo I no fígado, culminando na indução de genes estimulados pelo interferão (ISGs). A Viperina, uma molécula antiviral, é um dos ISGs mais induzidos durante a resposta anti-*Plasmodium*.

Esta tese tem como objetivos a caracterização das respostas mediadas pelo interferão durante a fase hepática da infeção, fornecendo uma visão de potenciais efetores celulares no controlo intra-hepático dos parasitas. Uma análise de expressão génica ao longo da infeção revelou que a expressão dos ISGs, regulada por interferões tipo I e II, apresenta dois picos de indução coincidentes com diferentes fases do ciclo de vida do parasita. Um primeiro pico ocorre às 42 horas após infecção (hpi) seguido de um segundo pico de indução mais alto que ocorre às 84 hpi e é potencialmente mediado por células linfóides inatas cuja funcionalidade se encontra por explorar.

Adicionalmente, propusemos desvendar o papel da indução da Viperina durante a infeção hepática. Ratinhos deficientes em Viperina exibem uma maior carga parasitária hepática comparando com ratinhos *wild type* às 42 hpi. A investigação dos mediadores celulares da expressão de Viperina no fígado foi realizada através de qRT-PCR e citometria de fluxo identificando os hepatócitos e monócitos como as principais fontes de Viperina às 42 e 84 hpi, respetivamente.

Esta tese revela uma população celular que exibe a assinatura de interferão tipo I, a qual pode atuar como efetora no controlo de uma infeção primária e/ou secundária, assim como pode contribuir para o *design* de estratégias contra o *Plasmodium* através do aumento do conhecimento acerca das interações hospedeiro-parasita.



**Palavras-chave:** Malária, *Plasmodium*, Sistema imunitário inato, Interferão, Células linfóides inatas, Viperina

# Table of contents

## Index of figures

## Index of tables

## Abbreviations

| | |
|---|---|
| **5'-dAdo** | 5'-deoxyadenosyl |
| **AC** | Assembly compartment |
| **ACK** | Ammonium-Chloride-Potassium |
| **ACT** | Artemisin combination treatment |
| **AMPK** | AMP-activated protein kinase |
| **AP-1** | Activator protein-1 |
| **APC** | Antigen presenting cell |
| **ATP** | Adenosine triphosphate |
| **BSA** | Bovine serum albumin |
| **CCL** | C-C motif chemokine ligand |
| **CCR** | C-C chemokine receptor type |
| **CD** | Cluster of differentiation |
| **cDC** | Conventional dendritic cell |
| **cDNA** | Complementary DNA |
| **CHC** | Chronic hepatitis C virus |
| **CHIKV** | Chikingunya virus |
| **ChREBP** | Glucose-responsive transcription factor |
| **CM** | Cerebral malaria |
| **CNS** | Central nervous system |
| **CSP** | Circumsporozoite protein |
| **Ct** | Threshold cycle |
| **CTP** | Cytidine triphosphate |
| **CX3CR1** | CX3C chemokine receptor 1 |
| **DAB** | 3,3'-diaminobenzidine |
| **DC** | Dendritic cell |
| **ddhCTP** | 3'-deoxy-3',4'-didehydro-CTP |
| **DENV** | Dengue virus |
| **DMEM** | Dulbecco's modified minimal essential medium |
| **DNA** | Deoxyribonucleic acid |
| **ECM** | Experimental cerebral malaria |
| **EEF** | Exo-erythrocytic form |
| **iRBC** | Infected red blood cell |
| **ER** | Endoplasmic reticulum |
| **FBS** | Fetal bovine serum |
| **FPPS** | Farnesyl diphosphate synthase |
| **FSC** | Forward scatter |
| **FVD** | Fixable viability dye |
| **GAS** | γ-activated sequence |
| **GFP** | Green fluorescent protein |
| **GPI** | Glycosylphosphatidylinositol |
| **hCMPK2** | Human cytidylate monophosphate kinase 2 |
| **HCMV** | Human cytomegalovirus |
| **HCV** | Hepatitis C virus |
| **HIV** | Human immunodeficiency virus |
| **hpi** | hours post-infection |
| **HPR** | Horseradish peroxidase |
| **HPRT** | Hypoxanthine guanine phosphoribosyltransferase |
| **HSPG** | Heparan sulphate proteoglycan |
| **hVAP-33** | Human vesicle-associated membrane protein-associated protein of 33 kDa |
| **ICAM** | Intercellular adhesion molecule |
| **Ifi44** | Interferon-inducible protein 44 |
| **Ifit-1** | Interferon-inducible protein with tetratricopeptide repeats 1 |
| **Ifit3** | Interferon-inducible protein with tetratricopeptide repeats 3 |
| **IFN** | Interferon |
| **IFNAR** | IFN-α receptor |
| **IFNGR** | IFN-γ receptor |
| **IFV** | Influenza virus |
| **Ig** | Immunoglobulin |
| **IL** | Interleukin |
| **IL-2R** | IL-2 receptor |
| **ILC** | Innate lymphoid cell |
| **iNOS** | inducible nitric oxide synthase |
| **IRAK1** | Interleukin-1 receptor-associated kinase 1 |
| **IRF** | IFN-regulatory factor |

| | | | |
|---|---|---|---|
| **iRNA** | RNA interference | **PRR** | Pattern Recognition Receptor |
| **IRS** | Indoor residual spraying | **qRT-PCR** | Quantitative real time PCR |
| **ISG** | IFN-stimulated gene | **RAG** | Recombinase activating gene |
| **ISGF3** | IFN-stimulated gene factor 3 | **RBC** | Red blood cell |
| **ISRE** | IFN-stimulated responses element | **RdRp** | RNA-dependent RNA polymerase |
| **ITN** | Insecticide treated bed-net | **RDT** | Rapid diagnostic test |
| **JAK** | Janus kinase | **RIG** | Retinoic acid-inducible gene |
| **JEV** | Japanese encephalitis virus | **RLR** | RIG-like receptor |
| **KO** | Knockout | **RNA** | Ribonucleic acid |
| **LD** | Lipid droplet | **ROI** | Region of interest |
| **LPS** | Lipopolysaccharide | **ROS** | Reactive oxygen species |
| **MAVS** | Mitochondrial antiviral-signaling protein | **RPMI** | Roswell Park Memorial Institute |
| **MCP** | Monocyte chemoattractant protein | **RSV** | Respiratory syncytial virus |
| **MDA5** | Melanoma differentiation-associated protein 5 | **RT** | Room temperature |
| **MHC** | Major histocompatibility complex | **SAM** | *S*-adenosyl-L-methionine |
| **MPS** | Mononuclear phagocyte system | **SD** | Standard deviation |
| **Myd88** | Myeloid differentiation primary response 88 | **shRNA** | short-hairpin RNA |
| **NF-κB** | Nuclear factor-kappa B | **SPECT** | Sporozoite microneme protein essential for cell traversal |
| **NFAT** | Nuclear factor of activated T cells | **spz** | sporozoite |
| **NK** | Natural killer cells | **STAT** | Signal transducer and activator of transcription |
| **NKT** | Natural killer T cells | **STING** | Stimulator of IFN genes |
| **NO** | Nitric oxide | **TBEV** | Tick-born encephalitis virus |
| **ORBEA** | Orgão Responsável pelo Bem-Estar Animal | **TBK1** | Tank-binding kinase 1 |
| **PAMP** | Pathogen-associated molecular pattern | **TCR** | T cell receptor |
| ***Pb*A** | *P. berghei* ANKA | **TFP** | Trifunctional protein |
| **PBS** | Phosphate-buffered saline | **TLR** | Toll-like receptor |
| **PCR** | Polymerase chain reaction | **TNF** | Tumour necrosis factor |
| **pDC** | Plasmocytoid dendritic cell | **TRAF6** | TNF receptor associated factor 6 |
| **PFA** | Paraformaldehyde | **TYK** | Tyrosine kinase |
| **PRDI-BF1** | Positive regulatory domain I-binding factor 1 | **UIS** | Upregulated in infective sporozoites |
| **PV** | Parasitophorous vacuole | **Usp18** | Ubiquitin specific peptidase 18 |
| **PVM** | Parasitophorous vacuole membrane | **Viperin** | Virus inhibitory protein, endoplasmic reticulum associated, interferon-inducible |

| | |
|---|---|
| **vMIA** | Viral mitochondrial inhibitor of apoptosis |
| **WHO** | World Health Organization |
| **WNV** | West Nile Virus |
| **WT** | Wild-type |
| **ZIKV** | Zika virus |
| **α-GalCer** | α-galactosylceramide |

# 1. Introduction

## 1.1. Malaria: General Facts

Malaria is a mosquito-borne infectious disease that remains a major health concern worldwide, especially in the tropical and subtropical regions[1]. In 2016 alone, nearly half of the world's population was at risk of contracting malaria, with 91 countries and areas presenting an ongoing set of malaria transmission[2]. The World Health Organization (WHO) estimated that in 2016 there were 216 million cases of malaria worldwide (95% confidence interval, 196–263 million) compared with 211 million cases in 2015 (95% confidence interval, 192–257 million; Fig. 1.1). Of these, approximately 90% were reported in the WHO African Region and 7% in the South-East Region (Fig.1.1). From the ninety-one countries that accounted for all malaria cases globally, a total of 445 000 deaths were reported, of which approximately 91% occurred in the WHO African Region. Children under five years old are at particularly high risk of contracting malaria, with the disease claiming the life of a child every two minutes[2].

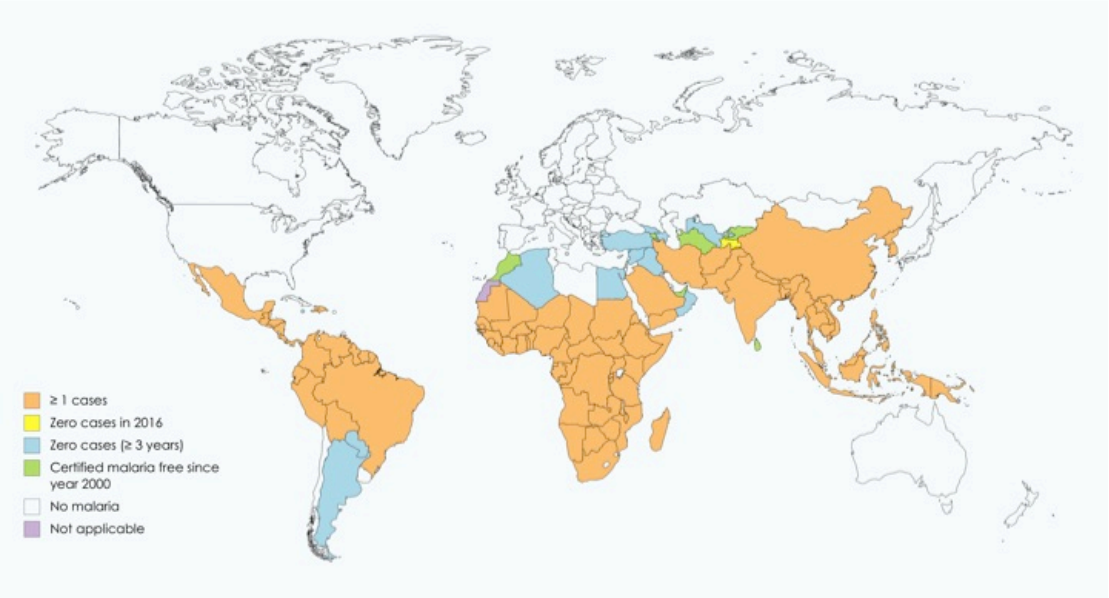


**Figure 1.1. Malaria incidence cases map.** World map showing the areas with malaria cases in 2000 and their status by 2016. Regions coloured in orange represent areas with 1 or more cases of malaria, regions coloured in yellow represent areas with no malaria cases in 2016 and regions coloured in blue represent areas with zero cases for more than 3 years. Countries with zero cases over at least the past 3 consecutive years are entitled with a certification of malaria free status from WHO. Adapted from World Malaria Report, 2017[(2)] (WHO database).

Malaria is caused by protozoan parasites of the *Plasmodium* (*P.*) genus, which belongs to the phylum Apicomplexa, and are transmitted through the bite of an infected female *Anopheles* mosquito[3]. In humans, malaria infections are caused by *P. falciparum, P. vivax, P. malariae, P. ovale* and by the simian parasites *P. knowlesi*[3] and *P. simium*[4]. In Africa, there is a predominance of *P. falciparum*, which is the species responsible for most malaria-associated mortality and disease severity, whereas *P. vivax* is more common in the Indo-Pacific and South American regions[3].

Remaining a major cause of morbidity and mortality worldwide, malaria poses a major challenge for the economic development of the poorest regions of the globe. In fact, malaria costs Africa's economy US$ 12 billion per year[5]. However, although the fight against this infectious disease may be prolonged and threatened by diverse challenges, a relatively stable funding effort has been put into the malaria control since 2010[(2)].

## 1.2. *Plasmodium* life cycle

Malaria infection begins when an infected *anopheline* mosquito injects hundreds of sporozoites into the skin of the mammalian host while taking a blood meal[3] (Fig.1.2.A). Sporozoites, the liver-infective forms of *Plasmodium* parasites, then rely on the locomotion process of gliding motility to reach a blood vessel[3,7]. Once in the bloodstream, parasites actively target the liver, possibly through the interaction of a *Plasmodium* sporozoite surface protein, named circumsporozoite protein (CSP) and the negatively charged heparan sulphate proteoglycans (HSPGs) of the hepatocytes surface[3,6,7]. Although HSPGs are present in most tissues, those in the liver seem to have a greater degree of sulphation, which may account for the possible binding to positively charged domains of the CSP[8], the thrombospondin-like cell-adhesive region II-plus and a positively charged motif upstream from the conserved region I[(6,9)].

After reaching the liver, sporozoites traverse the endothelial cells or the liver-resident macrophages, the Kupffer cells, which compose the liver sinusoids as well as several hepatocytes[3,6]. Two proteins of the rodent-infective parasite, *P. berghei*, sporozoite microneme protein essential for cell traversal (SPECT1) and SPECT2, seem to be crucial for the process of cell traversal and, consequently, for the infectivity of the parasites[6].

Ultimately, the sporozoites productively infect a final hepatocyte with the formation of a parasitophorous vacuole (PV; Fig.1.2.B), where the differentiation into exo-erythrocytic forms (EFFs) occurs[3,6,7]. Within the PV, a phase of asexual reproduction takes place. The EEF undergoes a process of schizogony (nuclear division without cell division) during which a massive DNA replication and parasite growth takes place[3] (Fig.1.2.C). Three *P. berghei* proteins have been identified has being essential for parasite development within the PV, upregulated in infective sporozoites (UIS)3, UIS4 and Pb36p. The host molecule ApoA1, which is localized in the PV membrane (PVM) seems to interact with the parasitic UIS4 contributing to the intrahepatocyte development[6].

Towards the end of the pre-erythrocytic phase, thousands of merozoites are formed and fill the merosomes, which bud off from the infected hepatocytes and are released into the bloodstream[3.6] (Fig.1.2.D). The merosome membrane derives from the host hepatocyte plasma membrane, allowing the merosome to pass uncovered in front of the immune system defences, such as the Kupffer cells, on its way to the bloodstream[10]. The duration of the liver stage is characteristic of each *Plasmodium* species and can take a minimum of 6 days in *P. falciparum* and a maximum of 16 days in *P. malariae* for human-infective parasites[11] and only 2 days for the rodent-infective parasites (*P. berghei* and *P. yoelii*)[12].

One major public health concern regarding the liver stage of the parasite development is the *P. vivax* and *P. ovale* dormant liver stages, also known as hypnozoites, parasite forms that remain quiescent until, through yet unknown mechanisms, they are reactivated and undergo schizogony, causing malaria relapse long after the mosquito bite[3,6].

Although asymptomatic, the liver stage is an obligatory phase of the *Plasmodium* life cycle. Therefore, it is the most appealing stage for prophylactic strategies as, if infection is blocked at this stage, there will be no pathology and therefore no disease[13].

Once in the bloodstream, merozoites are able to rapidly infect red blood cells (RBCs) and undergo successive cycles of invasion, intracellular growth, proliferation and re-invasion (Fig.1.2.E). The merozoite faces the erythrocyte through its apical end, where the specialized secretory organelles rhoptries and micronemes are localized. Following apical reorientation, the merozoite propels itself into a newly forming vacuole through a junction. Once inside the erythrocyte, the parasite remains surrounded by its own plasma membrane and a PVM[3].

Within the RBC, the parasite undergoes sequential and morphologically distinct phases starting at the ring stage. Then, at the throphozoite stage, the parasite is actively growing, consuming erythrocyte's contents and modulating the surface of the infected red blood cell (iRBC)[3]. At the beginning of the development, the asexual stages travel mostly at the peripheral circulation. However, from the throphozoite to the schizont stages, parasites start to be able to adhere to host cells, sequestering in various organs. This has been suggested to be a survival mechanism developed by the parasite in order to avoid splenic clearance[14]. The next parasite form is the schizont, where the parasite undergoes a series of nuclear divisions. Following the coordinated partition of the nuclei, the lysis of the PVM and the RBC membrane occurs and the merozoites are released into the bloodstream, being able to start more rounds of schizogony[15].

During the blood stage, a small proportion of parasites undergo a developmental switch initiating commitment to gametocytogenesis, the formation of gametocytes (Fig.1.2.F). Daughter merozoites from a single schizont-infected cell develop into either asexual or sexual stage parasites, with the sexually committed ones originating microgametocytes (males) or macrogametocytes (females)[7]. The pathogenesis of malaria occurs during the blood stage of the parasite life cycle, thus, being responsible for the emergence of all clinical symptoms[16].

The cycle progresses as a female *Anopheles* mosquito feeds from an infected host, with the ingested gametocytes ensuing the vector phase of the *Plasmodium* life cycle (Fig.1.2.G). In the posterior midgut lumen of the mosquito, the gametocytes, triggered by mosquito-specific and environmental factors, undergo a rapid transformation into gametes[7]. In turn, the recently formed microgametes fertilize the already emerged macrogametes within the mosquito blood meal to form diploid zygotes. These zygotes inherit the maternal gamete plasma membrane, cytoplasm and intracellular organelles[7,18]. Next, the recently formed zygote undergoes meiosis and genetic recombination, gradually transforming into an ookinete, which crosses the epithelium midgut in order to reach the basal lamina of the epithelium. Here, the parasite differentiates into oocysts. At the onset of sporozoite formation, the oocyst nuclei undergo their final mitosis. Consequently, the accumulation of thousands of sporozoites causes the rupture of the oocyst, releasing haploid invasive-competent

sporozoites that will actively invade the mosquito salivary glands through gliding motility[7,18] (Fig.1.2.H).

When the infectious mosquito seeks a blood meal, sporozoites present in the salivary glands are injected into the dermis of the vertebrate host, completing this way the malaria parasite life cycle[7] (Fig. 1.2.I).

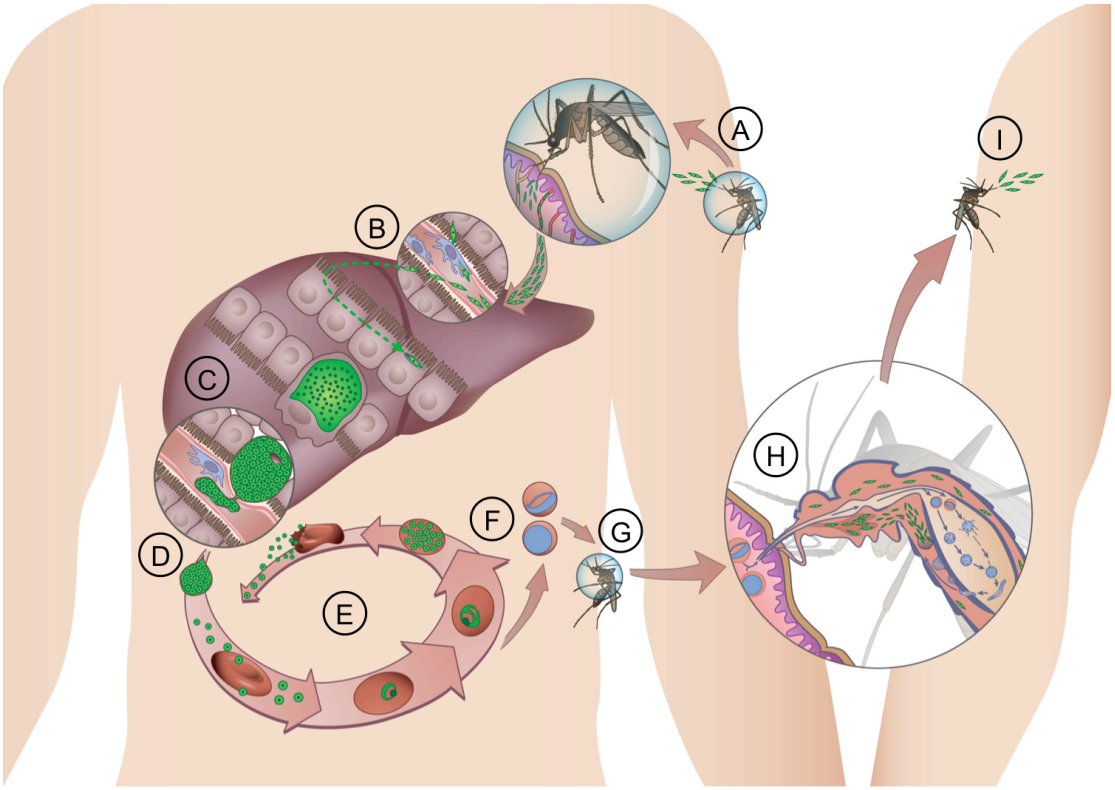


**Figure 1.2. *Plasmodium* spp. life cycle.** (A) While taking a blood meal, an infected female *Anopheles* mosquito injects sporozoites into the skin of the host. (B) Once in the liver, sporozoites will traverse several hepatocytes before productively infect a final one with the formation of a PV. (C) Inside the PV, sporozoites intensively replicate and differentiate into exo-erythrocytic forms, forming a schizont. (D) The merosomes, which are filled with merozoites, bud off from the infected hepatocytes and are released into the bloodstream, where the merosome membrane bursts releasing infectious merozoites. (E) The merozoites go through successive cycles of RBC invasion, intracellular growth, asexual proliferation and re-invasion. (F) During the erythrocytic stage, some parasites differentiate into sexual forms, the gametocytes. (G) When a female *Anopheles* mosquito feeds from an infected host, the gametocytes in circulation are up taken and ensure the vector phase of the parasite life cycle. (H) Within the mosquito, the formation of diploid zygotes takes place, which will then mature into motile ookinetes. The ookinetes cross the epithelium midgut, where the differentiation into oocysts takes place. As oocysts mature, sporozoites are formed within. With the rupture of the oocyst, the accumulated sporozoites are released invading the salivary glands of the mosquito. (I) Sporozoites present in the salivary glands are injected into the host's skin when the infected mosquito seeks a blood meal.

## 1.3. Clinical presentation of malaria and its diagnosis

During the blood stage of infection, *Plasmodium* spp. merozoites invade host RBCs, multiply asexually, egress and reinvade uninfected erythrocytes in a continuing cycle that is responsible for all the malaria-associated clinical symptoms[16]. Typically, the symptoms of the disease can appear as quickly as 7 days after the host is bitten by an infected mosquito, although it can take up to 18 days, depending on the *Plasmodium* species[3].

The clinical manifestations and progression of malaria depend on the infecting *Plasmodium* species, the immunological competence of the individual, the accuracy of the diagnosis and the timing and efficacy of treatment[3,19]. In the context of uncomplicated malaria, the symptoms are acute and mild to intense, albeit non-specific, being commonly mistaken by flu. These symptoms include acute fever, chills, fatigue, headache, gastrointestinal symptoms and cough. Thus, it is of extreme importance that severe malaria is ruled out of the picture[3].

The reference method for malaria diagnosis is the microscopic examination of the patient's blood through thin and thick blood films, which allows identification of the *Plasmodium* species and quantification of the infection load[20]. However, depending on resources availability, there are more precise methods such as rapid diagnostic tests (RDTs), through which soluble *Plasmodium* antigens are identified[21], and molecular techniques such as polymerase chain reaction (PCR), which allows identification of the parasite DNA[3,22].

### 1.3.1. Severe malaria

Severe malaria is a clinical form of the disease that is mainly caused by *P. falciparum* and that affects mostly children, pregnant women and immunocompromised individuals[23]. Although most malaria cases manifest as uncomplicated, around half million deaths occur yearly in sub-Saharan Africa as a result of severe disease[2]. The clinical features of severe malaria are highly variable but may include deep anaemia, renal complications, jaundice, pulmonary oedema with impaired respiratory function, impaired consciousness and, ultimately, coma[24,25].

For many years, severe malaria was simply perceived as two syndromes: (i) severe anaemia caused by the destruction of infected RBCs; and (ii) cerebral malaria (CM) caused by sequestration of trophozoite-infected RBCs in the small blood vessels and/ or rupture of infected RBCs and release of parasite-derived toxins[23,24,25]. However, a broader picture has emerged in the past few years identifying severe malaria as a highly complex disorder with multiple and inter-related processes and systems involved[25]. In fact, the pathophysiology of the disease seems to be a result of the contribution of parasitic virulence factors and host immune responses[24].

The study of severe malaria pathogenesis, mainly focused on the cerebral syndrome, has been conducted through *post-mortem* studies in humans, *in vivo* infections in mouse models and *in vitro* studies[25]. Much of our current understanding about the pathology of CM has come from the infection of susceptible mice strains, such as C57BL/6J and CBA, with *P. berghei* ANKA (*Pb*A), known as experimental cerebral malaria (ECM). This experimental model essentially recapitulates many of the characteristics of the human CM, including the immunogical, parasitological and neuropathological features, and is the best available experimental model so far[23]. Exaggerated production of pro-inflammatory cytokines[26], accumulation of $CD8^+$ T cells in the brain[27] and higher expression of the intercellular adhesion molecule-1[(28)] (ICAM-1) are some of the hallmarks of ECM. Typically, the clinical signs appear 5 to 10 days post-infection with death occurring within 4 to 5 hours after the appearance of neurological signs[23].

## 1.4. Malaria control and treatment

Malaria control measures occur at three levels: vector control through the use of insecticides, use of insecticide treated bed-nets (ITNs), and the use of efficient treatment drugs[3]. The WHO estimated that, between 2014 and 2016, a total of 582 million ITNs were distributed globally contributing to the decrease of malaria cases incidence[2]. However, fewer people at risk of contracting malaria are being protected by indoor residual spraying (IRS)[2]. Furthermore, although the access to antimalarial drugs has been improved, the emerging resistance to these medicines constitutes a threat to the control and elimination of malaria[2].

Although malaria is life-threatening, it is also a treatable disease. The main aim of antimalarial drugs is the treatment of uncomplicated malaria through the inhibition of parasite replication, whereas the objective of severe malaria treatment is to stop parasite maturation[3]. The present recommendation of the WHO and, consequently, the main approach for the treatment of uncomplicated malaria is the use of artemisin combination treatments (ACT). ACTs combine the rapidly acting and rapidly eliminated artemisin compounds with antimalarial drugs that have longer half-lives[3]. ACT kills asexual stage *P. falciparum* parasites, preventing gametocytogenesis[29]. Primaquine acts against pre-erythrocytic stages and is mainly used against dormant liver-stage hypnozoites, accounting for its prophylactic effect. Additionally, this antimalarial drug can be used against asexual stage parasites of *P. vivax, P. malariae* and *P. ovale* and is the only currently available anti-malarial active against mature *P. falciparum* gametocytes[30].

## 1.5. Malaria-related Immunity

The vertebrate immune system is equipped to deal with invading pathogens, whether by means of mechanical barriers or through an active immune response. *Plasmodium* has a very complex multistage and multiantigenic life cycle, which poses a challenge for the immune system of the vertebrate host. The immune reactions that the host develops once insulted are regulated by both the innate and adaptive immune system. Virtually, the immune system can target any stage of the parasite's life cycle[31].

### 1.5.1. Immunity elicited by *Plasmodium* liver stage infection

The clinically silent nature of the liver stage of *Plasmodium* infection led to the assumption that parasites massively replicate within this organ without being recognized by the host immune system. However, a set of seminal studies had already suggested that the mammalian host is able to detect the parasite and mount a cellular immune response during the liver stage of infection. Khan *et al.* (1991, 1992) observed inflammatory foci rich in neutrophils, eosinophils and macrophages in the livers of animals injected with live sporozoites but not with heat-killed sporozoites[32,33].

#### 1.5.1.1. Interferon-mediated innate immune responses

Interferons (IFNs) are cytokines first identified in 1957 by Alick Isaacs and Jean Lindenmann, named after their capacity to interfere with viral replication[34]. Currently, interferons are classified in three groups according to their main functions[35]:

1. Type I IFNs: family of cytokines comprehending 13 different isoforms of IFN-α (14 in mice) and a single IFN-β. Most cell types are able to produce IFN-β, whereas haematopoietic cells, particularly plasmocytoid dendritic cells (pDCs), were identified as the major producers of IFN-α. Therefore, type I IFNs can act in an autocrine and paracrine manner virtually in any tissue[35].
2. Type II IFN: composed only by one member, IFN-γ, which is produced by leukocytes, particularly T cells and natural killer (NK) cells. IFN-γ has been proven to be crucial for host defence against intracellular pathogens[35].
3. Type III IFN (IFN-λ): corresponds to the least well-studied group of interferons, although it seems to elicit similar responses to type I IFNs yet with a more restricted expression of its receptor[35].

The following sections will focus mainly on type I IFNs and in their crosstalk with IFN-γ.

Innate immunity plays a central role as the first line of defence against infections. Germline-encoded pattern recognition receptors (PRRs) recognize highly conserved pathogen-associated molecular patterns (PAMPs) mediating innate immunity recognition[36]. Activation of PRRs stimulates antimicrobial responses through signaling cascades that culminate in the production of type I IFNs. In turn, IFN-α and IFN-β bind to the transmembrane IFN-α receptor (IFNAR), which is composed by IFNAR1 and IFNAR2 subunits. In the canonical type I IFN signaling pathway, the engagement of the IFNAR activates two kinases that are associated with this receptor: the tyrosine kinase Janus kinase 1 (JAK1) and tyrosine kinase 2 (TYK2). These enzymes phosphorylate the cytoplasmic transcription factors signal transducer and activator of transcription 1 (STAT1) and STAT2. Tyrosine-phosphorylated STAT1 and STAT2 heterodimerize and translocate to the nucleus, where they bind to the IFN-regulatory factor 9 (IRF9), forming a trimolecular complex known as IFN-stimulated gene factor 3 (ISGF3). ISGF3 binds to consensus DNA sequences (TTTCNNTTTC) called IFN-stimulated responses elements (ISREs), eliciting the expression of various IFN-stimulated genes (ISGs)[37].

Type II IFN triggers a similar intracellular signaling cascade after binding to its receptor, the IFN-γ receptor (IFNGR), although with slight differences relative to the type I IFN pathway. IFN-γ activates JAK1 and JAK2, which phosphorylate STAT1 tyrosine residues leading to their homodimerization. Subsequently, STAT1 homodimers translocate into the nucleus where they will bind to γ-activated sequences (GAS; consensus DNA sequence TTCNNNGAA)[35].

In the past years, the development of genomic approaches has contributed to unravelling the nature of the innate immune responses that are activated upon parasitic infections. Protozoan parasites, including *Plasmodium*, are known to induce potent antimicrobial responses mediated by type II IFN[38]. However, it has also become apparent that protozoa, similarly to viruses, elicit a type I IFN response whose mechanistic details and functionality have been gradually broadened.

In 1970, Jahiel and colleagues suggested that IFNs induced by a viral infection could be harvested and administered to mice infected with liver-infective *P. berghei* sporozoites as a prophylactic measure to completely prevent malaria. This study revealed that exogenous IFNs are able to potently control liver stage infection[39]. However, the role of endogenously induced IFNs upon malaria infection remained undefined until recently. In 2011, Portugal *et al.* disclosed the first clues for the exploration of type I IFN-mediated responses in the context of malaria infection. The authors analysed the liver transcriptome of infected mice by genome-wide microarray analysis, identifying genes linked to a type I IFN signature as being upregulated[40].

In early 2014, two independent studies conducted by Liehl *et al.* and Miller *et al.* deciphered fundamental features of the *Plasmodium*-induced liver stage-specific innate immune responses, including: (i) the identity of the host PRRs that recognize *Plasmodium*, (ii) the identity of the parasite PAMPs detected by those PRRs, (iii) the type of innate immune response induced, (iv) whether this response impacts infection, and (v) the role of the recruited lymphocytes[41,42].

Following the productive invasion of a hepatocyte, the relatively few parasites that reach the liver enter an obligatory phase of asexual reproduction within the PV. During this asymptomatic development, *Plasmodium* was shown to engage an innate immune response. Liehl *et al.* and Miller *et al.* performed RNA sequencing experiments to compare the liver transcriptome between mice infected with the rodent-infective parasites, *P. berghei* and *P. yoelii*, respectively, and mock-infected mice (mice injected with an equivalent amount of non-infected salivary glands). Both studies concluded that all the genes whose expression was induced at least two-fold belonged to a group known as interferon-stimulated genes and were, thus, connected to the innate type I IFN response[41,42].

A model for the PAMP-PRR interactions that result in the engagement of the type I IFN response has been suggested for *Plasmodium* liver infection. Liehl *et al.* proposed that the melanoma differentiation-associated protein 5 (MDA5), a cytosolic retinoic acid-inducible gene (RIG)-I-like receptor, is responsible for the recognition of *Plasmodium* RNA[41]. The mechanism whereby this nucleic acid leaves the PV and makes their way into the hepatocyte cytosol remains yet elusive[41]. Then, MDA5 initiates a signaling cascade, transmitted through the adaptor molecule mitochondrial antiviral-signaling protein (MAVS) and the transcription factors interferon-regulatory factor 3 (IRF3) and IRF7, which culminates in the induction the type I IFNs and, subsequently, of several ISGs (Fig.1.3.A). In fact, mice individually knockout for MDA5 (*Mda5*$^{-/-}$), MAVS (*Mavs*$^{-/-}$), IRF3 (*Irf3*$^{-/-}$) and IRF7 (*Irf7*$^{-/-}$) showed a significant impairment on the induction of the type I IFN response upon *P. berghei* infection[41]. In contrast, Miller *et al.* found that MDA5 and MAVS as well as the Toll-like receptor (TLR)3, which can activate IRF3 once engaged, are dispensable for the sensing events of *P. yoelii*[42] (Fig.1.3.A).

Further studies towards understanding the cellular basis and functionality of the *Plasmodium*-induced type I IFN response were carried out by the aforementioned authors. By performing a time course of *Plasmodium* infection, Liehl *et al.* discovered that this response is evident already at 36 hours post-infection following the natural route of transmission, mosquito bite. The response peaks at 42 hours post-infection, before the release of the hepatic merozoites into the bloodstream, and is

abrogated in mice that lack the IFNAR1 specifically in hepatocytes (Alb-Cre-*Ifnar1*$^{flox/flox}$). Therefore, hepatocytes were identified as the primary source of ISG expression (Fig.1.3.B). In fact, hepatocytes are able to autocrinally respond to their own IFNs, unleashing a feed-forward loop that amplifies the initial response (Fig.1.3.C). Importantly, the liver infection load and the total parasitemia during initiation of blood stage infection were exacerbated when hepatocytes could not receive signals via IFNAR[41].

Liehl *et al.* got further insights into the effector cells through which the type I IFN signaling increases host resistance to liver stage infection. By exogenously inducing this innate immune response in primary hepatocytes *ex vivo*, the authors observed an ineffectiveness to control the parasite burden. This suggested that the hepatocyte-mediated response, although crucial for the propagation of the type I IFN signaling, needs accessory cells, such as leukocytes, as effectors in parasite killing[41].

Collectively, these studies showed that the type I IFN response initiated and propagated by the hepatocytes, although unable to control parasite replication in the liver, is essential for the activation and recruitment of effector immune cells that infiltrate in the liver between 40 and 72 hours post-infection (Fig.1.3.E and F). Miller and colleagues complemented this study by concluding that the hepatocyte-driven type I IFN cascade acts paracrinally to recruit $CD8^+$ T cells, NK cells and CD1d-restricted natural killer T (NKT) cells, with the latter being essential for the control of parasite burden, likely via IFN-γ production (Fig.1.3.G). Indeed, the liver stage burden in IFN-$\gamma^{-/-}$ mice was twice that of infected wild type (WT) mice, suggesting that an innate upregulation of the type II IFN following liver stage infection mediates the reduction in liver stage burden[42]. This type II pro-inflammatory cytokine can influence the destruction of *Plasmodium*-infected cells through three essential mechanisms: (i) increasing the cytotoxic potential of $CD8^+$ T cells, (ii) inducing the production of antibodies by plasma B cells and, (iii) enhancing the phagocytic capabilities of immune cells, such as macrophages[38].

Although the innate immune response may not be sufficient to completely eliminate the parasites during a primary infection, Miller *et al.* (2014), as well as Liehl *et al.* (2015), independently demonstrated that it can play a key role in preventing reinfection during an ongoing infection[42,43]. This host resistance is dependent on the IFN-mediated response, which achieves much greater magnitude during reinfection than during a primary infection, not only decreasing liver parasite load but delaying blood parasitemia and increasing survival. The IFN-mediated host resistance to reinfection explains why in regions of malaria hyperendemicity not all infective mosquito bites translate into infection[42,43].

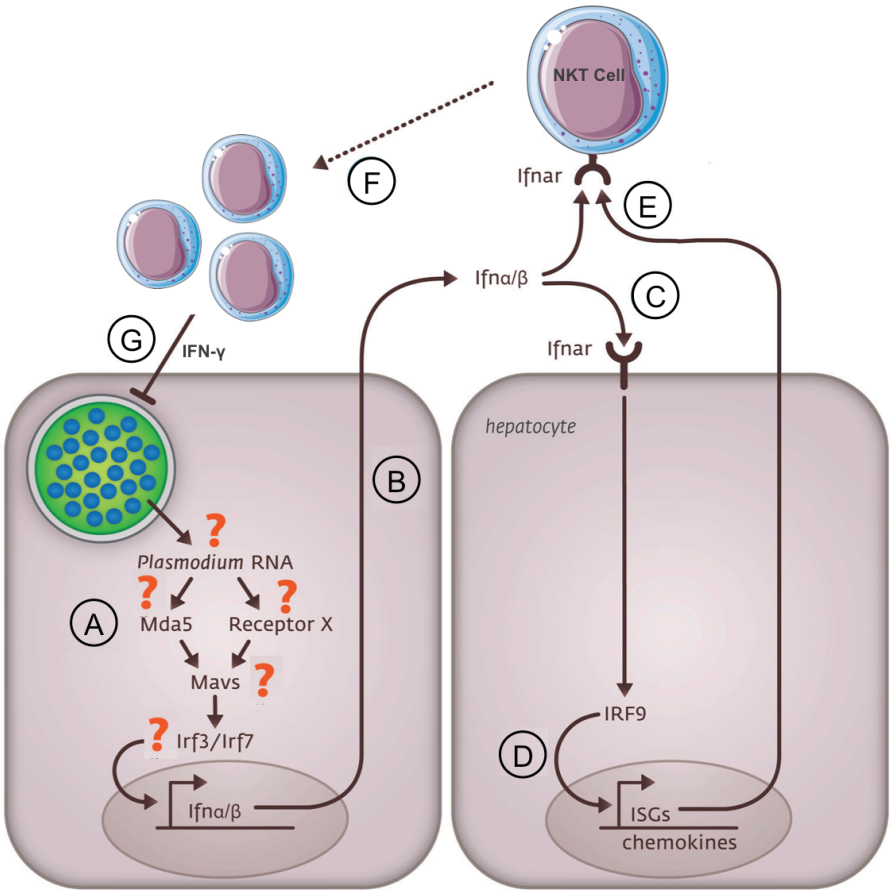


**Figure 1.3. *Plasmodium* liver infection induces an interferon-mediated immune response essential for the later recruitment of effector natural killer T cells.** Once in the liver, *Plasmodium* induces a type I IFN response initiated by the recognition of the *Plasmodium* RNA likely via the cytoplasmic receptor MDA5 and other yet unidentified receptors. The signaling cascade possibly progresses through MAVS and the transcription factor IRF7 and, potentially, IRF3 **(A)** culminating in the release of type I IFNs in the extracellular milieu **(B)**. IFN-α and IFN-β can, then, bind to the IFNAR in an autocrine or paracrine manner amplifying the initial response **(C)**. Engagement of the IFNAR leads to the upregulation of several ISGs and propagation of the response throughout the hepatocytes **(D)**. IFNs released from hepatocytes activate **(E)** and recruit **(F)** leukocytes, specifically NKT cells, to the infected hepatocytes, which through the production of IFN-γ are able to inhibit a secondary *Plasmodium* liver infection **(G)**. Adapted from "Host-cell sensors for *Plasmodium* activate innate immunity against liver-stage infection." by P. Liehl *et al.*, 2014, *Nature Medicine*, 20, 47-53 and "Interferon-Mediated Innate Immune Responses against Malaria Parasite Liver Stages" by J.L. Miller *et al.*, 2014, *Cell Rep.*, 7, 436-447.

#### 1.5.1.2. Cell-mediated immune responses

Once in the liver, sporozoites traverse Kupffer cells as well as several hepatocytes before invading a final one[3,6]. During this migration, traversed macrophages and infected hepatocytes are able to process malarial antigens, such as the CSP, into peptides that are presented in the context of major histocompatibility complex (MHC) molecules[44]. After recognition of the MHC-parasitic antigen complex, $CD8^+$ T cells are able to form pores in the hepatocyte cell membrane through key effector molecules known as perforins. Subsequently, granzymes, which are pro-apoptotic proteases, enter the hepatocyte through the recently formed pores and induce apoptosis likely by activation of caspases and induction of the production of reactive oxygen species (ROS)[45]. Moreover, $CD8^+$ T cells can also be activated by cytokines, such as IL-12 and IL-18, and, subsequently, kill parasites through oxygen-dependent cytolytic mechanisms such as the production of nitric oxide (NO)[46] or release of

IFN-γ. This type II cytokine can act autocrinally in the $CD8^+$ T cell population increasing their cytolytic capacity, or paracrinally on other effector cells, such as NK cells and macrophages, enhancing their cytotoxic and phagocytic activities[47]. In fact, it is widely acknowledged that $CD8^+$ T cells specific for the MHC-parasitic peptides complexes are important immune effectors for protective immunity against malaria[48].

In parallel, besides helping in the induction of $CD8^+$ T cell responses, $CD4^+$ T cells can help B cells producing antibodies that theoretically can block liver stage development, through yet undefined mechanisms[49].

T cells expressing the γδ T cell receptor (TCR) instead of the αβ TCR, were also shown to have protective functions against the liver stages of the malaria parasite. The role of γδ T cells was first demonstrated in a study using mice lacking αβ T cells. This study showed that mice lacking αβ T cells were still able to mount a response that conferred partial protective immunity after immunization with bites of irradiated *Plasmodium*-infected mosquitoes[50]. Furthermore, when γδ T cells were depleted from these sporozoite-immunized αβ T cell-deficient mice, the protective immunity was almost completely abrogated[50]. Also, γδ T cell-deficient mice showed an enhanced liver parasite burden, suggesting that this type of T cell contributes to the inhibition of the early development of intrahepatic parasites[51].

Natural killer T (NKT) cells are a subset of lymphocytes that co-express NK cell receptors and a semi-invariant TCR, which recognizes the MHC class I-like molecule CD1d[52]. Gonzalez-Aseguinolaza and colleagues discovered a role for this type of immune cell in the liver stage of malaria infection by showing that the administration of α-galactosylceramide (α-GalCer), a glycolipid known to activate CD1d-restricted NKT cells, resulted in inhibition of liver stage parasite development in mice inoculated with *Plasmodium* sporozoites. This inhibition was shown to be mediated through the IFN-γ produced by the α-GalCer-activated NKT cells[53].

### 1.5.2. Immunity elicited by *Plasmodium* blood stage infection

Following the obligatory phase of intense asexual reproduction in the liver, *Plasmodium* merozoites are released into the bloodstream initiating the successive cycles of RBCs' infection. In fact, the blood stage of infection is the one responsible for the emergence of all malaria-associated clinical symptoms, with the development of clinical disease at least partially resulting from the crosstalk between the parasite and the host's immune system[54]. Given the absence of expression of MHC molecules, erythrocytes are unable to present antigens, which is required to initiate cellular-mediated immune responses. Therefore, immunity elicited by blood stage parasites is primarily mediated by humoral immune responses. Interestingly, type I and type II gene expression are upregulated in response to blood stage infection in both humans and mice[55].

#### 1.5.2.1. Interferon-mediated immune responses

The mammalian host is able to recognize the parasite through different reported PAMP-PRR interactions in the context of the blood stage of *Plasmodium* infection. The parasite-derived molecules glycosylphosphatidylinositol (GPI) anchors, CpG DNA motifs, AT-rich DNA and haemozoin constitute PAMPs that are recognized by the host cell surface, endosomal or cytoplasmic PRRs[56]. In particular, Sharma *et al.* (2011) demonstrated that when the RBC membrane is lysed, haemozoin coated in parasite DNA is released into the bloodstream being, subsequently, phagocytosed. Haemozoin then physically destabilizes the phagolysosome and escapes into the cytosol where the AT-rich motifs (ATTTTTTAC) of the parasite's DNA, which are present over 6000 times in *P. falciparum* genome, interact with the cytosolic receptor stimulator of IFN genes (STING) and Tank-binding kinase 1 (TBK1), initiating a type I IFN-signaling cascade[57].

The identification of the major cell sources of type I IFNs during *Plasmodium* blood stage infection has been hindered by the lack of research tools that are able to detect IFN-α/-β protein production by specific cells. However, several experimental setups have already identified pDCs as the major source of type I IFNs during blood-stage of malaria infection[58]. This production is triggered by a TLR7-mediated signaling cascade, the myeloid differentiation primary response 88 (Myd88)[59] and IRF7[58]. Additionally, albeit at a lesser extent, conventional dendritic cells (cDCs) can also be a direct source of IFN-α/-β cytokines in mouse models of infection[60]. Hence, it is possible that a co-operation between different IFN-producing leukocytes is able to promote a robust type I IFN response.

Thus, it is clear that *Plasmodium* blood stage infection also induces an innate type I IFN-mediated response, at a time when IFN-γ is also abundantly produced by leukocytes[61]. However, the role of type I IFN-signaling in controlling blood stage infection is hitherto unclear and it seems to have positive or negative consequences for the host depending on whether it is exogenously or endogenously induced, as well as the host genetic background and parasite genetic background. As previously mentioned, Jahiel and colleagues discovered that exogenously induced IFNs are protective during the liver stage of infection. However, the effect on the blood stage parasites was much less pronounced suggesting that the role of type I IFN immunity might be different according to the stage of *Plasmodium* life cycle[39].

More recently, Vigário *et al*. attempted to further decipher the role of exogenously induced IFNs in the context of malaria blood stage infection. By engineering a hybrid of human IFN-α, termed BDBB, Vigário and colleagues demonstrated that BDBB was able to reduce blood stage parasitemia during infection with non-lethal strains of *P. yoelii*, although the previously seen effect on liver stage infection was absent[62]. Furthermore, Vigário and colleagues showed that BDBB prevented ECM caused by *Pb*A infection[63]. The mechanism whereby the engineered IFN-α prevented ECM is not clear, although some hallmarks of this form of severe malaria such as parasitemia, levels of pro-inflammatory cytokines, brain sequestration of parasites, number of pathogenic $CD8^+$ T cells and brain endothelial expression of ICAM-1 were reduced[63]. Collectively, these pioneering studies

revealed that exogenously induced IFNs could be beneficial during blood stage of malaria infection and impact the severity of the disease.

However, from 2009 onwards, studies about the potential role of endogenously induced IFNs in malaria infection started to emerge. In 2009, Voisine *et al*. employed an experimental setup in which IFNAR-knockout on mice with the 129Sv genetic background were infected with the non-lethal *P. chabaudi chabaudi* AS strain demonstrating that the absence of type I IFN signaling mediated by the IFNAR had no impact on blood stage infection when comparing with WT controls[64]. A contrasting conclusion was reached by Sebina and colleagues when using a slightly different experimental setup, IFNAR1-knockout on mice with the C57BL/6J background. These authors revealed that type I IFN signaling via IFNAR1 delays parasite control, not only with *P. chabaudi chabaudi* AS model but also during non-lethal infection with *P. yoelii*, which was linked to an incapacity to produce parasite-specific immunoglobulins (Ig)[65]. Similar conclusions were attained by Zander *et al*. (2016) by blocking the type I IFN signaling with an IFNAR-specific blocking antibody[66]. Taken together, these results seem to suggest that the role of type I IFN signaling via IFNAR1 may be dependent on the host genetic background. While in the 129Sv background, this endogenously-induced innate response seems to have no role in parasite control, in the C57BL/6J background, type I IFN response appears to hamper the control of primary blood stage infection, at least in non-lethal models of infection.

Conversely, in 2014, Wu *et al.* used mice with an impaired type I IFN-signaling, either genetic (*Ifnar1*$^{-/-}$) or through antibody blockade, non-lethally infected with another *P. yoelii* strain (N67) to demonstrate, for the first time, that endogenously induced type I IFNs can contribute to a decrease in parasitemia[67]. This highlights that *Plasmodium* genetics may also influence the effect of type I IFN during non-lethal blood stage infection.

Nevertheless, when the lethal *P. yoelii* YM strain was employed, more contrasting results arose. When using *Ifnar1*$^{-/-}$ mice, Spaulding *et al.* (2016) observed a decrease in blood parasitemia and increase in survival rates[59], whereas Yu and colleagues (2016) observed exactly the opposite when employing an IFNAR-blocking antibody[58]. Thus, further studies are necessary to unravel the role of type I IFN signaling via IFNAR1 regarding the lethal *P. yoelii* YM infection.

Therefore, it is difficult to reach any definitive conclusions regarding the effect of the type I IFN response upon blood stage malaria infection. This is partly due to differences obtained by independent experimental animal studies with different host-parasite combinations, but also due to the scarcity of human studies. Additional studies to understand more completely the key tenets of the type I IFN response in the context of the blood stage *Plasmodium* infection are required.

#### 1.5.2.2. Type I IFN response and experimental cerebral malaria

Although T cell activation and the type II IFN-γ are known to be essential for the development of ECM[68], the role of type I IFNs has only recently been assessed. In 2003, Aucan and coworkers found that genetic variants in *IFNAR1* led to protection from CM development in Gambian children[69]. Because IFNAR1 is a key initiator of type I IFN signaling, this study paved the way for the investigation of the role of this innate response in the context of cerebral malaria.

In 2011, Sharma *et al.* discovered that C57BL/6J mice lacking the type I IFN receptor, as well as the mediators of this signaling pathway IRF3 and IRF7, were resistant to otherwise lethal cerebral malaria[57]. In the same year, Haque and coworkers reached the same conclusion additionally showing that mice deficient in type I IFN signaling had reduced parasite burdens and the fatal neurological symptoms characteristic of a *Pb*A infection were absent[70]. Mechanistically, IFN-I inhibited the production of the type II IFN-γ by $CD4^+$ T cells, preventing this emerging Th1 response from controlling parasite burden[70].

Recently, Ball *et al.* and others got further insights into the mechanistic details behind the role of the type I IFN response during *Pb*A infection[71]. Ball *et al*. (2013) transferred splenocytes from donor mice that had received irradiated iRBCs, into IFNAR1-deficient mice in an effort to re-capitulate ECM symptoms. Using this pre-sensitization approach, the authors showed that IFNAR1 expression specifically on $CD8^+$ T cells was sufficient to restore susceptibility to ECM in *Ifnar1*$^{-/-}$ mice. Taken together, these results identified the specific expression of IFNAR1 in $CD8^+$ T cells as a key mediator of ECM development in mice[71].

Haque *et al.* (2014) used a combination of mixed bone marrow chimeras (with congenically marked *Ifnar1*$^{+/+}$ and *Ifnar1*$^{-/-}$ splenic cDCs in equal proportions) and cDC-specific IFNAR1-knockout mice (CD11c-Cre-*Ifnar1*$^{flox/flox}$) to implicate a role for cDCs, the major APC responsible for priming IFN-γ-producing Th1 cells, in mediating the deleterious effects of type I IFN signaling. In fact, the first group of mice revealed a 50% reduction in the activity of the cDCs and the second group of mice were completely protected from neurological symptoms and death compared with the controls, indicating that the type I IFN signaling cascade directly affects cDC function. However, it remains unclear what is the contribution of each cell type to the pathogenic type I IFN signaling during *Pb*A infection[60].

Based on these results, it was suggested that the type I IFN signaling mediated by the IFNAR present in various cell types, such as $CD8^+$ T cells and cDCs, has a negative impact on the progression of malaria disease potentiating the development of the cerebral syndrome[60,71].

## 1.6. Preliminary results: *Viperin*, an interferon-inducible gene

Extensive studies have been carried out to characterize the role of the innate immune system as the first line of defence against *Plasmodium* infection. In fact, a series of recent studies has indicated that *Plasmodium* specifically induces a type I IFN response during the liver stage of its life cycle, which has a strong impact on infection[41,42].

Genome-wide microarray investigations, conducted by the host laboratory, of *Plasmodium* infection-mediated transcriptional changes in the liver revealed that sporozoites induce the expression of 65 genes, mainly interferon-stimulated genes, at 42 hours post-infection compared to mock-infected mice (Fig.1.4). Interestingly, VIPERIN (virus inhibitory protein, endoplasmic reticulum associated, interferon-inducible), an ISG with a broad spectrum of notorious antiviral functions, was identified as one of the most transcriptionally induced genes within the *Plasmodium*-induced type I IFN response (Fig. 1.4).

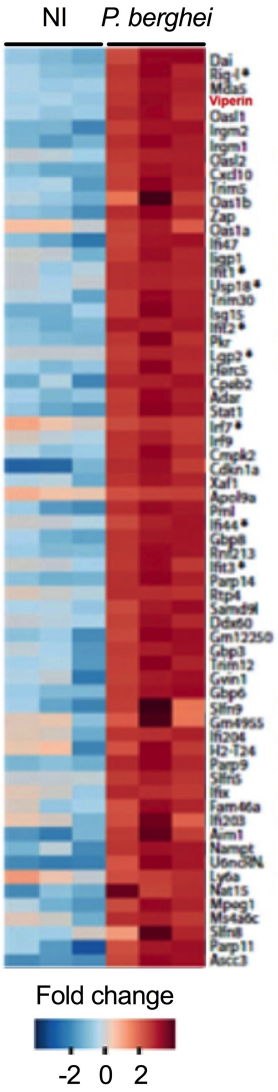


**Figure 1.4. *Plasmodium* parasites specifically induce a type I IFN response during the liver stage of infection.** C57BL/6J mice were infected with 5 × $10^4$ *P. berghei* sporozoites and genome-wide gene expression was measured in liver extracts 42 hours post-infection. Sporozoites induced the expression of 65 genes, mainly ISGs, being *Viperin* one of the most transcriptionally induced genes. Non-infected control mice were injected with an equivalent number of salivary glands extracted from non-infected mosquitoes. Columns represent individual mice and rows represent genes for which expression values increased more than two-fold compared to non-infected mice (F test p<0.05). Red and blue shades indicate upregulation and downregulation, respectively.

### 1.6.1. Structure and biochemical characterization of Viperin

Viperin (also known as cig5), the product of the gene *rsad-2*, was first identified in primary human macrophages treated with IFN-γ and in primary human fibroblasts infected with human cytomegalovirus (HCMV)[72]. Being highly conserved amongst species, Viperin is a 361-amino acid protein with a predicted molecular mass of 42.1 kDa[72].

Viperin is a three-domain globular protein with an N-terminal amphipathic α-helix, followed by a sequence motif found in the superfamily of radical *S*-adenosyl-L-methionine (SAM) enzymes and a C-terminal domain[73–75] (Fig.1.5).

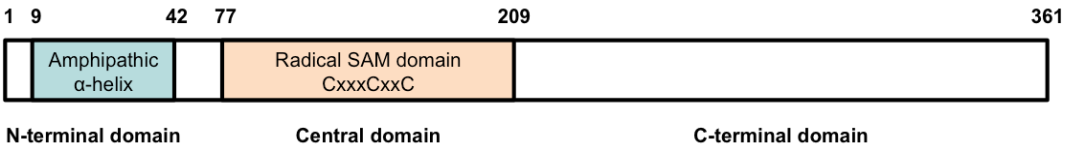


**Figure 1.5. Schematic representation of Viperin protein's structure.** Amino acid residues 1-42 form the N-terminal domain of Viperin, important as a mediator of Viperin's association to subcellular organelles. The highly conserved C-terminal domain ranges from residues 209-361 and it is involved in Viperin's dimerization. The radical SAM domain, characterized by the presence of a CxxxCxxC motif, corresponds to residues 77-209. All three domains were individually identified as mediators of Viperin's functions against different viruses. Adapted from "The role of viperin in the innate antiviral response." by K.J. Helbig and M.R. Beard, 2014, *J. Mol. Biol.*, 426, 1210-1219.

The protein's N-terminal region is a variable transmembrane domain approximately ranging from residues 1 to 42[(73)] and is known to mediate Viperin's localization to the endoplasmic reticulum (ER), to lipid droplets (LDs) and to the mitochondria[76]. The C-terminal (residues 209-361) is a highly conserved domain of Viperin amongst species[75]. Interestingly, Hinson *et al.* (2009) have hypothesized that the induction of morphological changes in the ER upon Viperin overexpression involves both the N-terminal and C-terminal of Viperin. Specifically, the N-terminal amphipathic α-helix is responsible for the induction of localized ER membrane curvature, which is further exacerbated upon Viperin dimerization through its C-terminus to cause crystalloid ER formation. The increase in membrane curvature may subsequently cause a reduction in protein secretion, a phenomenon that is also observed upon Viperin overexpression[77].

Viperin has been suggested to be a member of the radical SAM superfamily of enzymes due to the presence of a CxxxCxxC motif, a hallmark of this enzymatic family[73,75]. Typically, SAM enzymes coordinately bind a [4Fe-4S] cluster to cleave SAM reductively and generate a radical that is usually transferred to a substrate. The cysteine residues within the CxxxCxxC motif bind three of the iron atoms of the [4Fe-4S] cluster[75]. In fact, several biochemical analysis independently carried out by Duschene *et al.* (2010) and Shaveta *et al.* (2010) have concluded that Viperin binds a reducible [4Fe-4S] cluster and catalyses the reductive cleavage of SAM to yield methionine and 5'-deoxyadenosyl (5'-dAdo) radical intermediate[73,74]. Despite this discovery, a direct link between Viperin's enzymatic and antiviral activities is yet to be defined.

Little is known about the structure-activity relationship of Viperin. However, the development of Viperin constructs lacking each one of the protein's three domains has elucidated some important links between the structure of this protein and its involvement in the antiviral function. In particular, although it seems to be more important in directing Viperin to the ER rather than being responsible for its antiviral activity[78,79], the truncation of the N-terminal abolishes Viperin's antiviral activity against hepatitis C virus (HCV)[80] and Chikungunya virus (CHIKV)[79]. On the other hand, the C-terminal conserved domain is essential for Viperin's activity against HCV[76,80], Zika virus (ZIKV)[81], tick-born encephalitis virus (TBEV)[78] and Dengue virus (DENV)[82]. Lastly, mutations of SAM domains reversed Viperin mediated inhibition of TBEV[78] and human immunodeficiency virus-1 (HIV-1)[83].

### 1.6.2. Regulation of Viperin expression

Viperin is expressed in most cell types at very low basal levels[84]. Analysis of Viperin induction by both type I and type II IFNs in primary human macrophages revealed that IFN-α and IFN-β strongly induced this ISG, whereas IFN-γ induced Viperin to a lesser extent[72]. Since then, Viperin has been shown to be induced by several factors, such as lipopolysaccharide (LPS), the double-strand RNA analogue poly (I:C) and by a broad range of RNA and DNA viruses[85].

Viperin can be induced in an IFN-dependent or IFN-independent manner[84]. In the IFN classical pathway, the aforementioned factors bind to PRRs such as the transmembrane TLR3 and TLR4, the cytosolic RIG-like receptors (RLRs) or cytosolic DNA sensors. Consequently, IRF3 and IRF7 are activated and are translocated to the nucleus where they will regulate the expression of type I IFNs. These will, in turn, bind to the IFNAR, in an autocrine or paracrine manner, initiating a signaling cascade that culminates in the formation of the ISGF3. ISGF3 is able to bind to the Viperin promoter and induce its expression, amongst several other ISGs[84]. Interestingly, Severa *et al.* (2006) have identified a mechanism of counter-regulation, through which Viperin expression is blocked. This mechanism is mediated by the positive regulatory domain I-binding factor 1 (PRDI-BF1, also called BLIMP1), which competes with the ISGF3 complex for the ISRE sites, and seems to counteract the potential detrimental effects of excessive IFN production[86]. On the other hand, a number of viruses, such as Japanese encephalitis virus (JEV), CHIKV and HCMV, are able to induce Viperin independently of IFN production[79,87,88]. The stimulated RLRs interact with the adaptor protein MAVS to promote the activation of IRF1 and IRF3. In turn, these regulatory factors promote the simultaneous expression of type I IFNs and ISGs. Therefore, whereas Viperin IFN-dependent expression is mediated by ISGF3, its IFN-independent expression is mediated by IRF1 and IRF3[84].

### 1.6.3. Antiviral functions of Viperin

In 2001, Chin and Cresswell demonstrated for the first time that Viperin, an interferon-stimulated gene, exhibits antiviral activity against HCMV, the herpes virus, in primary human foreskin fibroblasts[72]. Since 2001, most research focusing on this ISG has employed *in vitro* infection systems of various cell lines, using stable or transient pre-expression (or overexpression) of Viperin to assess the impact on viral replication[88,89]. In a complementary manner, some studies also applied RNA interference (RNAi) techniques to knockdown Viperin and investigate a possible reversal of the Viperin-mediated phenotype[89]. Ectopic expression of Viperin is now known to inhibit a broad range of DNA and RNA viruses on several tissues in culture, including flaviviruses (HCV, West Nile Virus, DENV, JEV and ZIKV), the orthomyxovirus influenza A, the retrovirus HIV-1 and the alphavirus Chikungunya[84]. However, the effects of this protein *in vivo*, which have been investigated mainly through the use of mice knockout for the Viperin-encoding gene (*Viperin*$^{-/-}$), appear to be more limited, possibly due to redundant and, therefore, possible compensatory mechanisms exerted by other ISGs[90].

Two independent studies conducted by Wang *et al.* (2007) and Tan *et al.* (2012) revealed that the release of influenza virus (IFV) from the host cell plasma membrane was substantially inhibited by the ectopic expression of mouse and human Viperin, respectively, in an epithelial cell line (HeLa). Wang and colleagues further investigated the biological mechanism whereby this ISG is able to inhibit IFV egress, proposing that Viperin disrupts lipid rafts, crucial sites for virus budding and release, through the interaction, and subsequent inhibition, of the farnesyl diphosphate synthase (FPPS) enzyme[91]. FPPS is a key enzyme in the isoprenoid biosynthetic pathway, which culminates in the synthesis of cholesterol, an important component of lipid rafts. A similar mechanism was proposed to be involved in the inhibition of HIV-1 replication by Viperin[83]. Possibly through its radical SAM domain, Viperin colocalizes with the HIV-1 antigen p24 and again, via interaction with the FPPS enzyme, prevents HIV-1 particle egress. In fact, it was observed a reduction on the levels of extracellular p24 in HEK293T cells expressing WT Viperin but not in the ones expressing the SAM domain mutant[83].

In an attempt to translate the anti-IFV activity of Viperin *in vitro* to its function in an *in vivo* model, Tan and co-workers performed a time course analysis of IFV infection in *Viperin*$^{-/-}$ mice. However, no difference was observed in susceptibility, pulmonary damage, IFV titres or the ability to mount an adaptive immune response between WT and knockout mice. As previously mentioned, the authors suggested that the absence of Viperin can be masked by other ISGs activated in the lungs or that the natural induction of ISGs may not be early enough to counter acute influenza. Interestingly, the peak of Viperin expression occurred 5 days post-infection, when IFV infection is already well established[90].

In contrast with the observations made for IFV, Viperin has been shown to restrict the replication of West Nile Virus (WNV)[92], a neurotropic virus, and CHIKV[79] in mouse models. Contrary to WT mice, the absence of Viperin resulted in an increase in WNV lethality that was associated with a more significant increase in viral replication in the central nervous system (CNS)[92]. Similarly, Viperin is able to directly control CHIKV replication *in vivo* with CHIKV-infected *Viperin*$^{-/-}$ mice exhibiting higher viral titres and more severe joint inflammation than WT mice[79].

The only study to date to analyse the impact of Viperin overexpression *in vivo* was performed in the context of respiratory syncytial virus (RSV) infection in chinchillas. The previously demonstrated Viperin's antiviral effect *in vitro* was also accomplished in the animal model[93], with Viperin being able to significantly reduce viral titres of RSV in the chinchilla's upper airways[94].

#### 1.6.3.1. Viperin in the context of the liver-infecting Hepatitis C virus

In a study performing microarray analysis of liver biopsies from human patients chronically infected with HCV (CHC), Helbig *et al.* identified Viperin as being significantly upregulated in all cases of CHC, amongst 39 interferon-related genes[80]. This discovery laid the foundation for the investigation of Viperin's role in the context of HCV infection.

Strikingly, it was subsequently demonstrated that transient expression[80] or overexpression[89] of Viperin in the human hepatoma cell line Huh-7 harbouring the HCV replicon led to a significant ~50% reduction of HCV RNA levels at two different times post-infection[80,89]. These results suggested

that Viperin expression can in part directly supress HCV replication. The same conclusion was achieved when Helbig *et al*. (2011) and Wang *et al.* (2012) employed a more physiologically relevant system with the complete HCV life cycle in hepatocyte cell lines (a system named HCVcc)[76,89].

Further studies aimed at understanding the biological mechanism whereby Viperin exerts its anti-HCV activity were conducted by the authors mentioned above. Viperin was shown to interact with the host protein hVAP-33 (human vesicle-associated membrane protein-associated protein of 33 kDa) through its C-terminal domain. In the absence of Viperin, the C-terminus of hVAP-33 binds the viral non-structural protein NS5A, with this interaction being crucial for the assembly of the HCV replication complex on ER-derived membranes[89]. Therefore, when expressed prior to infection, Viperin competes with NS5A for the binding to hVAP-33, inhibiting the replication of HCV RNA, which may account for the *in vitro* anti-HCV activity[89]. Moreover, Viperin was also found to interact with NS5A surrounding the LDs, which may also destabilize HCV replication[76].

For the establishment of a persistent infection, HCV is able to supress innate antiviral function by cleavage of MAVS using NS3 protease function, which blocks downstream pathways. In fact, HCV NS3 protease activity downregulates the expression of ISGs, including Viperin, as a mechanism of evading host defences[95].

HCV is, in fact, highly prevalent in areas endemic for malaria with both pathogens developing in the liver and potentially synergistically interact[96]. Interestingly, Liehl *et al.* (2014) discovered that the innate type I IFN response elicited by the HCV is functional against *Plasmodium* infection leading to an IFNAR1-dependent reduction of the liver infection load when HCV RNA is administered prior to the parasitic infection[41]. This is an important finding in the understanding of a role for the type I IFN response in the context of coinfections with hepatotropic pathogens, in which Viperin could assume a biologically relevant role.

#### 1.6.3.2. A potential unifying mechanism of Viperin action against flaviviruses

Viperin has been suggested to elicit a plethora of antiviral activities through the promiscuous interaction with several functionally unrelated host (such as FPPS and hVAP-33) and viral (including HCV NS5A) proteins.

A recent study by Gizzi *et al*. (2018) demonstrated that Viperin can take advantage of its intrinsic catalytic activity to exert its antiviral activity, at least, against the flavivirus family. Viperin was shown to catalyse the conversion of cytidine triphosphate (CTP) to 3'-deoxy-3',4'-didehydro-CTP (ddhCTP) via a SAM-dependent mechanism. ddhCTP acts as a chain terminator for the RNA-dependent RNA polymerase (RdRp), an enzyme that catalyses the replication of RNA from multiple members of the Flavivirus genus. More strikingly, human cytidylate monophosphate kinase 2 (hCMPK2), an enzyme that is co-transcribed with Viperin upon IFN stimulation, catalyses the phosphorylation of CDP to CTP, ensuring sufficient substrate for Viperin-mediated production of ddhCTP during viral infection[97]. Consistently, the exploration of the ddhCTP effect on the RdRp activity of different members of the flavivirus family revealed that RdRps from WNV, DENV, ZIKV and HCV were susceptible to inhibition by ddhCTP acting as a chain terminator[97].

### 1.6.4. Viperin-mediated modulation of immune signaling

Viperin is now a well-recognized ISG with direct antiviral activity against most viruses being portrayed as a key antiviral protein. However, it is becoming apparent that Viperin may also exert key functions in the modulation of immune signaling.

Using *Viperin*-deficient mice (*Viperin*$^{-/-}$), Qiu *et al.* (2009) explored the potential role of Viperin in T cell development and function[98]. The activation of T lymphocytes depends on three signals: (i) engagement and subsequent signal transduction by the T cell receptor (TCR); (ii) costimulation through the interaction of CD28 with CD80/CD86 of antigen-presenting cells (APCs) and, finally, (iii) cytokine stimulation[99]. Several transcription factors have been shown to be involved in these processes, including those belonging to NFAT (nuclear factor of activated T-cells), AP-1 (activator protein 1), NF-κB (nuclear factor kappa B) and STAT families[98]. Although not necessary for the T cell development, Viperin was shown to be crucial for the activation and differentiation of $CD4^+$ T cells[98]. Upon TCR/CD28 engagement, Viperin appears to modulate the formation of NF-κB/AP-1 DNA binding complexes and subsequent induction of GATA-3, the master regulator of Th2 differentiation[98]. Consequently, *Viperin*-deficient $CD4^+$ T cells fail to differentiate into Th2 cells with a subsequent reduction in the production of Th2-characteristic cytokines (IL-4, IL-5 and IL-13)[98]. Th2 responses are responsible for targeting extracellular parasites, such as helminths, and facilitate tissue repair[100]. This unexpected finding signals the need for additional studies to uncover the mechanism whereby Viperin influences T cell activation and differentiation.

Moreover, it is now clear that Viperin intervenes in a multitude of pathways, modulating innate immune signaling through the interaction with various host organelles, including lipid storage organelles called lipid droplets[101]. Interestingly, through its N-terminal amphipathic α-helix, Viperin anchors to the membrane lipid layer of LDs where it acts as a regulator of PRR-mediated innate immune responses specifically in pDCs[101]. In fact, pDCs are a major source of IFN-α[102], in part, through the constitutive expression of endosomal TLRs (TLR7 and TLR9) and IRF7, a key transcription factor for type I IFNs expression[101]. Thus, Viperin emerges as a LD-associated transit point between TLR7- and TLR9-mediated signaling and IFN-α production[101]. Mechanistically, upon TLR-stimulation, Viperin recruits IRAK1 (interleukin-1 receptor-associated kinase 1) and TRAF6 (TNF receptor associated factor 6) to the LDs facilitating the subsequent lysine-63 (K63) ubiquitination of IRAK1 by TRAF6[101]. As a consequence, IRF7 is activated and induces the expression of type I IFNs[101]. On one hand, this finding may hint the presence of a direct link between the antiviral activity of Viperin and its localization to LDs, recognized replication sites of numerous viruses, including HCV. On the other hand, this IFN-independent induction of Viperin expression may function as a mechanism of positive feedback, given that Viperin expression is highly induced by IFNs[101]. If Viperin is essential for IFN induction, pDCs must basally produce certain amounts of this ISG even in the absence of IFN[101].

### 1.6.5. Viperin at the centre of viral evasion and host exploration mechanisms

While it is known that the vertebrate immune system is equipped to deal with invading pathogens, it has also become apparent that infectious agents have evolved strategies to escape detection by these lines of defence and to exploit the host cell resources in order to survive and successfully develop. Viruses are no exception, with Viperin being at the centre of immunity-exploiting and immunity-evading mechanisms developed by HCMV and JEV, respectively.

HCMV is able to induce the expression of Viperin but a prior expression gives cells resistance to this viral infection[72]. Curiously, it was proposed that Viperin could exert its anti-HCMV activity by inhibiting the synthesis or function of HCMV-encoded proteins critical for virus maturation and/or assembly[72]. Indeed, synthesis of the pp65, gB and pp28 viral proteins was significantly reduced in fibroblasts expressing Viperin[72]. However, when fibroblasts were infected with HCMV, the virus itself induced the expression of Viperin, which was shown to be redistributed from its usual ER-association to the Golgi apparatus, the site of viral glycoprotein maturation, and, ultimately, to virus assembly compartments (ACs)[103]. Although it was originally proposed to be a strategy of evading the antiviral effects of the ER-localized Viperin, Seo *et al.* (2011) added a twist to the story. These authors discovered that, before its transfer to the Golgi, Viperin is transported to the mitochondria, a strategy used by the herpes virus to increase viral infection. The HCMV viral protein vMIA (viral mitochondrial inhibitor of apoptosis) physically interacts with Viperin and relocalizes it to the mitochondria, where it interacts with and inhibits the trifunctional protein (TFP), a protein that mediates the fatty acid β-oxidation to generate ATP (adenosine triphosphate). The major consequence of this interaction between Viperin and vMIA is ATP depletion and the ensuing actin cytoskeleton disruption as a mean of enhancing viral infectivity[103]. Later, in 2013, Seo *et al.* revealed that Viperin also regulates the cellular lipid metabolism during HCMV infection[104]. In fact, Viperin-mediated ATP depletion activates the enzyme AMP-activated protein kinase (AMPK), which induces the expression of the glucose transporter GLUT4[104]. The GLUT4-mediated increase of intracellular glucose concentration induces the expression of a glucose-responsive transcription factor (ChREBP), which, upon nuclear translocation, leads to increased expression of genes encoding key lipogenic enzymes, increased lipogenesis and lipid droplet accumulation. An increase in total lipid biosynthesis is crucial for viral protein envelope formation and, subsequently, optimal production of infectious viruses[104].

Unlike other viruses of the Flaviviridae family, such as the WNV, ZIKV and HCV, the Japanese encephalitis virus, although inducing Viperin through an IFN-independent pathway, was not inhibited by a potential antiviral effect of this ISG. When infecting human epithelial A549 cells, Chan *et al.* (2008) were only able to detect Viperin protein in the presence of the proteasome inhibitor MG132. This observation highly suggested that JEV is able to degrade Viperin through a proteasome-dependent pathway as a way of circumventing its antiviral effects. However, as the authors noted, more work is necessary to uncover what is the mechanism whereby JEV is able to trigger proteasome-dependent Viperin degradation[87].

### 1.6.6. Viperin: linking the immune system with lipid metabolism?

It is now clear that Viperin can have a dual antiviral or proviral role: besides being able to directly inhibit the replication of numerous viruses through different and ill-defined mechanisms, it can also interfere with signaling pathways critical for an innate response via assembling of a signaling complex in LD, or even interfere with fatty acid β-oxidation, ultimately enhancing lipid synthesis which is essential for most pathogens replication. In fact, Viperin is now considered a key molecular link between lipid metabolism and immune defence or evasion[104,105].

In this context, Viperin induction upon *Plasmodium* liver stage infection assumes enhanced relevance because *Plasmodium* parasites strongly alter the hepatic lipid metabolism. A microarray-based approach to profile the host cell response to malaria infection in a time course experiment has identified the significant modulation of 35 (amongst 451) genes playing a role in lipid metabolism[106]. Furthermore, it was shown that parasites rely on host lipids, including phosphatidylcholine and lipoic acid, for their growth, development[107] and survival[108], significantly increasing the abundance of lipids typically associated with LD.

Collectively, the critical role of LD-associated lipids in parasite survival and the simultaneous increase in Viperin expression as well as the already described link between LDs and this ISG, provide the basis for hypothesizing that Viperin may be a key player in a cascade of events that allows the maintenance of host cell and parasite homeostasis and/ or parasite survival or elimination.

## 2. Aims

The asymptomatic nature of *Plasmodium* infection of the liver led to the assumption that its intense asexual replication inside hepatocytes occurred without being detected by the host immune system[6]. Only recently has *Plasmodium* been shown to specifically elicit a type I IFN-driven functional anti-parasite response, which results in the activation of numerous ISGs[41,42].

On this thesis, we propose to broaden the current knowledge on the innate immune response elicited by the liver stage of *Plasmodium* infection. We will focus on the dynamics of ISGs expression during infection and on the identification of its key cellular mediators, with the objective of contributing to a more integrated view of this parasite control mechanism. Furthermore, we intent to unravel the role of a well characterized antiviral ISG, Viperin, on *Plasmodium* infection.

Therefore, the following aims are established for this thesis:

- To characterize the dynamics of interferon-stimulated immune responses elicited by *Plasmodium* infection during the mid to late stages of parasite liver development and exiting to the bloodstream. An extensive time course expression analysis for type I and type II IFNs as well as ISGs, will be performed using quantitative real-time PCR (qRT-PCR) to unravel a potential crosstalk between the different IFN pathways in ISGs expression.

- To unveil the cellular mediators of the interferon-stimulated responses induced upon *Plasmodium* liver stage infection. Flow cytometry-based techniques and qRT-PCR analysis will be combined with knockout mouse models lacking specific subsets of immune cells and cell depletion antibodies to narrow down and pinpoint potential immune cellular mediators of the increased ISG expression during *P. berghei* liver stage infection.

- To characterize the role of Viperin in host resistance to *Plasmodium* infection. The impact of Viperin expression on liver and blood stage *Plasmodium* infection will be assessed by combining bioluminescence methodology with mice deficient for Viperin production (*Viperin*$^{-/-}$) and cellular mediators of Viperin's mRNA expression will be uncovered using flow cytometry methodology.

# 3. Materials and Methods

## 3.1. Parasite strains and sporozoite collection

Green fluorescent protein (GFP)- or luciferase-expressing *P. berghei* ANKA sporozoites were obtained from dissection of the salivary glands of infected female *Anopheles stephensi* mosquitoes in non-supplemented Roswell Park Memorial Institute 1640 (RPMI 1640; Gibco) medium, bred at the Instituto de Medicina Molecular (Lisbon, Portugal) before being employed for the experiments. To obtain free sporozoites, the salivary gland suspension was mechanically homogenized and filtered through a 70 µm strainer. Sporozoites were then counted in a Neubauer chamber using an Olympus CKX41 inverted microscope.

## 3.2. Cells and cell culture conditions

The human hepatoma cell line Huh-7 was maintained in monolayer culture in RPMI 1640 or Dulbecco's modified minimal essential medium (DMEM; Gibco) supplemented with 1% (v/v) glutamine (Gibco), 1% (v/v) non-essential amino acids (Gibco), 1% (v/v) penicillin/streptomycin (Gibco), 10% (v/v) fetal bovine serum (FBS; Alfagene) and 1% (v/v) HEPES pH 7 (Alfagene), in a humidified atmosphere at 37°C with 5% $CO_2$.

## 3.3. *In vitro* infection of Huh-7 cells with *P. berghei*

Huh-7 cells were seeded on coverslips in 24-well culture plates (30,000 cells/ well), 24 hours prior to infection. On the day of infection, 30,000 *P. berghei* sporozoites were added to each well, the plate was centrifuged for 5 min at 3000 rpm, and subsequently incubated at 37°C. At 42 hours post-infection, cells were either fixed with 4% paraformaldehyde (PFA; Santa Cruz Biotechnology) in 1× phosphate-buffered saline (PBS; NZYTech) and stored at 4°C for microscopy analysis, or collected for RNA extraction.

## 3.4. Huh-7 cell stimulation

Huh-7 cells were stimulated with 5000 U/mL of IFN-α (Thermo Fisher Scientific) for 24 hours before infection with *P. berghei* sporozoites.

## 3.5. Immunofluorescence microscopy of *P. berghei*-infected Huh-7 cells

At the previously indicated time point post-infection, coverslips of infected hepatoma cell lines were fixed with 4% PFA for 15 min at room temperature (RT) and washed 3 times with 1× PBS. Cells were then permeabilized and blocked with 0.1% (v/v) Triton X-100 (Roth) in 1× PBS containing 1%

(v/v) bovine serum albumin (BSA; VWR Chemicals) for 30 min. Primary and secondary antibodies, as well as the Hoechst were diluted in the same permeabilization/ blocking solution. Parasites were stained with a goat anti-UIS4 antibody (dilution 1:300, Sicgen). Viperin was detected using a monoclonal mouse anti-Viperin (Merck Millipore) or a polyclonal rabbit anti-Viperin (Abcam), both at 1:300 dilution. After incubation at RT for 1h in a humid box, the coverslips were washed three times with 1× PBS. Cells were then incubated in 1:300 dilution of anti-goat Alexa Fluor 594 (Donkey IgG) and anti-mouse Alexa Fluor 488 (Donkey IgG) or anti-rabbit Alexa Fluor 488 (Donkey IgG) (Jackson ImmunoResearch Laboratories) secondary antibodies, as well as with Hoechst 33342 (Invitrogen) in a dilution of 1:1000 for nuclei staining. Coverslips were mounted on microscope slides with Fluoromount G (SouthernBiotech). Widefield images were acquired in a Zeiss Axiovert 200M microscope.

## 3.6. Mice

Mice were housed in the animal house facility of Instituto de Medicina Molecular in specific pathogen-free conditions and in a 12-hour night-light cycle. All *in vivo* experiments were performed in compliance with national and European Union regulations and were approved by ORBEA (Órgão Responsável pelo Bem-Estar Animal).

C57BL/6J WT mice aged 6 to 12 weeks-old were purchased from Charles River Laboratories International. Recombinase activating gene (RAG)-$2^{-/-}$/$\gamma c^{-/-}$ mice were bred in the animal house facility of Instituto de Medicina Molecular in specific pathogen-free conditions. RAG-$2^{-/-}$ mice, 11 to 13 weeks-old, were ordered from Instituto Gulbenkian de Ciência. *Viperin*$^{-/-}$ mice on the C57BL/6J background were a kind gift from Peter Cresswell, Department of Immunobiology, Yale University School of Medicine. TCRd$^{-/-}$ mice were a kind gift from Ângelo Chora, Mota Lab, Instituto de Medicina Molecular. Liver samples collected at 42 hours post-infection from *Ifnar1*$^{-/-}$ mice were kindly provided by Patrícia Meireles, Prudêncio Lab, Instituto de Medicina Molecular.

Breeding of heterozygous (*Viperin*$^{+/-}$) mice on the C57BL/6J background was carried out to produce littermate controls (*Viperin*$^{+/+}$) that were categorized as WT mice with intact Viperin expression, and as homozygous knockout (KO) mice (*Viperin*$^{-/-}$), in which the Viperin gene was knocked out and replaced with a neomycin-resistance gene[98]. Genotyping of the mice was based on the detection of Viperin (WT) or neomycin-resistance (KO) genes. Genomic DNAs were isolated from the mouse ear and subjected to two independent PCR reactions for amplification of the Viperin gene and the neomycin resistance gene, respectively, using NZYTaq II 2× Colourless Master Mix (NZYTech), according to the manufacturer's instructions. Amplification of the Viperin gene was performed using the following program: 2 min at 95°C followed by 25 cycles of 30 sec at 95°C, 1 min at 55°C and 1 min at 70°C and a final step of 10 min at 70°C. The neomycin resistance gene was amplified as follows: 5 min at 95°C followed by 25 cycles of 30 sec at 95°C, 30 sec at 61°C and 17 sec at 72°C and a final step of 10 min at 70°C. Primer pairs used to detect target genes are listed in Table 3.1.

**Table 3.1.** List of primer sequences used for mice genotyping and the correspondent amplicon size.

| Gene | Foward primer (5' → 3') | Reverse primer (5' → 3') | Amplicon size |
|---|---|---|---|
| *Viperin* | CTCACAGGTTTGGAGAAGATC | CCATTGCTCACTATGCTCAC | 134 bp |
| *Neomycin* | TGACTGGGCACAACAGAC | TTTCTCGGCAGGAGCAAG | 271 bp |

The amplified PCR products were analysed by gel eletrophoresis on a 2% agarose gel stained with RedSafe™ Nucleic Acid Staining Solution and revealed on Chemidoc XRS+.

## 3.7. Natural Killer Cell Population Depletion

The TM-beta 1 antibody for depletion of the NK cell population (including NK and NKT cells) was kindly provided by Geert Leroux-Roels, Center for Vaccinology, Ghent University. C57BL/6J mice, aged 6-8 weeks-old, were intraperitonially injected with 150 µg of the depleting antibody dissolved in 1× PBS two hours after *P. berghei* sporozoite injection. Depletion of the NK and NKT cells subsets was confirmed by flow cytometry. Briefly, isolated liver nonparenchymal cells were stained in PBS 1× with the following flow cytometry (FACS) antibodies: PerCPCy5.5-CD3 (1:100 dilution; BioLegend) and PE-NK1.1 (1:300 dilution; BioLegend). FACS samples were run on a BD LSRFortessa X-20 and analysed using FlowJo software (version 10, FlowJo).

## 3.8. Mice irradiation

C57BL/6J mice were whole body irradiated with 900 rads of gamma radiation 24 hours prior infection with *P. berghei* sporozoites using a Gammacell ELAN 3000 irradiator.

## 3.9. *In vivo* infection of mice with *P. berghei* sporozoites

Mice were anaesthetized using isoflurane (Steve) and infected intravenously, through retro-orbital injection, with 30,000 freshly collected *P. berghei* sporozoites, unless specified otherwise, diluted in RPMI 1640.

## 3.10. Bioluminescence measurement of *P. berghei* liver infection *in vivo*

Luciferase acitivity in animals was visualized through imaging of whole bodies using the IVIS Lumina animal imager (Caliper Life Sciences, USA). The bellies of C57BL/6J mice were shaved prior to imaging in order to minimize the absorption of light by the fur[109,110]. Mice were intradermally injected with 100 µL of D-Luciferin (Perkin Elmer) before being anesthesized using a mixture of Imalgene 1000 (Merial) and Rompun 2% (Bayern) diluted in 1× PBS. Animals were kept anesthesized during the measurements, which were performed within 10 minutes after the injection of D-Luciferin. Bioluminescence imaging was acquired at medium binning factor and an exposure time of 3 minutes. Quantitative analysis of bioluminescence was performed by measuring the luminescence signal

intensity using the Region of Interest (ROI) settings of the Living Image 3.0 software (PerkinElmer). ROIs were placed around the abdominal area at the location of the liver. ROI measurements are expressed as average radiance (photons/second/$cm^2$/sr).

## 3.11. Assessment of blood parasitemia

The presence of luciferase-expressing blood stage parasites was monitored at specific times post-infection (days 2, 3, 4, 6, 7, 8, 10, 11, 13 and 20) by luminescence. For luminescence measurements, 5 µL of blood was collected from the tail vein into 45 µL of lysis buffer[111]. Luminescence was determined by adding 50 µL of D-Luciferin dissolved in luciferase assay buffer, according to the manufacturer's instructions, to 15 µL of lysate and immediately measured using a multiplate reader (Tecan, Switzerland). Values of luciferase activity are expressed as relative luminescence units.

## 3.12. Sample collection from mice

At specific times post-infection (42, 48, 60, 72, 84 and 96 hours post-infection), mice were sacrificed by isoflurane overdose, blood was collected by cardiac puncture using sodic heparin (100 U/mL; Braun) as an anticoagulant, and mice were perfused extensively with 20 mL of 1× PBS prior to liver harvesting. The liver was further divided in lobes for processing as follows: the left lateral lobe was fixed in 4% PFA overnight and then stored in 1× PBS at 4°C for microscopy analysis; the right lateral and caudate lobes were homogenized in 3 mL of denaturing solution (4 M guanidine thiocyanate; 25 mM sodium citrate pH 7, 0.5% (v/v) *N*-lauroylsarcosine and 0.7% (v/v) β-mercaptoethanol in DEPC-treated water) for RNA extraction; the left and right medial lobes were further processed for isolation of nonparenchymal cells as described below.

## 3.13. RNA extraction and quantification

For RNA extraction from cultured Huh-7 cells, cells were washed with 1× PBS, incubated with trypsin (Gibco) for 5 min at 37°C, and collected in 300 µL of complete RPMI medium. Cells were then centrifuged at 13,200 rpm for 5 min and the pellet containing the Huh-7 cells was flash-frozen in liquid nitrogen. For extraction of mouse liver RNA, the designated lobes of each liver were mechanically homogenized in 3 mL of denaturing solution.

RNA was then extracted from both Huh-7 cells and mouse liver using the TripleXtractor direct RNA kit (Grisp) according to the manufacturer's instructions. The concentration of RNA in each sample was assessed by measurement of absorbance at 260 nm on a NanoDrop 2000 spectrophotometer.

## 3.14. cDNA synthesis and qRT-PCR

Complementary DNA (cDNA) was synthesized from 1 µg of RNA using the NZYTech First-Strand cDNA synthesis kit, according to the manufacturer's instructions, in a total volume of 20 µL. The cDNA was synthesized in a Biometra Personal thermocycler employing the following parameters: 25°C for 10 min, 55°C for 30 min and 85°C for 5 min.

The qRT-PCR reaction was performed in a total volume of 8 µL in a ViiA7 Applied Biosystems real-time thermal cycler using the SYBR® Green (BioRad) reagent. The program employed was the following: 2 min at 50°C and 10 min at 95°C followed by 40 cycles of 15 sec at 95°C and 1 min at 60°C, and a melting stage at 95°C for 15 sec, 60°C for 1 min and 95°C for 30 sec. For the analysis, the expression levels of all target genes were normalized against the hypoxanthine guanine phosphoribosyltransferase (*Hprt*) housekeeping gene using the comparative threshold cycle (Ct). Gene expression values were then calculated based on the ΔΔCt method[112], using the mean of the control group as a calibrator to which all other samples were compared. Primer pairs used to detect target gene transcripts are listed in Table 3.2.

**Table 3.2.** List of primer sequences used for qRT-PCR analysis.

| Gene | Species | Foward primer (5' → 3') | Reverse primer (5' → 3') |
|---|---|---|---|
| *HPRT* | *Homo sapiens*/ *Mus musculus* | TTTGCTGACCTGCTGGATTAC | A CAAGACATTCTTTCCAGTTAAAGTTG |
| *18S* | *P. berghei* | AAGCATTAAATAAAGCGAATACATCCTTAC | GGAGATTGGTTTTGACGTTTATGTG |
| *Viperin* | *Homo sapiens* | TCCTTTGTGCTGCCCCTTGAGGA | TGCTCACGATGCTCACGCTGG |
| | *Mus musculus* | CTTCAACGTGGACGAAGACA | GACGCTCCAAGAATGTTTCA |
| *IFN-α* | *Mus musculus* | CACCCCTCTTTCCTGCCTAA | TCTGCTGGGTAAGATCTCGC |
| *IFN-β* | | CCCTATGGAGATGACGGAGA | CTGTCTGCTGGTGGAGTTCA |
| *IFN-γ* | | ATGAACGCTACACACTGCATC | CCATCCTTTTGCCAGTTCCTC |
| *Ifit-1* | | CCTTTACAGCAACCATGGGAGA | GCAGCTTCCATGTGAAGTGAC |
| *Ifi44* | | TCGATTCCATGAAACCAATCAC | CAAATGCAGAATGCCATGTTTT |
| *Usp18* | | CGTGCTTGAGAGGGTCATTTG | GGTCGGGAGTCCACAACTTC |
| *Ifit3* | | CTGAACTGCTCAGCCCACAC | TGGACATACTTCCTTCCCTGA |
| *Irf7* | | CTTCAGCACTTTCTTCCGAGA | TGTAGTGTGGTGACCCTTGC |
| *CD68* | | AGCTGCCTGACAAGGGACACT | AGGAGGACCAGGCCAATGAT |

## 3.15. Isolation of mouse liver nonparenchymal cells

To obtain mouse liver nonparenchymal cells, perfused livers were squeezed in 1× PBS solution containing DNase (2 U/mL), filtered through a 100-µm filter followed by 5 min centrifugation at 2,000 rpm. The pellet was resuspended in 10 mL of 35% Percoll (Sigma) and centrifuged at 2,600 rpm, for 20 min without break at 20°C. The pellet containing the nonparenchymal cells was

ressuspended in 3 mL of Ammonium-Chloride-Potassium (ACK) buffer for 3 min at RT to lyse the RBCs. This reaction was stopped with FACS buffer (1× PBS containing 2% (v/v) FBS) followed by 5 min centrifugation at 2,000 rpm.

## 3.16. Tissue isolation and flow cytometry

For flow cytometry analysis, mice livers were harvested at the previously indicated times post-infection, manually homogenized and then filtered through a 100-µm filter for isolation of liver leukocytes as described above.

One million cells were surface stained in PBS 1× with the flow cytometry (FACS) antibodies and respective dilutions indicated on Table 3.3, followed by a 20 min incubation at 4°C. All antibodies were obtained from BioLegend. Cells were then incubated with Fixation/ Permeabilization buffer (eBioscience) for 30 min at 4°C to allow intracellular staining with rabbit polyclonal anti-Viperin antibody (Abcam; 1:500 dilution). Following a 30 min incubation at 4°C, cells were incubated in a 1:750 dilution of anti-rabbit Alexa Fluor 488 (Donkey IgG) (Jackson ImmunoResearch Laboratories). All FACS samples were run on a BD LSRFortessa X-20 and analysed using FlowJo software (version 10, FlowJo).

**Table 3.3.** List of FACS conjugated antibodies and dilutions employed for flow cytometry analysis of mouse liver nonparenchymal cells.

| FACS Conjugated Antibody (Fluorochrome-Cell marker) | Dilution Factor |
|---|---|
| eF506-FVD | 1:100 |
| PECy7-CD3 | 1:100 |
| APC-CD4 | 1:300 |
| PerCPCy5.5-CD8 | 1:300 |
| APCCy7-NK1.1 | 1:500 |
| PE-TCRγδ | 1:200 |
| BV785-MHC II | 1:200 |
| BV711-CD11c | 1:200 |
| AF700-CD11b | 1:200 |
| Pacific Blue-Ly6G | 1:200 |
| BV605-Ly6C | 1:400 |
| AF488-CD8 | 1:400 |

## 3.17. Immunohistochemical staining of liver slices

Paraformaldehyde-fixed livers were embedded in paraffin and cut into 10 µm-thick slices using a Microtome Leica RM2245. Liver slices were prepared for immunohistochemistry staining using heat-induced antigen retrieval in citrate buffer, pH 6.0 at 95°C for 20 min in Dako PT Link equipment. Endogenous peroxidase activity was blocked with 3% hydrogen peroxyde ($H_2O_2$) diluted in methanol for 30 min at RT. Liver slices were then washed 3 times for 5 min with 1× PBS and

blocked with Dako Protein Block for 40 min at RT. Primary and secondary antibodies were diluted in antibody diluent. Viperin was detected using a monoclonal mouse anti-Viperin (Merck Millipore) at 1:300 dilution. After incubation at RT for 1h in a humid box, the slides were washed three times with 1× PBS. Liver slices were then incubated with Dako EnVision horseradish peroxidase (HRP) conjugated with anti-mouse secondary antibody for 30 min at RT. After washing the slides with 1× PBS, 3,3'-diaminobenzidine (DAB) was added to the slices for 5 min, resulting in a brown-coloured precipitate at the antigen site. Following counterstaining with Harris Haematoxylin, slides were cleared and mounted using Fluoromount G (SoutherBiotech). Whole slide images were obtained using a NanoZoomer SQ (Hamamatsu). This work was performed by the Histology and Comparative Pathology Laboratory of the Instituto de Medicina Molecular.

## 3.18. Immunofluorescence staining of liver slices

Paraformaldehyde-fixed livers were paraffin-embedded and cut into 10 µm-thick slices using a Microtome Leica RM2245. This work was performed by the Histology and Comparative Pathology Laboratory of the Instituto de Medicina Molecular. Liver slices were prepared for immunofluorescence staining using heat-induced antigen retrieval in citrate buffer, pH 6.0 at 95°C for 20 minutes in Dako PT Link equipment. Tissue autofluorescence was quenched by treatment with 3% $H_2O_2$ diluted in methanol for 30 min at RT. Liver slices were then washed 3 times for 5 min with 1× PBS and blocked with Dako Protein Block for 40 min at RT. Primary and secondary antibodies, as well as the Hoechst were diluted in Dako antibody diluent. Parasites were stained with a goat anti-UIS4 antibody (dilution 1:300, Sicgen). Viperin was detected using a monoclonal mouse anti-Viperin (Merck Millipore) at 1:300 dilution. After incubation at RT for 1h in a humid box, the slides were washed three times with 1× PBS. Liver slices were then incubated for 1h in 1:300 dilution of anti-goat Alexa Fluor 488 (Donkey IgG) and anti-mouse Alexa Fluor 568 (Donkey IgG) (Jackson ImmunoResearch Laboratories) secondary antibodies, as well as with Hoechst 33342 (Invitrogen) in a dilution of 1:1000 for nuclei staining. The slides were then mounted with Fluoromount G (SouthernBiotech). Confocal images were acquired using a Zeiss LSM 710 confocal microscope.

## 3.19. Statistical analysis

Data are expressed as mean ± standard deviation (SD). Statistically significant differences between two different groups were analysed using the Mann-Whitney test. *P*-values less than 0.05 were considered significant. Significances are represented in the figures as follows: ns - not significant, $*P < 0.05$, $**P < 0.01$, $***P < 0.001$ and $****P < 0.0001$. Correlation analyses were performed using Spearman's correlation analysis, in which Spearman correlation coefficients (*R*) greater than 0.6 was considered a strong correlation. All statistic tests were performed using Graph Pad Prism 7 software.

# 4. Results and Discussion

## 4.1. Characterization of interferon-mediated responses elicited by *Plasmodium* infection

Innate immune responses mediated by both type I and type II IFNs were recently found to play a central role in controlling *Plasmodium* liver stage infection[41,42]. In fact, although type I and type II IFNs may exhibit distinct roles in the immune mechanisms elicited by the insulted host, the potential crosstalk between these cytokines may trigger similar cellular responses and result in the transcriptional induction of the same genes[61].

As proposed by Liehl *et al.* (2014), *Plasmodium* RNA is recognized by the cytosolic receptor MDA5, which, through the adaptor molecule MAVS and the transcription factors IRF3 and IRF7, leads to the induction of type I IFNs[41]. IFN-α and IFN-β are then the key cytokines responsible for the propagation of the signaling cascade that characterizes the type I IFN response[35]. Interestingly, the pro-inflammatory cytokine IFN-γ, known to kill liver stage parasites *in vitro* via yet unknown mechanisms[113], was also identified as an important regulator of the innate immune response triggered by *Plasmodium* liver infection[42]. This suggests that an orchestrated response encompassing both type I and type II IFNs may be regulating the response elicited by *Plasmodium* infection.

Therefore, we started by characterizing the kinetics of both type I and type II IFNs, and the potential crosstalk between them, during *Plasmodium* liver infection by performing a time course analysis. To this end, 6-12 weeks-old C57BL/6J mice were infected with 30,000 *P. berghei* sporozoites (spz) and euthanized at specific times post-infection (hpi; 42 hr, 48 hr, 60 hr, 72 hr, 84 hr and 96 hpi) to include the mid liver stage of parasite development, as well as later time points after merozoite egress from infected hepatocytes and the initiation of erythrocytic replication[3].

Quantitative real-time PCR data revealed that both IFN-α and IFN-β were upregulated upon *Plasmodium* infection when compared with non-infected control mice. These results are in accordance with the notion that *Plasmodium* specifically induces a type I IFN response during the liver stage of infection which is detectable in whole-liver extracts even when mice are infected by a physiologically relevant route of infection, mosquito bite[41]. Furthermore, IFN-α and IFN-β mRNA expression exhibit identical kinetics and magnitudes of induction with the first statistically significant peak already appearing at 42 hpi (1.619±0.555 and 1.573±0.595 fold induction for IFN-α and IFN-β, respectively), before the exit of the parasites to the bloodstream, after which continues to increase in an exponential manner. Within the temporal window of our experiment, the maximal induction of the type I IFNs occurred at 96 hpi (14.890±14.110 and 16.350±16.410 fold induction for IFN-α and IFN-β, respectively; Fig.4.1. A and B).

The time course analysis also revealed that, contrarily to what was observed with type I IFNs, IFN-γ begins to be induced at a later time point, specifically at 60 hpi (1.495±0.403 fold induction), after or concurrent with the egress of the merozoites into the bloodstream[3]. Following a steadily increase in the levels of mRNA expression, the peak of IFN-γ expression occurs at 84 hpi (4.127±1.464 fold induction), after which it declines (Fig. 4.1. C). When comparing our results to those

of Liehl *et al.* (2015)[43], it should be noted that, although the profile of IFN-γ expression is identical in the two studies, the magnitudes of induction are different and the maximum peak occurs at different times post-infection. IFN-γ expression peaking at around 68-72 hpi could be explained by the difference in the number of *P. berghei* spz injected. While Liehl and colleagues employed 50,000 spz, our experimental setup was performed with 30,000 spz, which could explain the relative delay in the peak of IFN-γ expression.

These results reveal a temporal difference in the kinetic profile of the two types of IFNs, with the liver stage parasites initially triggering the type I IFN pathway and simultaneously stimulating IFN-γ expression at later time points. This overlapping expression may hint the existence of pleiotropy and crosstalk between these two types of cytokines and the potential intervention in sequentially occurring events[61], as initially hypothesized.

After binding to their specific receptors, type I and type II IFNs initiate distinct, albeit similar, signaling cascades that culminate in the expression of several ISGs[35]. In order to characterize the activation of interferon-mediated responses, the measurement of mRNA expression levels of six ISGs (*Ifit-1, Ifi44, Usp18, Ifit3*, *Irf7* and *Viperin*) were used as a readout for the type I IFN pathway activation[41]. Our time course results demonstrated that the mRNA levels of these ISGs present two waves of induction, which coincide with different phases of the parasite's life cycle (Fig.4.1. D). The first statistically significant peak occurs at 42 hpi (1.975±0.686 fold induction of the averaged genes), while parasites are still in the phase of intense asexual replication in the liver[3]. Interestingly, ISG induction starts to increase further after parasites have exited the liver, up to an averaged ~36-fold peak at 84 hpi. A similar pattern of results was obtained by Liehl *et al.* (2015)[43], although the higher peak of induction was reported to occur at 72 hpi and started to decline already at 82 hpi. This disparity can again potentially be explained by the difference in the number of sporozoites injected, which could explain the delay in the response and is in agreement with what we observed for the IFN-γ expression profile.

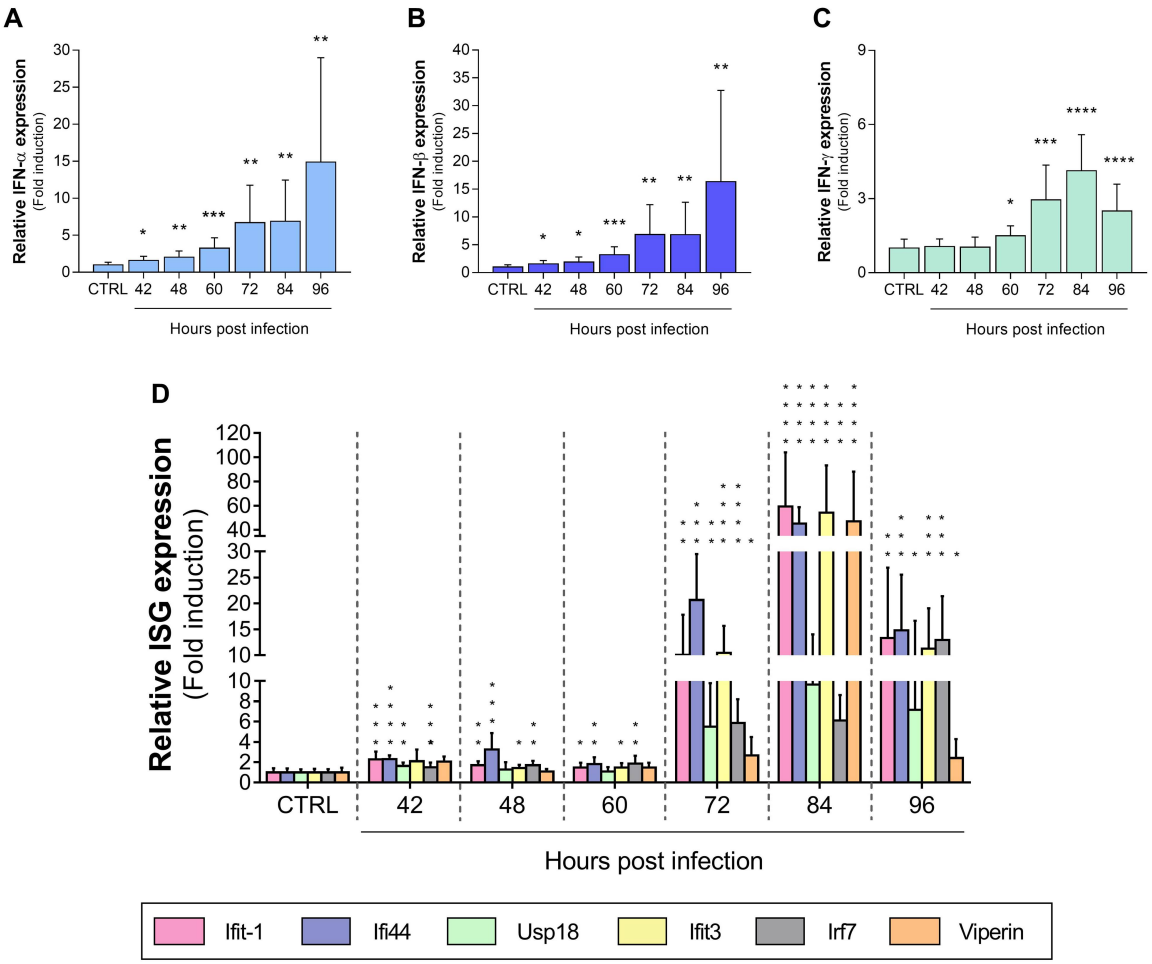


**Figure 4.1. *Plasmodium* liver stage parasites induce an innate response mediated by the type I IFNs, IFN-α and IFN-β, as well as the type II IFN, IFN-γ, which culminates in the induction of interferon-stimulated genes.** IFN-α **(A)**, IFN-β **(B)** and IFN-γ **(C)** expression in whole liver extracts of C57BL/6J WT mice infected with $3\times10^4$ *P. berghei* ANKA spz and euthanized at the indicated times post-infection. **(D)** Expression of the ISGs *Ifit-1*, *Ifi44*, *Usp18*, *Ifit3*, *Irf7* and *Viperin* in whole liver extracts of WT mice at multiple times post *P. berghei* spz injection. The relative expression of each gene was analysed through qRT-PCR. Non-infected WT mice were used as controls. For each time point, data are expressed as means ± SD of the results of two independent experiments (CTRL, *n* = 10; 42 h, *n* = 6; 48 h, *n* = 6; 60 h, *n* = 6; 72 h, *n* = 6; 84 h, *n* = 6; 96 h, *n* = 6). Complete statistics are present in Appendices, Supplementary Table 1.

## 4.2. Unveiling the cellular mediators of the interferon-stimulated responses

Once in the liver, *Plasmodium* parasites induce an ISG response that is not able to directly and completely kill or at least mediate the elimination of the hepatic parasites[41]. However, hepatocytes are responsible for the propagation of this type I IFN response which, acting paracrinally, leads to the activation of liver-resident immune cells and/or recruitment of infiltrating leukocytes that also exhibit a type I IFN signature[41,42]. These leukocytes further target the infected hepatocytes and mediate the elimination of *Plasmodium* parasites, likely through the production of IFN-γ[42].

The ISG response during *Plasmodium* infection is characterized by two expression peaks with quite different magnitudes (Fig.4.2. J). The first ~2-fold induction peak occurs at 42 hpi and it is thought to be primarily mediated by hepatocytes and to be responsible for the activation and/ or recruitment of effector leukocytes to the vicinity of parasitized hepatocytes. However, at 84 hpi, after

parasites have already exited the liver[3], a striking ~36-fold induction peak takes place whose functional consequence was only assessed through a reinfection model[42,43]. Not only is the liver an organ composed by a plethora of lymphocytic populations[114] as it is long-time known that recruited immune cells start to infiltrate the liver between 40 and 72 hpi with rodent-infective *Plasmodium* parasites[32,33]. Given the kinetic and magnitude profiles of the ISG response studied (Fig.4.2. J), it is conceivable to envisage that the ISG response may be differently mediated at the two relevant time points and have different functional consequences.

Thus, we sought to identify the cellular mediators of the ISG response during *Plasmodium* liver infection and, subsequently, to gain further insights into the potential effectors of biologically relevant events. To this end, we started by characterizing the interferon-mediated responses throughout infection using the same experimental setup as described above in mice knockout for certain populations of leukocytes so we could establish a link between the type I IFN signature observed and a corresponding cell type.

Our first approach was to target all lymphoid cells by using a completely alymphoid mouse strain deficient in both RAG-2 and the γ chain ($RAG2^{-/-}/\gamma c^{-/-}$). $RAG2^{-/-}/\gamma c^{-/-}$ mice were generated by crossing the RAG-2 mutant ($RAG\text{-}2^{-/-}$) with the $\gamma c^{-/-}$ mouse model. The former was generated through the targeted deletion of the RAG-2 gene, whereas the latter was generated by targeting the common cytokine receptor γ chain for interleukin-2 (IL-2), IL-4, IL-9 and IL-15[115]. Since these cytokines are important regulators of the activities of lymphocytes, the $RAG2^{-/-}/\gamma c^{-/-}$ mouse model reveals a complete absence of T cells (including αβ and γδ T cells as well as NKT cells), B cells and innate lymphoid cells (ILCs)[115].

Quantitative RT-PCR analysis revealed that, in contrast with WT mice (Fig.4.2. A, D and G), $RAG2^{-/-}/\gamma c^{-/-}$ mice failed to upregulate any of the assessed interferons at any time point upon *Plasmodium* infection (Fig.4.2. B, E and H). This result was not unexpected since lymphocytes, which are chronically absent in the mouse model in study, are also responsible for the production of IFNs[35].

On the other hand, in an environment of complete IFN absence, one would expect to observe a similar pattern of ISG response. However, the 2-fold peak at 42 hpi observed in WT mice was maintained in the knockout mice (3.407±2.315 fold induction; Fig.4.2. K). Likewise, the induction of ISGs at 48, 60 and 72 hpi also reached statistical significance and, except for the 72 hpi time point (1.857±0.713 at 42 hpi; 1.635±0.708 at 60 hpi; 2.611±1.480 at 72 hpi), the fold induction was identical to that observed in WT mice (1.752±1.025 at 42 hpi; 1.527±0.584 at 60 hpi; 8.878±7.582 at 72 hpi).

In the same line of thought, the complete absence of ISG induction at 84 hpi (Fig.4.2. K) suggests that lymphoid cells are the major mediators/ contributors for the establishment of a highly-induced interferon-like response at this time point.

Since $RAG2^{-/-}/\gamma c^{-/-}$ mice lack the whole class of lymphoid cells, we chose to perform the same experiment on another knockout mouse model, the $RAG\text{-}2^{-/-}$ model, in order to narrow down the range of cell types that might be responsible for the 84 hpi ISG peak of induction. Mouse mutants for the RAG-2 gene fail to generate mature B and T lymphocytes (including NKT) owing to a complete inability to initiate the V(D)J recombination process[116], but have increased levels of NK cell activity[117].

Similarly to what we observed in RAG2$^{-/-}$/γc$^{-/-}$ mice (Fig.4.2. B and E), the induction of the type I IFN response mediators, IFN-α and IFN-β, was not detectable in the whole liver extracts of RAG-2$^{-/-}$ mice infected with *P. berghei* spz (Fig.4.2. C and F). Once again, this result can be explained by the absence of both B and T cells, which, like most cells, are able to produce type I IFNs[35].

In contrast, the time course analysis revealed a profile of IFN-γ induction (Fig.4.2. I) similar to that observed in WT mice (Fig.4.2. G), with the difference that the maximum peak of induction occurred at 72 hpi instead of 84 hpi, as observed in WT mice. The major cell types responsible for the production of the type II IFN are lymphocytes, particularly T cells and NK cells[35]. Thus, although RAG-2$^{-/-}$ mice are deficient in T cells, the liver-resident or recruited NK cells could compensate the chronic absence of IFNγ-producing T cells and even being recruited earlier upon *Plasmodium* infection to compensate for the absence of T lymphocytes.

The analysis of ISG expression throughout infection of RAG-2$^{-/-}$ mice indicates that at 42 hpi the ISGs are induced ~2-fold when compared with naive RAG-2$^{-/-}$ mice (Fig.4.2. L). This result strengthens the conclusion drawn from the analysis performed with RAG2$^{-/-}$/γc$^{-/-}$ mice (Fig.4.2. K), the 42 hpi peak of ISG induction is independent of cells from the immune system. Moreover, although the magnitude of induction is significantly lower when compared with the WT mice (*p*-value < 0.0001; Fig.4.2. J), the ISGs are still 10-fold induced at 84 hpi. This reinforces the aforementioned hypothesis that the 84 hpi peak may be a result of the crosstalk between the type I IFNs, which are not upregulated, and the type II IFN which presents an induction comparable to that of WT mice (6.523±1.903 for RAG-2$^{-/-}$ and 4.127±1.464 for WT mice at 72 hpi).

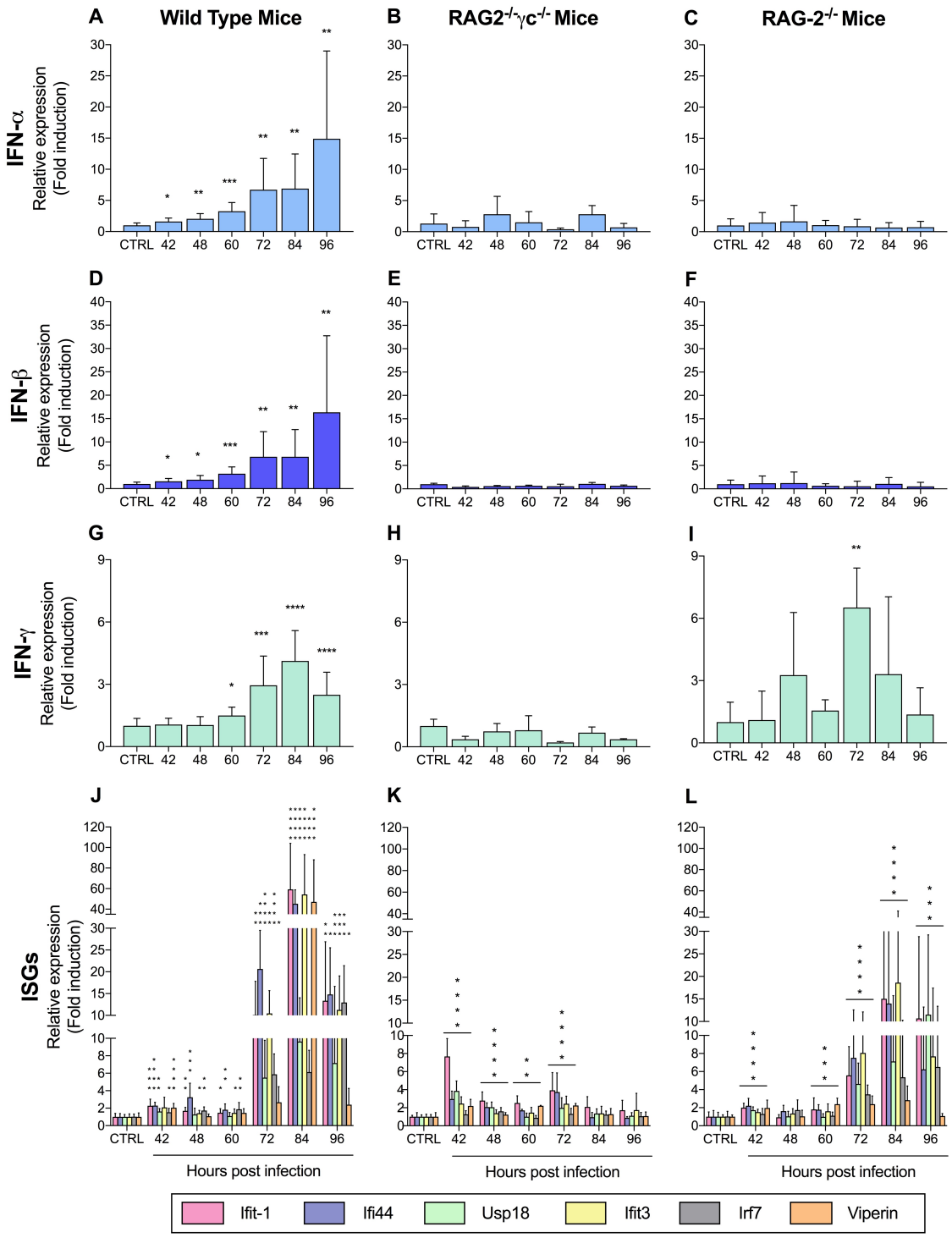


**Figure 4.2. *Plasmodium* liver stage parasites induce an interferon-mediated innate response whose signature depends on both hepatocytes and immune cells of the lymphoid lineage. (A-L)** WT C57BL/6J, RAG2$^{-/-}$/γc$^{-/-}$ and RAG-2$^{-/-}$ mice were infected with 3×10$^4$ *P. berghei* ANKA spz and euthanized at the indicated times post-infection. IFN-α, IFN-β and IFN-γ mRNA expression in whole liver extracts of WT C57BL/6J **(A, D, G)**, RAG2$^{-/-}$/γc$^{-/-}$ **(B, E, H)** and RAG2$^{-/-}$ mice **(C, F, I).** Expression of the ISGs *Ifit-1*, *Ifi44*, *Usp18*, *Ifit3*, *Irf7* and *Viperin* in whole live extracts of WT **(J)**, RAG2$^{-/-}$/γc$^{-/-}$ **(K)** and RAG2$^{-/-}$ mice **(L)** at multiple times post *P. berghei* spz injection. The relative expression of each gene was analysed through qRT-PCR. Non-infected mice were used as controls. For each time point, data are expressed as means ± SD of the results of two independent experiments for the WT (CTRL, *n* = 10; 42 h, *n* = 6; 48 h, *n* = 6; 60 h, *n* = 6; 72 h, *n* = 6; 84 h, *n* = 6; 96 h, *n* = 6) and RAG-2$^{-/-}$ mice (CTRL, *n* = 6; 42 h, *n* = 6; 48 h, *n* = 6; 60 h, *n* = 6; 72 h, *n* = 6; 84 h, *n* = 6; 96 h, *n* = 6) and one experiment for RAG2$^{-/-}$/γc$^{-/-}$ mice (CTRL, *n* = 4; 42 h, *n* = 3; 48 h, *n* = 3; 60 h, *n* = 2; 72 h, *n* = 3; 84 h, *n* = 3; 96 h, *n* = 3). *P*-values of the average of fold inductions of all ISGs for each time point are shown. Complete statistics are present in Appendices, Supplementary Table 1.

Overall, these results show that the absence of lymphoid cells does not appear to impact the induction of ISGs at 42 hpi in both knockout mouse models employed. Nevertheless, the ~36-fold induction of the interferon-related genes at 84 hpi in WT mice is absent in RAG2$^{-/-}$/γc$^{-/-}$ mice and is strongly reduced in RAG-2$^{-/-}$ (36.570±35.200 for WT mice, 1.386±0.694 for RAG2$^{-/-}$/γc$^{-/-}$ mice and 10.490±14.760 for RAG-2$^{-/-}$ mice), suggesting an involvement of lymphoid cells in this phase of the response. The difference in the induction of the response between the two knockout mice can only be attributable to NK cells and ILCs since the remaining lymphocytes (B and T cells) are commonly absent in both mouse models. On the other hand, given that ISG induction is partially lost in RAG-2$^{-/-}$ mice, one cannot exclude the possibility of a pool of lymphoid cells contributing to the highly induced peak.

Unlike the RAG2$^{-/-}$/γc$^{-/-}$ model, RAG-2$^{-/-}$ mice exhibit normal population numbers of NK cells and ILCs, which can be implicated in the 84 hpi ISG phenotype observed (Fig.4.2. J, K and L). Thus, in order to pinpoint the cell type responsible for the type I IFN signature observed in WT mice, we sought to target the NK cell population. To this end, 6-8 weeks-old WT mice of the C57BL/6J genetic background were injected with the neutralizing antibody, TM-beta 1. The TM-beta 1 monoclonal antibody recognizes the murine IL-2 receptor (IL-2R) beta chain, which is constitutively expressed on a subpopulation of CD8$^{+}$ T cells and NK cells[118]. The high affinity binding of IL-2 to the IL-2R is inhibited by TM-beta 1 abolishing the generation and differentiation of T lymphocytes and NK cells[118]. Two hours prior the injection of the antibody, each mouse was infected with 30,000 *P. berghei* spz and the same time course experiment previously described was performed. At each time point (except at 96 hpi), the depletion of the NK cell population (including NK and NKT cells) was assessed by flow cytometry analysis (See Appendices, Supplementary Fig.1 and Table 2).

To determine whether the absence of the NK cell population would alter the pattern of IFN-α and IFN-β mRNA expression observed in WT mice (Fig.4.1. A and B), we measured the expression levels of these IFNs in whole liver extracts by qRT-PCR. The depletion of NK and NKT cells resulted in low levels of type I IFNs expression throughout the infection with only one peak of induction at 72 hpi (2.268±0.475 for IFN-α and 2.594±0.619 for IFN-β; Fig.4.3. A and B). Although this peak did not reach statistical significance, the ~3-fold induction observed suggests that it may result from a type I IFN-producing cell population that was acutely activated or recruited at that specific time point.

In addition to their cytotoxic activity, NK cells are one of the major cell populations implicated in the production of IFN-γ[119]. Despite this, in NK-depleted mice, IFN-γ expression exhibits a kinetic profile similar to that observed in WT mice (Fig.4.3. C). Type II IFN expression starts to increase while parasites are still in the pre-erythrocytic stage of development, until it reaches a 2.7-fold peak at 48 hpi. At 60 hpi, when parasites are egressing from the liver into the bloodstream, there is a reduction of IFN-γ expression to values similar to those of non-infected controls (1.272±1.646). When parasites have already initiated the erythrocytic stage of infection, a new peak is detectable in mice euthanized at 72 hpi (14.200±10.250), after which type II IFN expression decreases. As observed in RAG-2$^{-/-}$ mice, the higher induction peak occurred at a time point sooner than the peak observed in WT mice. Additionally, the peak observed at 72 hpi was approximately 5 times higher in magnitude than that observed in WT mice. These two striking differences can result from compensatory mechanisms

exerted by T lymphocytes. With the host defence being compromised by the depletion of one of the effectors involved in the innate reduction of liver stage parasites[42], it is not unlikely that the host compensates this defect with the remaining IFNγ-producing cells.

When measuring mRNA expression levels for the panel of ISGs previously mentioned, the kinetic profile observed is identical to that of WT mice. The first statistically significant peak of ISG induction occurs at 42 hpi (2.614±1.252) followed by a highly induced peak at 84 hpi (51.470±38.370; Fig.4.3. D). When comparing the magnitudes of the inductions in WT mice (1.975±0.686 at 42 hpi and 36.570±35.200 at 84 hpi), it is clear that there is a slightly higher induction of the ISGs at both time points in NK-depleted mice (2.614±1.252 at 42 hpi and 51.470±38.370 at 84 hpi), which, again, may result from compensation mechanisms exerted by the host in the absence of NK cells, or may be a consequence of the low numbers of mice employed in this experiment.

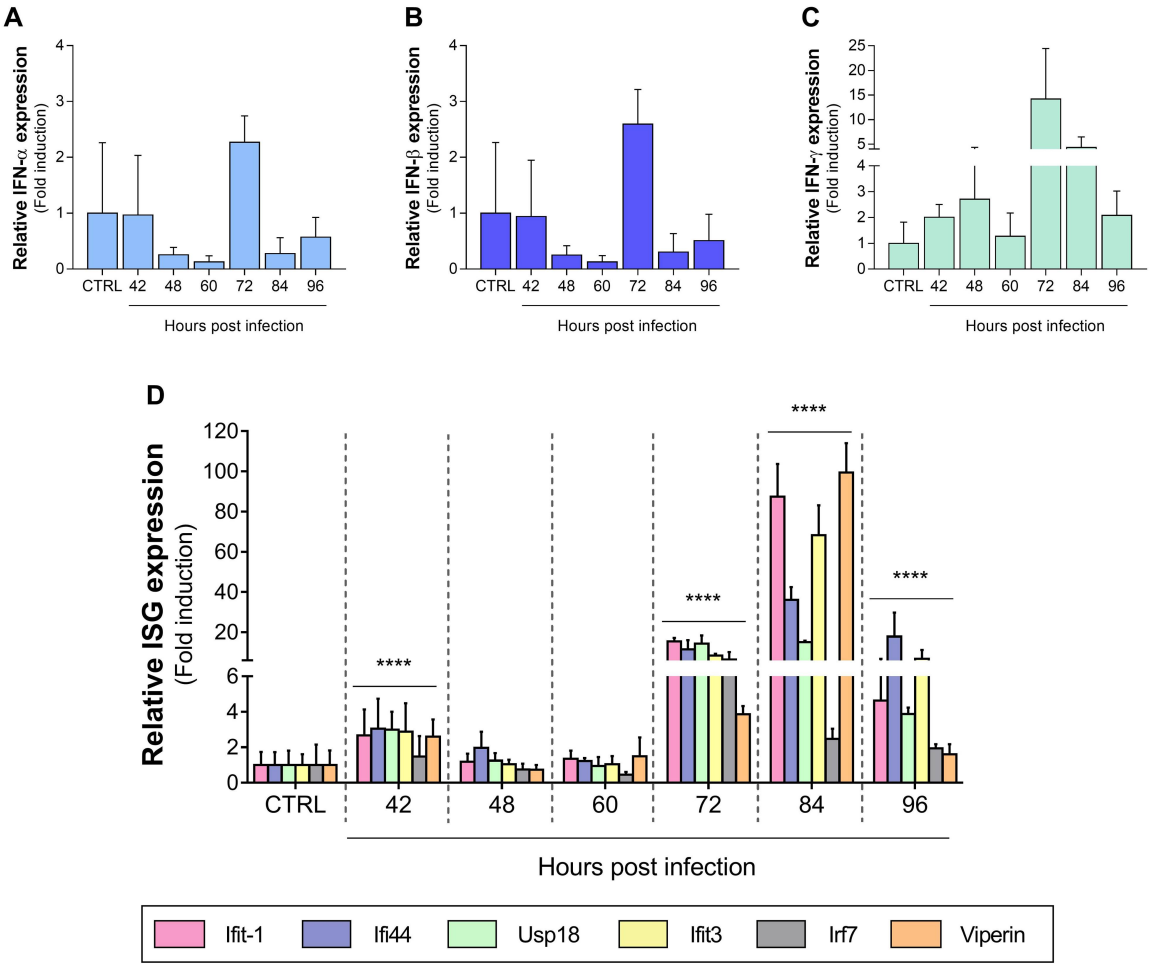


**Figure 4.3. Characterization of the interferon-mediated innate response elicited by *Plasmodium* liver stage parasites in mice depleted in the natural killer cell population.** IFN-α **(A)**, IFN-β **(B)** and IFN-γ **(C)** expression in whole liver extracts of NK-depleted mice infected with $3\times10^4$ *P. berghei* ANKA spz and euthanized at the indicated times post-infection. **(D)** Expression of the ISGs *Ifit-1*, *Ifi44*, *Usp18*, *Ifit3*, *Irf7* and *Viperin* in whole liver extracts of NK-depleted mice at multiple times post *P. berghei* spz injection. The relative expression of each gene was analysed through qRT-PCR. Non-infected NK-depleted mice were used as controls. For each time point, data are expressed as means ± SD (CTRL, *n* = 3; 42 h, *n* = 3; 48 h, *n* = 3; 60 h, *n* = 3; 72 h, *n* = 3; 84 h, *n* = 3; 96 h, *n* = 3). *P*-values of the average of fold inductions of all ISGs for each time point are shown. Complete statistics are present in Appendices, Supplementary Table 1.

Having excluded the NK cell population, the results above described suggest that a novel cell population, the ILCs, may be the major contributors to the type I IFN signature observed at 84 hpi in the whole liver extracts of *Plasmodium*-infected mice. Therefore, our results cast a new light on a previously unstudied cell population which may be implicated in the reduction of the liver stage burden of a secondary infection through yet unknown mechanisms.

## 4.3. Viperin: an ISG that stands out from the crowd

When analysing the profile of ISG mRNA expression in WT, RAG2$^{-/-}$/γc$^{-/-}$ and RAG-2$^{-/-}$ mice, we identified a gene with a different signature from that of the remaining ISGs, Viperin.

In WT mice infected with *P. berghei* sporozoites, Viperin mRNA expression follows a pattern similar to that of the other ISGs, with 2-fold and 47-fold induction peaks at 42 and 84 hpi, respectively (Fig.4.4. A). However, a slight different pattern of expression is observed when we focus on the 84 hpi peak. We observe that, while the expression of the other ISGs progressively increases from the 72 hpi (8.878±7.582) until they peak at 84 hpi (36.570±35.200) and continue to progressively decrease (9.911±0.418 at 96 hpi), Viperin presents a more acute peak of induction (2.668±1.804 at 72 hpi; 47.140±40.980 at 84 hpi and 2.408±1.864 at 96 hpi). The different behaviour of Viperin upregulation in comparison with the other group of ISGs suggest a possible involvement of another cell type in Viperin expression and, potentially, a unique role for this ISG. A comprehensive analysis of the immune cells that are activated and/or recruited to the liver throughout *Plasmodium* infection would potentially allow the identification of a cell population acutely recruited at this time point and that could be involved in Viperin production.

In RAG2$^{-/-}$/γc$^{-/-}$ mice, where we observed the presence of the 42 hpi peak and the absence of the 84 hpi ISG peak (Fig.4.2. K), Viperin also follows the same pattern (Fig.4.4. B). Conversely, while the other ISGs are 10-fold induced at 84 hpi in RAG-2$^{-/-}$ mice (Fig.4.2. L), Viperin was less upregulated presenting only an approximate 3-fold induction, similarly to what happens at 42 hpi (Fig.4.4. C).

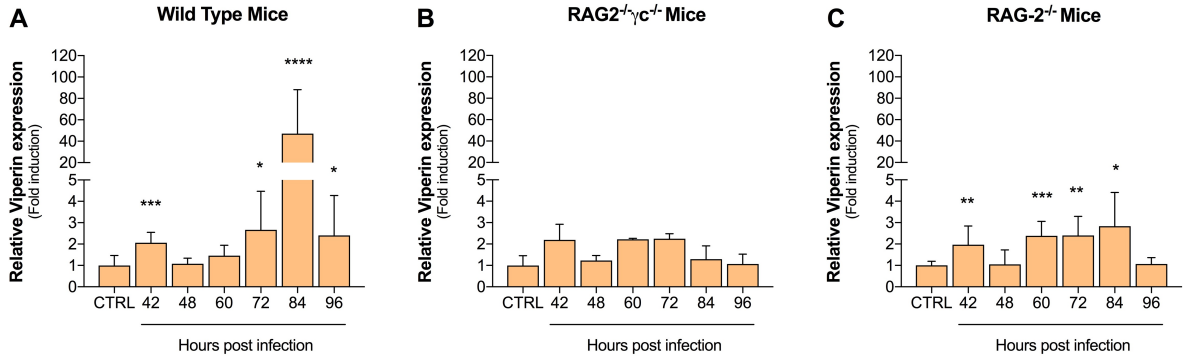


**Figure 4.4. Viperin mRNA follows a different pattern of expression in wild type mice and mice knockout for lymphoid cells.** Viperin mRNA expression in whole liver extracts of C57BL/6J WT **(A)**, RAG2$^{-/-}$/γc$^{-/-}$ **(B)** and RAG-2$^{-/-}$ **(C)** mice infected with 3×10$^4$ *P. berghei* ANKA spz and euthanized at the indicated times post-infection. The relative Viperin expression was analysed through qRT-PCR. Non-infected mice were used as controls. For each time point, data are expressed as means ± SD of the results of two independent experiments for the WT (CTRL, *n* = 10; 42 h, *n* = 6; 48 h, *n* = 6; 60 h, *n* = 6; 72 h, *n* = 6; 84 h, *n* = 6; 96 h, *n* = 6) and RAG-2$^{-/-}$ mice

(CTRL, *n* = 6; 42 h, *n* = 6; 48 h, *n* = 6; 60 h, *n* = 6; 72 h, *n* = 6; 84 h, *n* = 6; 96 h, *n* = 6) and one experiment for RAG2$^{-/-}$/γc$^{-/-}$ mice (CTRL, *n* = 4; 42 h, *n* = 3; 48 h, *n* = 3; 60 h, *n* = 2; 72 h, *n* = 3; 84 h, *n* = 3; 96 h, *n* = 3). Complete statistics are present in Appendices, Supplementary Table 1.

These results prompted us to focus on this ISG attempting to unravel its potential role in the context of the type I IFN response elicited by the liver stage of *Plasmodium* infection, as well as to identify the subset of immune cells responsible for its production at 84 hpi.

### 4.3.1. Role of Viperin during *Plasmodium*-liver stage infection

The immune system of the vertebrate host is equipped to deal with the liver-invading *Plasmodium* sporozoites by recognizing them and eliciting a robust innate immune response capable of controlling the liver stage burden and reducing the number of merozoites that bud off from hepatocytes[41,42]. As previously mentioned, during the first obligatory phase of the parasite's life cycle, *Plasmodium* triggers an interferon-mediated immune response, which is characterized by a specific profile of ISG induction (Fig.4.1. D). Indeed, during viral infections, several genes are upregulated in the context of the interferon-induced antiviral state that act as direct effectors of the response, with different ISGs targeting different viruses[41]. However, to the best of our knowledge, no specific ISG has been studied and characterized in the context of malaria infections.

Viperin is an ISG with a broad spectrum of vastly explored antiviral functions[85]. Thus, it is equally plausible that Viperin may also play a role in parasitic infections. Interestingly, genome-wide microarray studies developed by the host laboratory aiming at identifying *Plasmodium* infection-mediated transcriptional changes, pinpointed Viperin as one of the most highly transcriptionally induced genes in the context of the interferon-mediated immune responses elicited.

Although being preferentially stimulated by type I IFNs in a variety of cell types[80], IFN-γ is also able to induce Viperin expression[72,80]. In fact, Chin and Cresswell have suggested that the transcriptional induction of Viperin via IFN-γ could depend on the signaling pathway that is activated or on the accessibility of regulatory elements in the gene promoter[72]. Intriguingly, the profile of Viperin expression in WT mice infected with *P. berghei* sporozoites seems to better illustrate the kinetics of IFN-γ stimulation rather than the type I IFNs (Fig.4.1. C and 4.4. A). However, one cannot exclude the involvement of IFN-α and IFN-β, the existence of cooperation between the two types of cytokines in yielding the upregulation of Viperin, or even the contribution of different types of IFNs in different stages of the parasite's life cycle.

Therefore, we aimed at exploring the unknown role of Viperin by indirectly assessing the impact of Viperin induction on *Plasmodium* liver infection.

To address whether an absence of Viperin would affect *Plasmodium* liver infection, we infected WT (*Viperin*$^{+/+}$) mice, which were used as littermate controls, heterozygous *Viperin*$^{+/-}$ mice, and homozygous *Viperin*$^{-/-}$ mice with 30,000 luciferase-expressing *P. berghei* sporozoites. These mice show a dose-dependent decrease in Viperin mRNA expression by qRT-PCR (See Appendices, Supplementary Fig.2). The assessment of the liver infection load at 42 hpi by *in vivo* imaging of bioluminescent parasites revealed that the liver burden was inversely proportional to Viperin

expression in the mice. While WT mice exhibited a liver infection load correspondent to $1.10 \times 10^6 \pm 1.58 \times 10^5$ p/s/cm$^2$/sr, the hepatic burden of *Viperin*$^{-/-}$ mice was increased by approximately 2-fold ($2.29 \times 10^6 \pm 4.98 \times 10^5$ p/s/cm$^2$/sr; Fig.4.5. A and B). The presence of half of Viperin mRNA expression in *Viperin*$^{+/-}$ mice relative to the WT controls was proportionally reflected in the liver infection load they displayed, with an approximate increase of 1.6-fold ($1.84 \times 10^6 \pm 1.96 \times 10^5$ p/s/cm$^2$/sr; Fig. 4.5. A and B). Our findings on the impact of the absence of Viperin on the liver infection load of *P. berghei*-infected mice indicate that Viperin has an *in vivo* biological significance and can have a critical role in controlling *Plasmodium* infection.

Since Viperin upregulation is detectable in the whole liver extracts of *P. berghei*-infected mice, we next investigated which cell types in the liver are required for the induction of Viperin. As previously hypothesized and partially confirmed by the time course analysis with RAG2$^{-/-}$/γc$^{-/-}$ and RAG-2$^{-/-}$ mice, it is likely that the ISGs' induction at 42 hpi is mainly mediated by the hepatocyte. In order to further investigate this hypothesis, WT C57BL/6J mice were subjected to 900 rads irradiation in order to eliminate all cells of haematopoietic origin, infected with *P. berghei* sporozoites and euthanized at 42 hpi. Quantitative RT-PCR analysis of the whole liver extracts revealed no reduction in the induction of Viperin compared to the WT mice (0.853±0.353 fold reduction; Fig.4.5. C), which suggests that hepatocytes are the primary source of Viperin expression.

Moreover, to confirm that, at 42 hpi, Viperin is induced through the activation of a *Plasmodium*-elicited type I IFN response, mice lacking the IFNAR subunit IFNAR1 (*Ifnar1*$^{-/-}$) were infected with *P. berghei* sporozoites, euthanized at 42 hpi and Viperin expression was assessed through qRT-PCR of whole liver extracts. *Ifnar1*$^{-/-}$ mice, which are unable to respond to the type I IFNs due to the lack of the receptor subunit IFNAR1, showed a ~4-fold reduction in Viperin mRNA expression compared to the infected WT mice, confirming that the activation of Viperin expression is mediated by the type I IFN response at this time point (Fig.4.5. D).

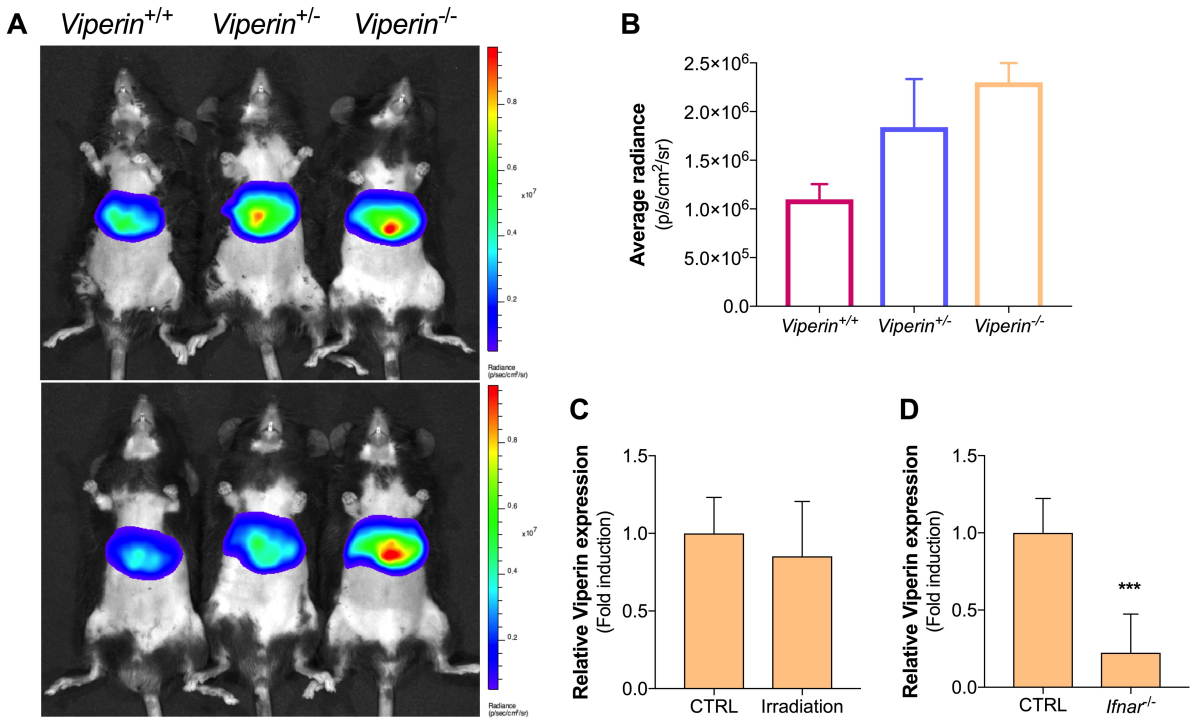


**Figure 4.5. Interferon-stimulated Viperin is required for *in vivo* host defence controlling *Plasmodium berghei* liver infection load. (A)** Rainbow images of luminescence in livers of WT *Viperin*$^{+/+}$, heterozygous *Viperin*$^{+/-}$ and homozygous *Viperin*$^{-/-}$ mice 42 hours after infection with $3\times10^4$ luciferase-expressing *P. berghei* spz. Rainbow scales are expressed in radiance (p/s/cm$^2$/sr). **(B)** Quantification of bioluminescent signal in average radiance (p/s/cm$^2$/sr) at 42 hpi (*n* = 2 per condition). **(C)** Relative Viperin mRNA expression in whole liver extracts of C57BL/6J WT mice irradiated with 900 rads (CTRL, *n* = 10; Irradiation, *n* = 8) **(C)** and *Ifnar1*$^{-/-}$ mice (CTRL, *n* = 8; *Ifnar1*$^{-/-}$, *n* = 8) **(D)** infected with $3\times10^4$ *P. berghei* ANKA sporozoites and euthanized at 42 hpi. The relative Viperin expression was analysed through qRT-PCR. Infected C57BL/6J mice were used as controls. Data are expressed as means ± SD. Complete statistics are present in Appendices, Supplementary Table 1.

We further characterized the Viperin protein localization in the livers of *P. berghei*-infected C57BL/6J mice by immunohistochemical (IHC) analysis in order to provide an insight into how Viperin inhibits *Plasmodium* replication. As shown in Fig.4.6. A and B, IHC analysis revealed foci containing Viperin throughout the liver, whose number and intensity is elevated in the *P. berghei*-infected mouse euthanized at 42 hpi (Fig.4.6. B) compared with the non-infected mouse (Fig.4.6. A). The increase in number and signal intensity of the Viperin protein in the *P. berghei*-infected WT mouse compared with non-infected mouse is in accordance with what is observed regarding the levels of Viperin mRNA expression assessed by qRT-PCR in the two groups of mice (Fig.4.4. A). However, it was not possible to observe any parasite by Harris Haematoxylin staining, which rendered impossible to establish any correlation between the localization of Viperin and the parasite.

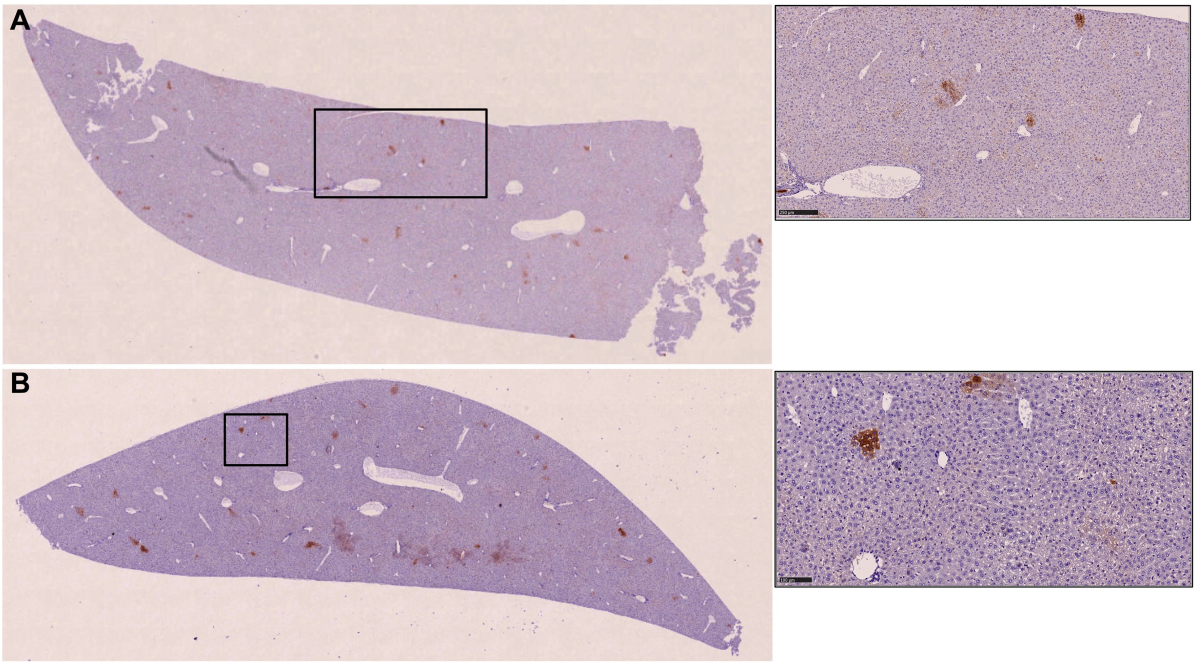


**Figure 4.6. Viperin staining in the liver slices of non-infected and *P. berghei*-infected C57BL/6J WT mice.** Histology of liver slices from a non-infected WT mouse **(A)** and a mouse infected with $3\times10^4$ *P. berghei* ANKA spz and euthanized at 42 hpi **(B)**. Analysis was made by haematoxylin & eosin staining and IHC staining with anti-Viperin antibody (brown-coloured foci). Boxed regions are shown at higher magnification at right. Scale bars: 250 µm **(A)** and 100 µm **(B)**. *N* = 1 per condition.

In an attempt to establish a relationship between the localization of Viperin and the parasite in the liver, C57BL/6J WT mice were infected with 100,000 *P. berghei* sporozoites, euthanized at 42 hpi and the livers collected and fixed in 4% PFA. Paraffin-embedded livers were cut into 10 µm-thick slices, stained with anti-*Pb*UIS4 and anti-Viperin primary antibodies and analysed by confocal microscopy. As it was observed by immunohistochemistry analysis, Viperin was found to localize in foci throughout the liver (Fig.4.7. B) with no specific relationship with the localization of the parasite (Fig.4.7. A and C).

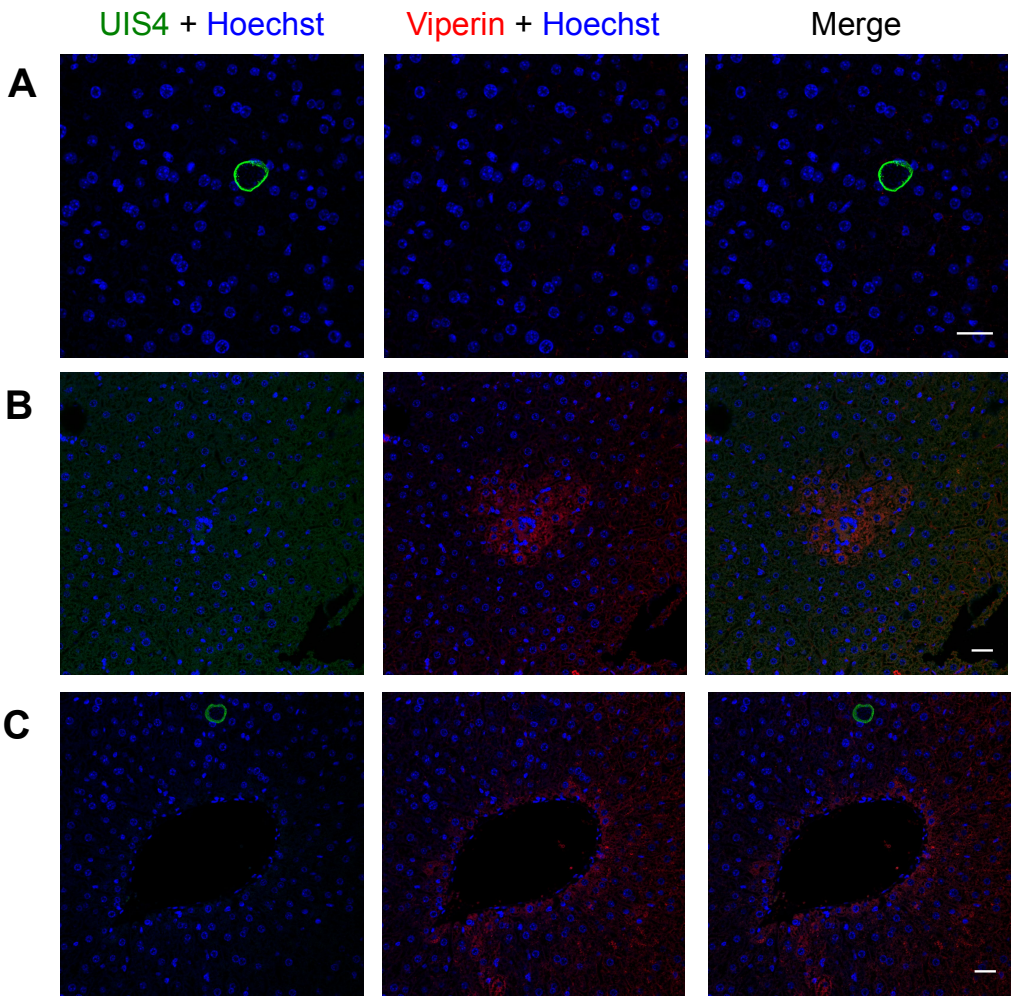


**Figure 4.7. Viperin and *Pb*UIS4 proteins localization in the liver slices of *P. berghei*-infected C57BL/6J WT mice.** Immunofluorescence of the liver slices from mice infected with $1\times10^5$ *P. berghei* ANKA spz and euthanized at 42 hpi (*n* = 2). Livers were fixed in 4% PFA and immunostained for *Pb*UIS4 and Viperin, with detection of stained structures with anti-goat 488 (green) and anti-mouse 568 (red), respectively. Nuclei were stained with Hoechst (blue) and representative images of the *Pb*UIS4 **(A)**, Viperin **(B)** and *Pb*UIS4 simultaneously with Viperin **(C)** were acquired by confocal microscopy. Scale bars: 30 µm.

### 4.3.2. Absence of Viperin does not impact *P. berghei* blood stage infection

Finally, we sought to determine whether the absence of Viperin would affect *P. berghei* blood parasitemia and mouse survival. To this end, we infected WT *Viperin*$^{+/+}$ mice, which were used as littermate controls, heterozygous *Viperin*$^{+/-}$ mice, and homozygous *Viperin*$^{-/-}$ mice with 30,000 luciferase-expressing *P. berghei* sporozoites. As previously mentioned, at 42 hpi, liver stage burden was assessed by *in vivo* bioluminescent imaging, a non-invasive method that allows the infection to proceed to the blood stage in the same animals[121], and blood parasitemia was monitored throughout infection by bioluminescence assay[111]. No difference in parasitemia was observed between the three groups of mice (Fig.4.8. A). Unfortunately, it was not possible to withdraw any conclusion regarding the impact of Viperin absence in mice survival since littermate controls did not die from CM as expected (Fig.4.8. B). This a sporadic phenomenon observed when using this experimental model

and more biological replicates will be required before being able to assess the impact of Viperin expression on CM onset.

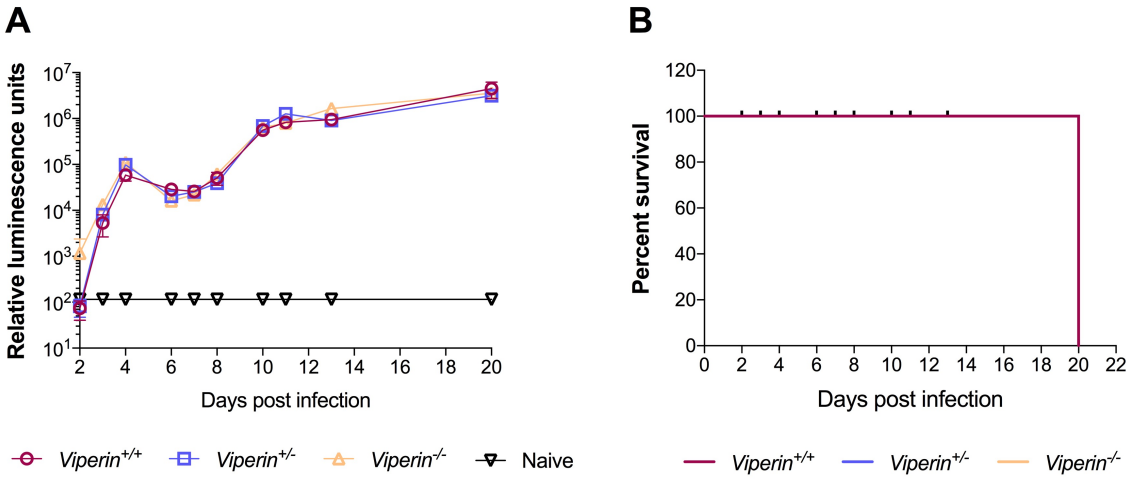


**Figure 4.8. Impact of the absence of Viperin on blood stage parasitemia and mouse survival. (A)** Blood parasitemia in WT *Viperin*$^{+/+}$, heterozygous *Viperin*$^{+/-}$ and homozygous *Viperin*$^{-/-}$ following injection with $3\times10^4$ luciferase-expressing *P. berghei* spz, assessed by bioluminescence assay (*n* = 2 per condition). **(B)** Survival percentage of WT *Viperin*$^{+/+}$, heterozygous *Viperin*$^{+/-}$ and homozygous *Viperin*$^{-/-}$ (*n* = 2 per condition).

### 4.3.3. Identification of the cellular mediators of Viperin expression

Viperin mRNA expression at 84 hpi was increased 47-fold when compared to the non-infected WT mice, whereas no upregulation was observed at the same time point in RAG2$^{-/-}$/γc$^{-/-}$ mice and only a 3-fold peak was observable in RAG-2$^{-/-}$ mice. Thus, although we speculate that some cell population of the RAG-2$^{-/-}$ mice, which is absent in the RAG2$^{-/-}$/γc$^{-/-}$ model, such as the NK cells and ILCs, may be contributing to the peak of Viperin expression at 84 hpi, it is plausible that a cell type absent in both mouse models, such as B and T cells, is the major responsible for the striking upregulation of Viperin at 84 hpi.

Therefore, we aimed at identifying which cell type is responsible for the 47-fold Viperin induction observed in WT mice (Fig 4.9. A). To this end, we started by targeting the NKT cell population taking advantage of the same NK cell-depleting antibody previously mentioned. Two hours prior to the injection of the TM-beta 1 antibody, each mouse was infected with 30,000 *P. berghei* sporozoites and the same time course experiment as previously described was employed, focusing on 42 hr and 84 hpi time points. At each time point, the depletion of the NK cell population (including NK and NKT cells) was assessed by flow cytometry analysis (See Appendices, Supplementary Fig.1 and Table 2).

Quantitative RT-PCR analysis of the Viperin mRNA expression revealed that the depletion of the NK cell population did not affect the upregulation of Viperin at both time points analysed (Fig.4.9. B). Moreover, a stronger induction of Viperin expression was observed in NK cell-depleted mice, compared to WT mice (2.603±0.963 at 42 hpi and 99.500±14.570 at 84 hpi), which may result from the low numbers of mice employed in this experiment, or may suggest the existence of compensatory

mechanisms for the absence of the NK cell population, probably through the higher activation/ recruitment of the yet unidentified cell population actually responsible for Viperin production.

Having excluded the NKT cells, we then assessed the impact of the absence of the γδ T cell population on the expression of Viperin at 84 hpi using TCRd$^{-/-}$ mice. TCRd$^{-/-}$ mice were generated by targeting the TCR δ constant gene segment (Cδ), which results in a deficiency in γδ T cells but a normal development of αβ T cells[122]. As it was observed for the NKT-depleted mice, no change in the pattern of Viperin mRNA expression was observed in the TCRd$^{-/-}$ mice when compared with WT mice (Fig.4.9. C). In fact, both peaks at 42 and 84 hpi were present and with magnitudes comparable to those of WT mice (1.729±0.265 at 42 hpi and 22.620±10.270 at 84 hpi).

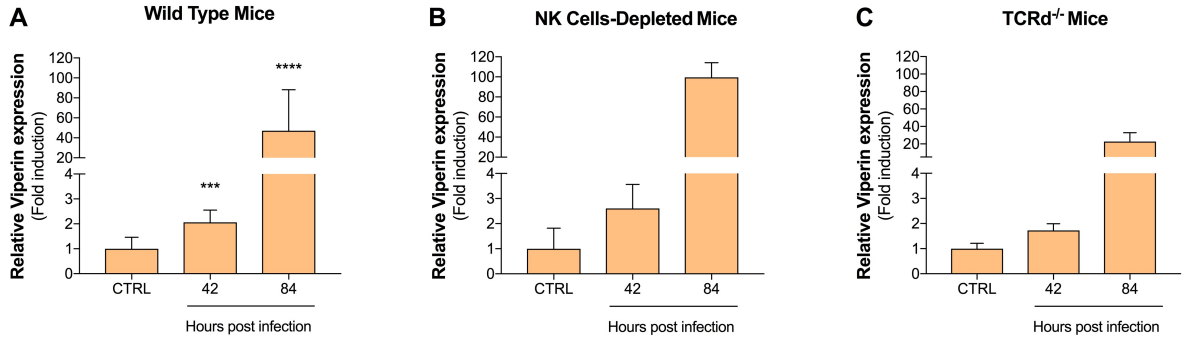


**Figure 4.9. The absence of NKT and γδ T cells does not impact the upregulation of Viperin at both 42 hpi and 84 hpi time points.** Viperin mRNA expression in whole liver extracts of C57BL/6J WT **(A)**, NK cells-depleted **(B)** and TCRd$^{-/-}$ **(C)** mice infected with $3\times10^4$ *P. berghei* ANKA spz and euthanized at the indicated times postinfection. The relative Viperin expression was analysed through qRT-PCR. Non-infected mice were used as controls. For each time point, data are expressed as means ± SD of the results of two independent experiments for the WT (CTRL, *n* = 10; 42 h, *n* = 6; 84 h, *n* = 6) and one experiment for NKT cells depletion (CTRL, *n* = 4; 42 h, *n* = 3; 84 h, *n* = 3) and TCRd$^{-/-}$ mice (CTRL, *n* = 4; 42 h, *n* = 3; 84 h, *n* = 3). Complete statistics are present in Appendices, Supplementary Table 1.

The maintenance of the Viperin induction peak at 84 hpi in both NKT-depleted and TCRd$^{-/-}$ mice excluded these lymphoid cells as being the major contributors of Viperin mRNA expression at this time point of *P. berghei* infection. Thus, the leukocytes that remain to be assessed and that are commonly absent in RAG2$^{-/-}$/γc$^{-/-}$ and RAG-2$^{-/-}$ mice are B cells and αβ T cells.

### 4.3.4. Dynamics of leukocyte populations at 84 hours post *P. berghei* infection

Besides nonhematopoietic cells, Viperin was found to be expressed in most leukocytes during lymphocytic choriomeningitis virus Armstrong infection, with neutrophils and macrophages showing the higher levels of type I and II IFNs-dependent Viperin induction[123]. Furthermore, CHIKV was also found to induce Viperin in an IFNα-dependent manner, with a higher induction observed in monocytes, the major immune cell subset targeted by CHIKV during the acute phase of infection[79].

Therefore, in order to perform a more comprehensive analysis of the immune cells that are activated or that are being recruited to the liver at this time point, and which may contribute to Viperin expression, we sought to determine the dynamics of the immune cells populations following *P. berghei* sporozoite infection through flow cytometry. To this end, WT C57BL/6J mice were infected

with 30,000 *P. berghei* sporozoites and at 84 hpi, the liver leukocytes of each mouse were isolated, purified and analysed by flow cytometry.

$CD8^+$ T and $CD4^+$ T cells were identified based on the surface expression of CD3, CD8 and CD4, whereas γδ T cells were identified by the surface expression of CD3 and TCR γδ. NK and NKT cells were identified based on the expression of the cell marker NK1.1; macrophages were identified based on the expression of CD11b, whereas the surface expression of Ly6C and Ly6G identified monocytes and neutrophils, respectively. Finally, dendritic cells (DCs) were identified through the expression of CD11c and the MHC class II molecule (Fig.4.10. A and Supplementary Fig.3).

Most cell populations revealed an increase (approximately 1.2 fold for $CD8^+$ T cells, macrophages and neutrophils and 2 fold for NK cells) or decrease (approximately 1.5 fold for $CD4^+$ T cells and γδ T cells and 8.5 fold for NKT cells) in the fold induction when compared with the non-infected WT C57BL/6J mouse. Nevertheless, a striking ~6.5-fold increase in the percentage of monocytes was observed in the livers of *P. berghei*-infected mice. No differences in the percentage of the DCs population were observed between *P. berghei*-infected mice and the non-infected mouse (Fig.4.10. B and C). However, the approach employed is limited by the fact that only one non-infected mouse was used as a control. Thus, as already described by Miller *et al.* (2014) for the 72 hours post-*P. yoelii* infection time point[42], *P. berghei* infection alters the leukocyte composition of the liver and, in our case, with a special highlight for the myeloid population of monocytes, providing hints to which cell type may be mediating the Viperin mRNA expression at this time point.

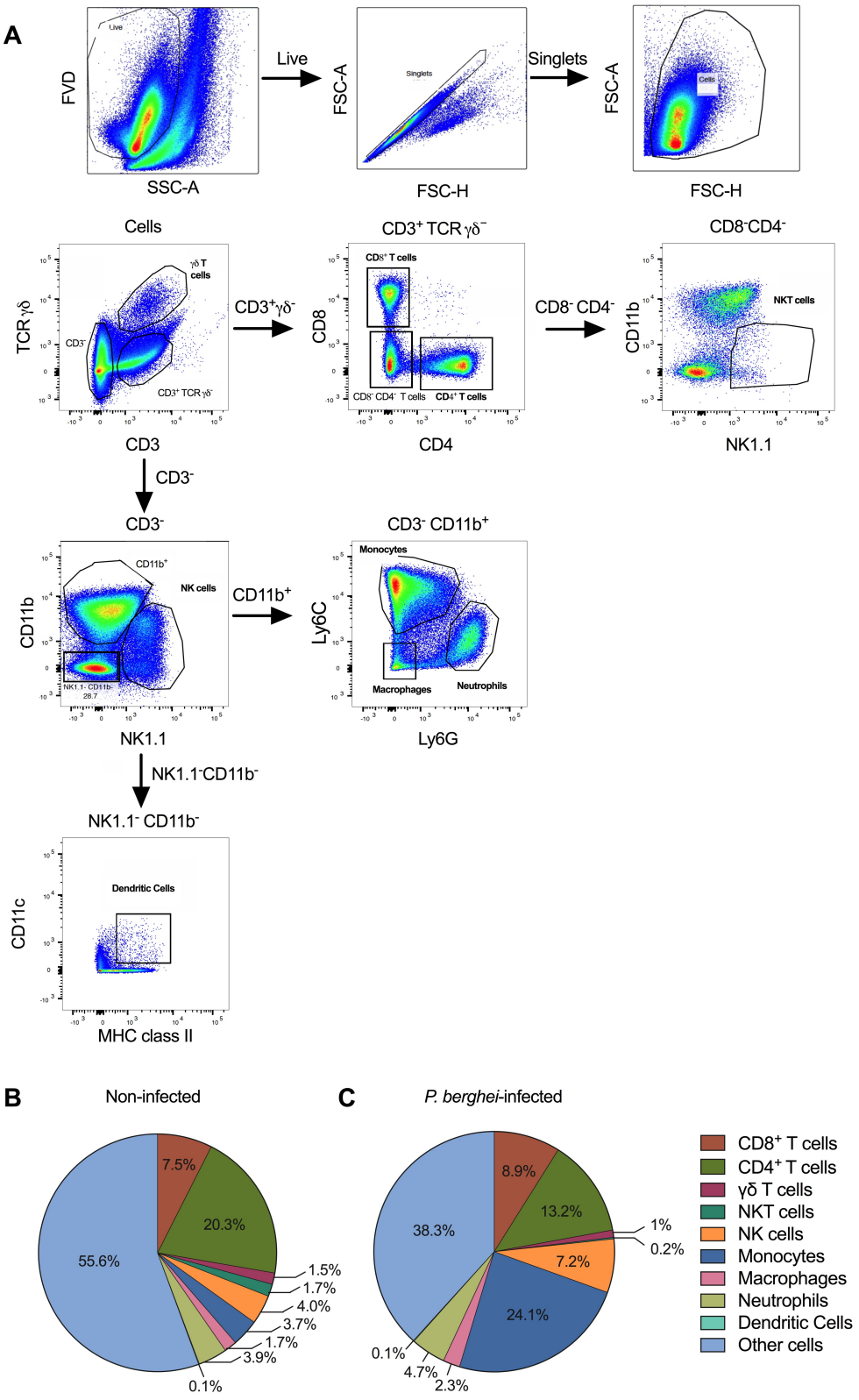


**Figure 4.10. Dynamics of the leukocytes activated and/ or recruited to the liver 84 hours post-*P. berghei* infection.** C57BL/6J mice were infected with $3\times10^4$ *P. berghei* ANKA spz. Non-parenchymal cells were isolated from non-infected and infected livers at 84 hpi, purified on a density gradient and analysed by flow cytometry. **(A)** Gating strategy for the identification of a wide range of immune cells activated and/ or recruited to the liver 84 hours post-*P. berghei* infection. Dead cells were excluded using the fixable viability dye (FVD) followed by selection of single cells based upon forward scatter (FSC) properties. Cell populations were then identified by the following staining pattern: γδ T cells ($CD3^+TCR\ \gamma\delta^+$), CD4 helper T cells ($CD3^+TCR\ \gamma\delta^-CD4^+$), CD8 cytotoxic T cells ($CD3^+TCR\ \gamma\delta^-CD8^+$), NKT cells ($CD3^+CD8^-CD4^-NK1.1^+$), NK cells ($CD3^-NK1.1^+$), monocytes ($CD3^-CD11b^+Ly6C^+$), neutrophils ($CD3^-CD11b^+Ly6G^+$), macrophages ($CD3^-CD11b^+Ly6C^-Ly6G^-$) and DCs

(CD11c$^+$MHC class II$^+$). **(B)** Quantification of CD8$^+$, CD4$^+$, γδ T cells, NKT cells, NK cells, monocytes, macrophages, neutrophils and DCs in the liver of non-infected **(B)** and *P. berghei*-infected **(C)** mice at 84 hpi (Non-infected, *n* = 1; *P. berghei*-infected, *n* = 3). Colours corresponding to each cell type are shown in legend and exact percentages are shown in each slide.

Previous results suggested that Viperin mRNA expression at 84 hpi is primarily mediated by leukocytes, which prompted us to identify which immune populations significantly contribute to Viperin expression. To this end, nonparenchymal cells isolated from non-infected and *P. berghei*-infected mice euthanized at 84 hpi were stained for intracellular Viperin and analysed by flow cytometry. Our results showed a substantial increase in the total number of Viperin-expressing leukocytes (45167±10100 for the infected mice compared with 21000 for the control) and, interestingly, in Viperin-expressing monocytes in the total cell population, as defined by positive staining for Viperin, CD11b and Ly6C (22298±4995; Fig. 4.11.A) compared with the non-infected mouse (3402). Although not so striking, an increase in Viperin-expressing CD4$^+$ T cells (3510±967.8 for the infected mice compared with 2799), NK cells (1549±204.1 for the infected mice compared with 888), macrophages (1173±219.8 for the infected mice compared with 474) and neutrophils (3397±915.2 for the infected mice compared with 1784) was also observed.

Additionally, within the cell population positive for the Viperin staining, only the proportion of monocytes increased approximately 3-fold relative to the non-infected control while the proportion of the other cell types either slightly increased (approximately 2-fold for macrophages), decreased (approximately 2-fold for CD8$^+$, CD4$^+$ T cells and γδ T cells, 13-fold for NKT cells and 1.2-fold for NK cells and neutrophils) or did not show any alterations (DCs; Fig. 4.11.B and C).

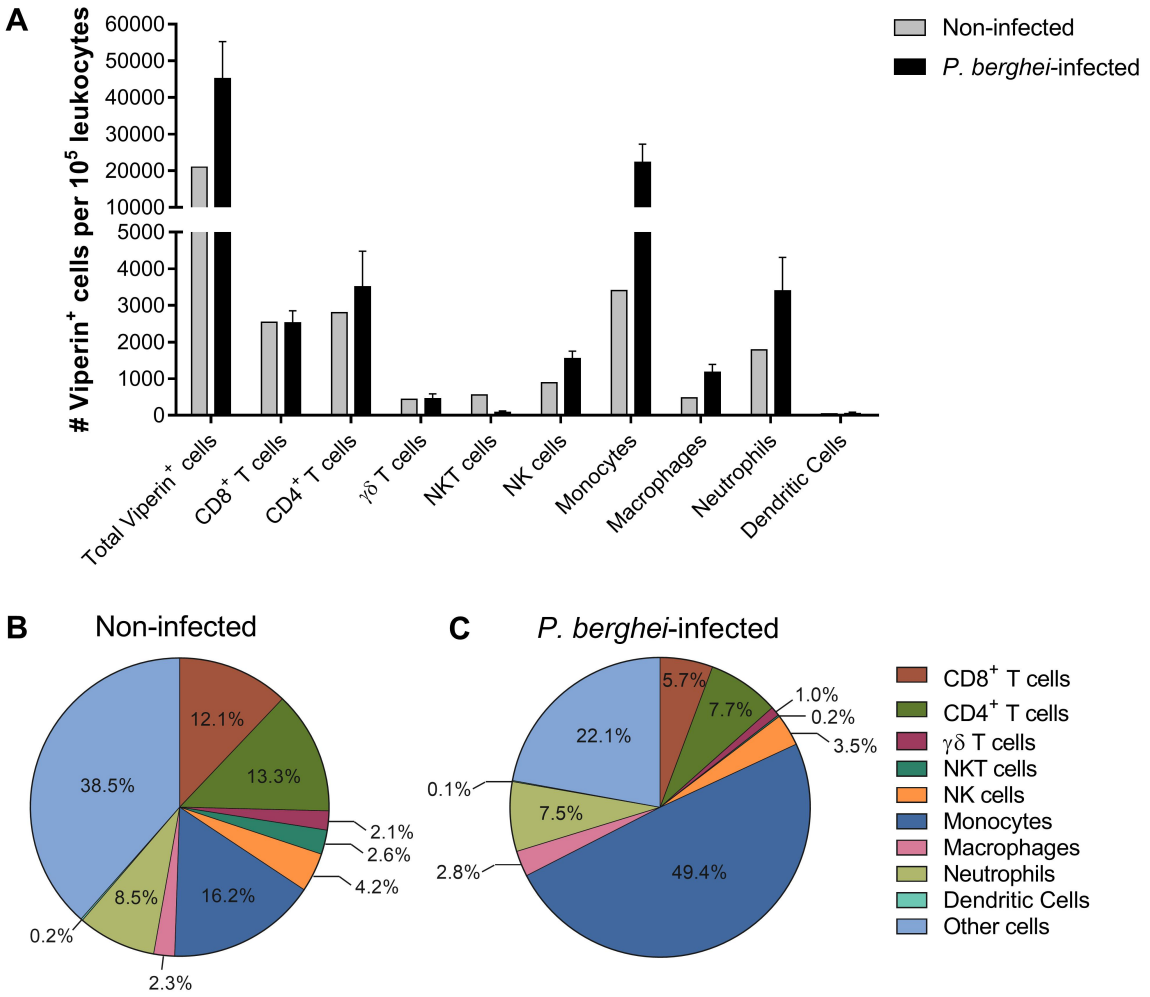


**Figure 4.11. Dynamics of Viperin-positive cell populations activated and/ or recruited to the liver 84 hours post *P. berghei* infection.** Nonparenchymal cells from the livers of non-infected and *P. berghei*-infected mice were extracted and purified 84 hpi and analysed for intracellular Viperin expression as well as surface expression of the molecules above mentioned. **(A)** Total number of Viperin-positive cells per 100,000 leukocytes by cell type. **(B, C)** Percentage of Viperin-positive leukocytes by cell type in non-infected **(B)** and *P. berghei*-infected **(C)** mice (Non-infected, *n* = 1; *P. berghei*-infected, *n* = 3). Colours corresponding to each cell type are shown in legend and exact percentages are shown in each slide.

Altogether, these results suggest that myeloid cells, and specifically monocytes, are highly recruited and appear to be essential for Viperin production in the liver at 84 hpi.

Although these are promising results, conflicting conclusions also emerge. At 84 hpi, Viperin mRNA expression was found to be 36-fold induced in WT mice while only a 3-fold induction was observed in RAG-2$^{-/-}$ mice and RAG2$^{-/-}$/γc$^{-/-}$ failed to upregulate this ISG. These observations led us to hypothesize that a population of leukocytes that is absent in both knockout mouse strains is the major contributor to Viperin mRNA expression, while flow cytometry analysis results suggest that monocytes, a population of myeloid cells that is present in both knockout models studied, may potentially constitute the most relevant producers of Viperin in the liver at 84 hpi.

These divergent results prompted us to question if monocyte recruitment to the liver at 84 hpi was altered in the RAG2$^{-/-}$/γc$^{-/-}$ and RAG-2$^{-/-}$ mouse models when compared to WT mice. To this end, we analysed the relative mRNA expression of CD68, a highly expressed protein in cells of the monocyte lineage[124], in whole liver extracts from the time course experiments performed with these

mouse strains. Quantitative RT-PCR analysis revealed that, in WT mice, the relative mRNA expression of CD68 increases gradually during infection reaching the first statistically significant peak already at 42 hpi (1.359±0.227; Fig.4.12. A) and rising to a 7-fold induction relative to the non-infected control mice at 84 hpi. In contrast, the analysis of CD68 mRNA expression in RAG2$^{-/-}$/γc$^{-/-}$ revealed that this cell marker is not induced during infection compared to the non-infected mice (Fig.4.12. B), which indicates an absence of activated or recruited monocytes to the liver of RAG2$^{-/-}$/γc$^{-/-}$ mice upon infection. Although Mazurier *et al.* (1999) reported that the absolute numbers of monocytes/ macrophages were at the lower limits of normal range[115], this should not be sufficient to impair the normal recruitment of monocytes upon infection and therefore, our results indicate that the lymphoid cell populations absent in the RAG2$^{-/-}$/γc$^{-/-}$ mice are somehow involved in the activation and/ or recruitment of monocytes to the site of infection. The pattern of CD68 mRNA expression in RAG-2$^{-/-}$ mice follows a different behaviour from the previously described mouse strains. Between 42 and 60 hpi, the CD68 levels remain low and no induction was detected when compared with the uninfected mice (Fig.4.12. C). After merozoites have egressed from the infected hepatocytes, the mRNA expression starts to increase until it reaches a 5-fold induction at 84 hpi, suggesting that monocytes start to be recruited to the liver at 72 hpi leading to an increase in the proportion of these myeloid cells, and subsequently in the CD68 expression in the infected liver.

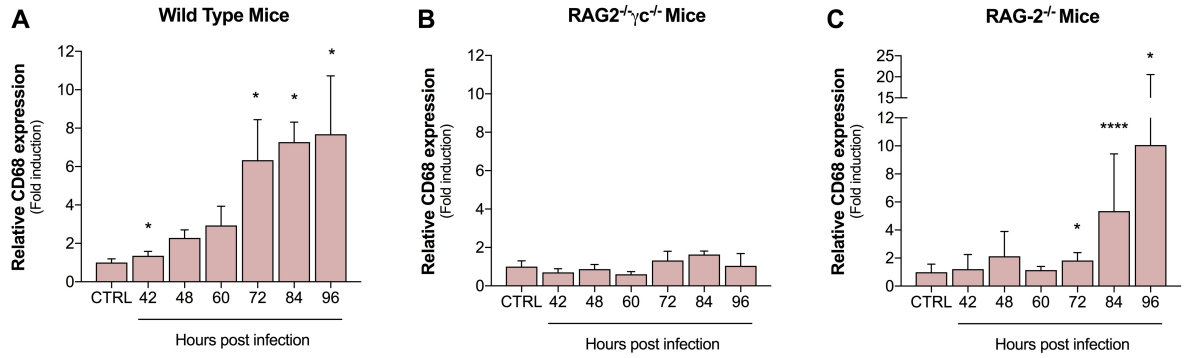


**Figure 4.12. CD68 mRNA expression in the liver upon *P. berghei* infection is impaired in RAG2$^{-/-}$/γc$^{-/-}$ and reduced in RAG-2$^{-/-}$ mouse models.** CD68 expression in whole liver extracts of C57BL/6J WT **(A)**, RAG2$^{-/-}$/γc$^{-/-}$ **(B)** and RAG-2$^{-/-}$ **(C)** mice infected with 3×10$^4$ *P. berghei* ANKA spz and euthanized at the indicated times post-infection. The relative CD68 expression was analysed through qRT-PCR. Non-infected mice were used as controls. For each time point, data are expressed as means ± SD of the results of two independent experiments for the WT (CTRL, *n* = 10; 42 h, *n* = 6; 48 h, *n* = 6; 60 h, *n* = 6; 72 h, *n* = 6; 84 h, *n* = 6; 96 h, *n* = 6) and RAG-2$^{-/-}$ mice (CTRL, *n* = 6; 42 h, *n* = 6; 48 h, *n* = 6; 60 h, *n* = 6; 72 h, *n* = 6; 84 h, *n* = 6; 96 h, *n* = 6) and one experiment for RAG2$^{-/-}$/γc$^{-/-}$ mice (CTRL, *n* = 4; 42 h, *n* = 3; 48 h, *n* = 3; 60 h, *n* = 2; 72 h, *n* = 3; 84 h, *n* = 3; 96 h, *n* = 3). Complete statistics are present in Appendices, Supplementary Table 1.

Collectively, these results strengthen the hypothesis that the monocytes are the major cell population contributing to the 36-fold induction peak of Viperin mRNA expression at 84 hpi observable in the whole liver extracts of *P. berghei*-infected WT mice.

The above described results urged us to monitor the dynamics of the CD11b$^+$Ly6C$^+$ monocytes at 84 hpi in the NKT-depleted and TCRd$^{-/-}$ mice via flow cytometry. In the NK-depleted mice there was a ~9,5-fold increase in monocytes when compared to the non-infected NKT-depleted

mice (Fig.4.13. A and Supplementary Fig.1), whereas in TCRd$^{-/-}$ mice, a 9-fold increase in the proportion of monocytes was observed (Fig.4.13. B and Supplementary Fig.4).

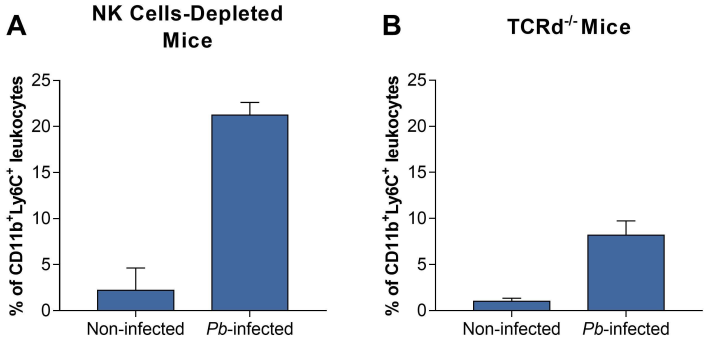


**Figure 4.13. Percentage of monocytes recruited to the liver 84 hours post-*P. berghei* infection in NK cells-depleted and TCRd$^{-/-}$ mice.** NK cells-depleted and TCRd$^{-/-}$ mice were infected with $3\times10^4$ *P. berghei* ANKA spz. Nonparenchymal cells were isolated from non-infected and infected livers at 84 hpi, purified on a density gradient and analysed by flow cytometry. **(A, B)** Quantification of monocytes in NK cells-depleted **(A)** and TCRd$^{-/-}$ **(B)** non-infected and *P. berghei*-infected mice. Monocytes were identified based on the expression of the surface cell markers CD11b and Ly6C. For each condition, data are expressed as means ± SD of the results of one experiment for the NK cells depleted (Non-infected, *n* = 3; *P. berghei*-infected, *n* = 3) and TCRd$^{-/-}$ (Non-infected, *n* = 3; *Pb*-infected, *n* = 3). Complete statistics are present in Appendices, Supplementary Table 1.

From these analyses, it is possible to conclude that, as it was observed in WT mice, monocytes are highly increased in *P. berghei*-infected mice compared with non-infected controls (Fig. 4.13). Furthermore, a raw comparison indicates that NKT-depleted mice, which showed the highest fold induction in Viperin mRNA expression at 84 hpi (99.500±14.570; Fig.4.9. B) also displayed the highest monocyte activation/ recruitment when compared to control mice (~9 fold induction; Fig.4.13. A). Likewise, RAG2$^{-/-}$/γc$^{-/-}$ mice, which exhibit the lowest fold-induction of Viperin expression at 84 hpi (1.296±0.619; Fig.4.4. B), also present the lowest expression of CD68 mRNA expression (1.631±0.184; Fig.4.13. B).

To test whether the levels of Viperin expression correlate with the proportion of monocytes present in the liver at 84 hpi, we calculated the Spearman correlation coefficient comparing the relative expression of Viperin and CD68 mRNA or relative proportion of monocytes (for the time courses with NKT-depleted and TCRd$^{-/-}$ mice; Fig.4.14). Spearman correlation coefficient (*R*) greater than 0.6 was considered a strong correlation. In WT C57BL/6J and RAG-2$^{-/-}$ mice, Viperin mRNA levels positively correlate with the CD68 expression (*R* of 0.2925 and 0.1985, respectively) although the correlation is weak (Fig.4.14. A and C, respectively). In RAG2$^{-/-}$/γc$^{-/-}$ mice, a Spearman's correlation coefficient of -0.05307 suggests the absence of correlation between the two variables (Fig.4.14. B). In contrast, the Viperin mRNA levels significantly correlate with the relative proportion of monocytes in the NKT-depleted (Fig.4.14. D) and TCRd$^{-/-}$ mice (Fig.4.14. E; *R* of 0.8694 and 0.8903, respectively). However, one limitation of this analysis is that, while in the WT, RAG2$^{-/-}$/γc$^{-/-}$ and RAG-2$^{-/-}$ mice, the variable used for correlation was the CD68 expression assessed by qRT-PCR, in the NK cells-depleted and TCRd$^{-/-}$ mice, correlation was based on the relative proportion of monocytes analysed through flow cytometry. The CD68 is a protein highly expressed in the monocyte lineage but also by circulating and tissue-resident macrophages, such as the Kupffer cells. Therefore, a simple correlation between the expression of Viperin and the proportion of monocytes as a function of the

expression of CD68 cannot be established since macrophages also express CD68 and a dilution effect might be occurring. In fact, a very low or non-existing correlation was obtained when relating Viperin expression with CD68 expression in the NKT-depleted and TCRd$^{-/-}$, which strengthens the previous conclusion regarding the use of CD68 as a monocyte-specific marker (*R* of 0.3025 and -0.1758, respectively; Appendices, Supplementary Fig.3). The only way to overcome this limitation would have been to characterize the dynamics of monocytes throughout the infection in all time courses by flow cytometry, through which we could directly assess the proportion of monocytes.

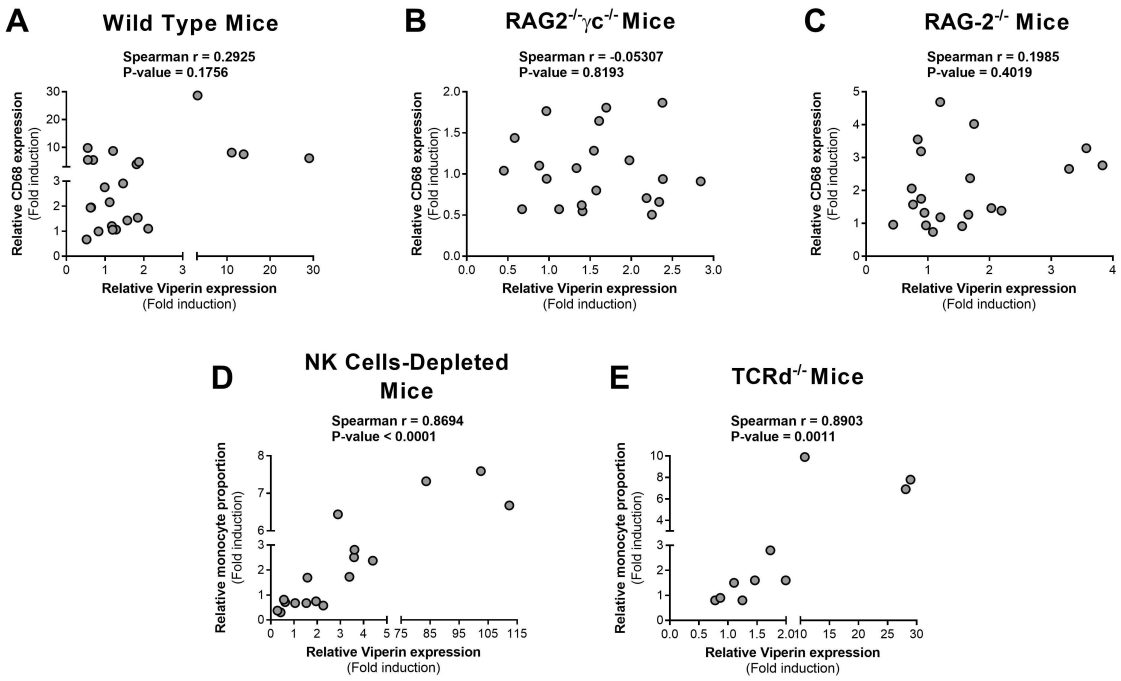


**Figure 4.14. Correlation of relative Viperin and CD68 mRNA expression or monocyte's proportion in the liver of different mouse strains infected with *P. berghei*.** Spearman's correlation coefficients relating relative Viperin and CD68 mRNA expression in WT C57BL/6J **(A)**, RAG2$^{-/-}$/γc$^{-/-}$ **(B)** and RAG-2$^{-/-}$ **(C)** mice or relative proportion of monocytes in NK cells-depleted **(D)** and TCRd$^{-/-}$ **(E)** mice. Spearman correlation coefficients and corresponding *p*-values are indicated. *R* greater than 0.6 was considered a strong correlation.

# 5. Conclusion

Malaria remains a major health concern as a significant cause of morbidity and mortality worldwide. The development of effective vaccines as well as therapeutic measures is urgent, although it is challenged by the lack of knowledge about *Plasmodium* parasites, the causative agents of the infection, and about the immune responses elicited on the vertebrate host. The clinically silent nature of the liver stage of *Plasmodium* infection led to the assumption that parasites pass undiscovered through this organ on their way to the bloodstream.

In 2014, Liehl *et al.* and Miller *et al.* started to decipher fundamental features of the *Plasmodium*-induced liver stage-specific innate immune response, identifying the host PRRs that recognize PAMPs of the *Plasmodium* parasite, the type of innate immune response that is induced as well as the impact of this response on infection and on the recruitment of effector leukocytes to the liver[41,42].

We proposed to extensively characterize the innate immune response elicited by *Plasmodium* parasites during the liver stage of infection, concentrating on the cellular mediators of the observed interferon signature and on the potential role of the interferon-stimulated gene Viperin. Overall, our observations are in accordance with the findings of the aforementioned authors, which are at the basis of the proposed model for the interferon responses elicited by *Plasmodium* liver stage parasites. Our results further expand this knowledge by identifying a novel cell population mediating the type I IFN signature and unveiling the impact of Viperin induction on liver stage *Plasmodium* infection.

During the obligatory liver stage of their life cycle, *Plasmodium* parasites trigger an immune response mediated by IFN-α and IFN-β. Primarily acting as signaling molecules, the mRNA expression of these type I IFNs increases exponentially throughout infection (Fig.4.1. A and B). These results are in agreement with previous studies indicating that *Plasmodium*-infected hepatocytes are able to amplify the type I IFN signaling through an autocrine and paracrine feed-forward loop, increasing the levels of these cytokines during infection[41].

The engagement of the IFNAR receptor by type I IFNs culminates in the induction of several ISGs, whose peaks of expression during liver stage infection occur at 42 hpi (Fig.4.1. D). Liehl *et al.* (2014) observed that this ISG response is not able to directly eliminate *Plasmodium* parasites, instead being essential for the later activation or recruitment of liver-resident or infiltrating leukocytes that target infected hepatocytes[41]. Since hepatocytes do not produce IFN-γ[35], it was hypothesized that the type I IFN pathway may be responsible for the recruitment of IFNγ-producing leukocytes which, in turn, act as effectors in controlling parasite development[41,42]. Thus, the observed upregulation of IFN-α and IFN-β at 42 hpi in whole liver extracts may lead to the recruitment of immune cells to the liver and to the subsequent significant induction of IFN-γ expression observed from 60 hpi onwards, peaking at 84 hpi (Fig.4.1. C). In particular, Miller *et al.* (2014) demonstrated that CD1d-restricted NKT cells, whose numbers increase in the liver following *Plasmodium* infection, act as the main effectors of liver stage parasite control, through the production of the type II IFN[42].

Hence, although the 42 hpi peak in ISG expression is essential for liver parasite control indirectly through the recruitment of effector immune cells[41,42], the physiological relevance of the 84

hpi peak remains to be fully ascertained. Miller *et al.* (2014) and Liehl *et al.* (2015) employed a mouse reinfection model to show that the type I IFN pathway induced by a primary infection is essential for the impairment of a secondary infection, with IFN-γ being the key mediator of this impairment. In fact, both IFNAR-deficient mice and IFNγ-knockout mice were unable to supress the liver stage of infection observed in control WT mice[42].

Additionally, the comparison between the kinetics and magnitude of the induction of the interferons and ISGs assessed in this study reveals that the 42 hpi peak and the corresponding magnitude of induction is similar for type I IFNs and ISGs, indicating that, at this time point, the ISGs are primarily induced by IFN-α and IFN-β (Fig.4.1. A, B and D). Moreover, the kinetics of ISG expression between 60 and 96 hpi show a profile similar to that observed for type II IFN (Fig.4.1. C and D). Therefore, the 84 hpi peak in expression of ISGs may reflect a crosstalk between type I and type II IFNs, yielding a stronger induction, whose physiological relevance remains undefined. This is supported by the hypothesis raised by Gough *et al.* (2010) suggesting that the expression of STAT1, a transcription factor shared by both cytokines' signaling cascades, could be a point of crosstalk between the two types of IFNs[125]. Interestingly, Miller *et al.* (2014) identified STAT1 as one of the major regulators of the transcriptional changes observed in *Plasmodium*-infected mice at 72 hpi when compared with mock-infected counterparts[42].

We subsequently investigated the cellular mediators of the 84 hpi peak of the ISG response during the liver stage of *Plasmodium* infection. The characterization of the interferon-mediated immune responses in a completely alymphoid mouse model (knockout for B and T cells as well as NK cells and ILCs) revealed that, in contrast with WT mice, RAG2$^{-/-}$/γc$^{-/-}$ mice were unable to upregulate neither the type I IFNs nor the type II IFN upon *Plasmodium* infection, likely due to the chronic absence of interferon producers[35] (Fig. 4.2. B and E). On the other hand, at 42 hpi, while parasites are still developing in the liver, the profile of ISG expression observed in the WT mice was identical to that observed in RAG2$^{-/-}$/γc$^{-/-}$ mice, suggesting that this first response is mediated by hepatocytes or myeloid cells, with no involvement of lymphoid cells (Fig.4.1. K). In fact, Liehl *et al.* (2014) had already reported that mice specifically knockout for the IFNAR1 on hepatocytes (Alb-Cre-*Ifnar1*$^{flox/flox}$) did not induce a type I IFN response, while the lack of the same IFNAR subunit specifically in myeloid cells (LysM-Cre-*Ifnar1*$^{flox/flox}$) did not affect the response[41]. Furthermore, it is possible that the 42 hpi ISG peak may be induced by interferons upregulated in a temporal window which was not assessed, comprised between the entry of the parasite in the liver and the 42 hpi, or that other types of IFNs, such as the relatively unexplored type III IFNs[123], could be involved in the ISGs upregulation.

Nonetheless, in the RAG2$^{-/-}$/γc$^{-/-}$ mouse model, *Plasmodium* infection did not lead to a high induction of ISGs at 84 hpi (Fig.4.2. K), suggesting that different cellular mediators are involved in the immune response during different stages of the parasite's life cycle.

The conclusions of this study are in agreement with the ones withdrawn by Miller *et al.* (2014) who assessed the dynamics of cell populations activated or recruited to the liver at 72 hours post-*P. yoelii* spz injection. A flow cytometry analysis revealed that, at this time point post-infection, the liver was enriched in CD8$^{+}$ T cells, NK and NKT cells, all of which are absent in the RAG2$^{-/-}$/γc$^{-/-}$ model[42]. However, the presence or absence of a type I IFN signature was not the object of the study.

A similar type of analysis performed upon *Plasmodium* infection of RAG-2$^{-/-}$ mice, which lack B and T cells, also revealed an inability of these mice to upregulate the type I IFNs at 84 hpi, although the profile of IFN-γ mRNA expression across infection was similar to that of WT mice (Fig.4.2. C, F and I). This is likely due to compensatory mechanisms exerted by NK cells, a cell population that is known to produce type II IFN[35], and which is present in normal levels in this mouse model. The analysis of ISG expression reinforced the prior observation that the 42 hpi peak may be mostly mediated by hepatocytes, while the 10-fold induction of ISG expression observed at 84 hpi is likely mediated by a cell population that is present in the RAG-2$^{-/-}$ mouse model but absent from the RAG2$^{-/-}$ /γc$^{-/-}$ mouse model, the NK cells and/or ILCs. Nonetheless, one cannot exclude that cells simultaneously absent from both mouse models may also be involved in the observed signature, which would explain why the ISGs are not induced in the RAG-2$^{-/-}$ mice exactly to the same magnitude as that observed in the WT mice.

Having hypothesized that the NK cells and/or the ILCs may be responsible for the peak of ISG expression at 84 hpi, we sought to analyse the impact of NK cell depletion on that expression profile. We initially observed that the depletion of the NK cell population, which includes NK and NKT cells, alters the characteristic profile of type I IFN expression observed in in WT mice, while maintaining the profile of IFN-γ expression (Fig.4.3. A-C). The NK-depleted mice showed no induction of type I IFNs between 42 hr and 60 hpi, revealing only an acute peak of expression at 72 hpi, likely due to a type I IFN-producing cell population that was only activated or recruited to the liver at that specific time point. The maintenance of a similar IFN-γ expression profile in NK-depleted and WT mice was unexpected given that the NK cells are one of the major producers of the type II cytokine[35], which suggests a possible activation of mechanisms that could compensate the absence of this IFNγ-producing population, such as earlier activation/ recruitment of T cells. Finally, the signature of ISG expression in the NK-depleted mice is kinetically similar to that observed in WT mice; there is a primary upregulation at 42 hpi, while parasites are still in the liver, with a second peak of induction occurring at 84 hpi, after parasites have already exited the liver and initiated the blood stage of infection (Fig.4.3. D).

Two conclusions can be drawn from these results: first, NK cells are not required for the observed 42 hpi induction of ISGs, supporting the notion that hepatocytes are the primary source of ISGs at this time point. However, the identity or time window of expression of the cytokines that regulate ISG induction at 42 hpi is still unclear given that type I IFNs' induction was absent in all the knockout mouse models employed. Second, the presence of the 84 hpi peak excludes the NK cell population as the main responsible for the high induction of ISG expression at this time point. Intriguingly, previous studies have stated that, at 72 hours post-*P. yoelii* infection, the liver is enriched in NK and NKT cells, with the latter limiting the liver stage parasite infection through the production of IFN-γ[42]. However, these do not seem to be the cell population that is contributing to the type I IFN signature observed at 84 hpi. Once again, the profile of IFNs' expression suggests that ISGs' induction at this time point may be jointly coordinated by both type I and type II IFNs, which show an upregulation just prior the ISGs' expression peak.

The exclusion of the NK cell population points to ILCs as possibly being the major contributors to the type I IFN signature observed in *Plasmodium*-infected WT mice. ILCs are a relatively unexplored cell population in the context of malaria infections. To the best of our knowledge, the only studies to date reporting a role for ILCs in the immune responses elicited by *Plasmodium* infection were performed in the context of CM. Palomo *et al.* (2017) suggested that IL33-mediated expansion of the group 2 of ILCs prevents ECM in mice through a mechanism dependent on M2 macrophages, a type of macrophage that decreases inflammation and stimulates tissue repair[120], and regulatory T cells[126]. Thus, these results may suggest a possible involvement of a novel cell population in a biologically relevant phenomenon that is occurring in the liver long after parasites have egressed from this organ. Furthermore, these cells, alongside with the previously identified NKT cells[42], may be involved in the inhibition of a secondary infection while the host is still dealing with an ongoing primary infection.

When analysing the mRNA expression profile of the panel of selected ISGs, a striking observation emerged: while *Ifit-1*, *Ifi44*, *Usp18*, *Ifit3*, *Irf7* were, on average, 10-fold induced at 84 hpi in RAG-2$^{-/-}$ mice, Viperin was only induced 3-fold relative to non-infected mice (Fig.4.4). Moreover, the peak of Viperin induction at this time point seems to be more acute than that of other ISGs, whose expression progressively increases from 72 hpi, peaking at 84 hpi and then gradually decreases until 96 hpi. These striking results prompted us to focus on this ISG, exploring a potential role in the context of the *Plasmodium* mediated-type I IFN response in the liver and identifying the subset of immune cells responsible for its production at 84 hpi.

Viperin is an ISG with antiviral activities against a plethora of viruses. Viperin revealed *in vitro* antiviral activity against HCV[76], DENV[82], ZIKV[81], influenza A[91], HIV-1[83] and CHIKV[79] and, more importantly, *in vivo* antiviral functions against WNV[92] and CHIKV[79]. However, the role of Viperin in the context of parasitic infections and, in particular, of *Plasmodium* infections, has not yet been investigated. Viperin is expressed in most cell types at very low basal levels[84], but it can be highly induced in an IFN-dependent manner by both type I and type II IFNs[72].

Key features of the *Plasmodium*-elicited type I IFN response have recently begun to be unravelled. However, the impact of specific ISGs on the progression of the parasite's life cycle remains elusive. In the present study, we indirectly demonstrated a role for Viperin in controlling *Plasmodium* infection using *Viperin*$^{-/-}$ mice. Loss of Viperin expression resulted in a 2-fold increase of the liver burden at 42 hpi relative to *Viperin*$^{+/+}$ littermates (Fig.4.5. A and B). Furthermore, we demonstrated that Viperin is induced in the context of the type I IFN response after the engagement of IFNAR, with hepatocytes likely being the primary source of expression of this ISG at this time point (Fig.4.5. C and D). Although Viperin was shown to play a role in controlling the liver stage of *Plasmodium* infection, microscopy analysis did not reveal any relationship between the localization of Viperin, which is distributed in foci throughout the liver, and that of the parasite (Fig.4.6 and 4.7). Moreover, the absence of this ISG does not seem to impact blood parasitemia (Fig.4.8. A)

We next sought to get further insights into the cellular mediators of Viperin induction at 84 hpi. The lower induction of Viperin expression at 84 hpi in the RAG2$^{-/-}$/γc$^{-/-}$ and RAG-2$^{-/-}$ mice compared to WT mice suggests that a cell type simultaneously absent from both knockout mouse models is the

main responsible for Viperin production at this time point. Upon analysis of Viperin mRNA expression in NKT-depleted mice, we excluded this cell type as the main contributor to Viperin expression (Fig.4.9. B). Therefore, one or more of the remaining shared T cell populations, such as the αβ and the γδ T cells, as well as B cells, might be responsible for the observed induction. Subsequent analysis of Viperin mRNA expression in mice depleted of γδ T cells has allowed the exclusion of this population of immune cells as well (Fig.4.9. C).

We then opted for a flow cytometry-based analysis, to identify the immune cells that are activated or infiltrating the liver at this time point, and which may contribute to the increase of Viperin expression. Our results showed that the liver stage of *Plasmodium* infection leads to an enrichment of $CD8^+$ T cells, macrophages, neutrophils and NK cells in the liver at 84 hpi, as well as a very significant increase in Viperin-producing cells in the livers of *P. berghei*-infected mice (Fig.4.10. B and 4.11. A). Strikingly, a 6-fold increase in the proportion of monocytes was observed, which also corresponds to the largest fraction of the Viperin-positive cell population (Fig.4.10. B and 4.11). A similar type of analysis performed by Miller *et al.* (2014) at 72 hr post-*P. yoelii* infection only analysed the dynamics of the lymphoid cells[42]. Thus, these results suggest that myeloid cells may also be essential in the inhibition of the reinfection or have another yet unknown biological relevance.

Overall, these results suggest that myeloid cells, and specifically monocytes, are highly activated and/or recruited to the insulted liver at 84 hpi, contributing to the high levels of Viperin observed. However, these results differ from those obtained from the $RAG2^{-/-}/\gamma c^{-/-}$ and $RAG\text{-}2^{-/-}$ knockout mouse models, which suggested that lymphoid cells, likely αβ T cells or B cells, might be responsible for the expression of Viperin. Thus, these results led us to hypothesize that a chemoattractant molecule potentially secreted by lymphoid cells is necessary for the recruitment of Viperin-positive monocytes to the *P. berghei*-infected liver. In fact, the expression of CD68, a marker for the cells of the monocyte-lineage, qualitatively correlates with that of Viperin mRNA (Fig.4.12). At 84 hpi, WT mice displayed the highest expression of Viperin, followed by $RAG2^{-/-}$ mice, and with the $RAG2^{-/-}/\gamma c^{-/-}$ mice exhibiting the lowest Viperin expression at this time point. The profile of the CD68 mRNA expression followed a similar pattern. However, the calculation of the Spearman correlation revealed a very low or non-existent correlation between the relative mRNA expression of Viperin and CD68. This is possibly due to the fact that CD68 is not a monocyte-specific marker as it is also expressed by tissue-resident macrophages such as the Kupffer cells[124]. In fact, flow cytometry analysis of the proportion of monocytes in NK-depleted and $TCRd^{-/-}$ mice allowed a more specific correlation analysis between the proportion of monocytes in the liver at 84 hpi and the levels of Viperin expression, with a strong correlation being observed between these two variables.

So far the results indicate that monocytes are the major producers of Viperin at 84 hpi, however, it is still not possible to ascertain the biological relevance of this phenomenon and, in particular, of the increase in Viperin-positive monocytes, during the late liver stage of *Plasmodium* infection. Monocytes are myeloid cells pertaining to the innate mononuclear phagocyte system (MPS) and considered to be a two-edged sword either playing a role in the control or clearance of the disease or contributing to the persistence of the infection[127]. Monocytes are a heterogeneous population of cells with various functions, which complexifies their characterization[127]. However, one

subset of murine peripheral blood monocytes has been identified based on the expression of GR1 (Ly6C and Ly6G) as well as the cell trafficking receptors CCR2 and the low expression of the fractalkine receptor CX3CR1, known as inflammatory or Ly6C$^{hi}$ monocytes[127,128]. If signaling through CCR2 via the CCL2, CCL7, CCL8 and/ or CCL12 chemokines is impaired, migration of inflammatory monocytes from the bone marrow, a major reservoir of these myeloid cells, is prevented[129].

The role of monocytes has been studied in a variety of experimental infection models, including parasitic infections. Murine infection with the enteric pathogen *Toxoplasma (T.) gondii* results in an enrichment of inflammatory monocytes in the gastrointestinal tract[130]. These monocytes expressed iNOS, IL-12 and TNF, and were indirectly associated with decreased pathology and lethality and, subsequently, to decreased susceptibility to oral toxoplasmosis[130]. Similarly, monocytes were found to adhere to the surface of *Leishmania major* parasites causing modifications in their morphology with a final respiratory burst of superoxides being able to kill parasites[131]. Interestingly, monocytes were also found to play a role in the blood stage of malaria infection. Sponaas *et al*. (2009) showed that *P. chabaudi* infection in mice resulted in an influx of inflammatory monocytes to the blood and spleen[132]. These monocytes expressed iNOS and TNF and exhibited the ability to phagocytose parasites *in vivo* contributing to the control of the infection[132]. In contrast, in an experimental model of African trypanosomiasis, inflammatory monocytes exhibited a pathogenic role[133]. Mouse infection with *Trypanosoma brucei* resulted in an increase in the numbers of inflammatory monocytes at the sites of infection where the differentiation into inflammatory DCs occurred[133]. These DCs revealed to be pathogenic, aggravating the disease and reducing survival[133]. In 2015, a study revealing a pathogenic role in the context of *Plasmodium* infection also emerged. In this study, the impairment of monocyte recruitment resulted in prevention of ECM with a decrease in brain inflammation and immune cell recruitment, in particular IFNγCD8$^{+}$ T effector cells.

Despite the fact that the role of Viperin-positive monocytes present in the liver at 84 hours post *P. berghei* infection remains undefined, their activation and/ or recruitment seems to be impaired in RAG2$^{-/-}$/γc$^{-/-}$ and RAG-2$^{-/-}$ mice, resulting in low levels of Viperin mRNA expression at this specific time point. The trafficking of monocytes and recruitment into tissues may be mediated by different chemoattractant molecules that bind to the CCR2, although CCL2 (also known as MCP1) and CCL7 (also known as MCP3) are the ones most rapidly produced[134,135].

A study conducted by Cohen *et al.* (2013) established a key link between CD4$^{+}$ T cells and recruitment of inflammatory monocytes to the intestinal mucosa[128]. In particular, CD4$^{+}$ T cells expressing CXCR3 mediate activation of intestinal mucosa inflammatory monocytes via secretion of IFN-γ, which will, in turn, be involved in control of *T. gondii* intestinal infection[128]. Another study developed in the context of myocardial infarction identified B cells as being essential for the recruitment of inflammatory monocytes to the heart through the production of CCL7[136]. The recruitment of these myeloid cells lead to enhanced tissue injury and deterioration of myocardial function rendering monocytes a pathogenic role[136]. A more relevant study developed in the context of a parasitic infection with *T. gondii* was developed by Schulthess *et al.* (2012)[137]. These authors observed that a crosstalk between IL-15 and IL-18 is crucial for the intestinal recruitment of inflammatory monocytes, which, in turn, controls parasite replication as well as tissue damage[137]. On

the one hand, stromal cells produce IL-15, which promotes the development of the ILC1 subset, specifically, the $NKp46^{+}NK1.1^{+}$ cells[137]. On the other hand, IL-18 produced in the context of the infection stimulates the $NKp46^{+}NK1.1^{+}$ cells to produce CCL3, a ligand involved in the chemoattraction of monocytes via their receptor CCR1[(137)]. Additionally, a study conducted by Lee *et al.* (2009) concluded that in chronic inflammation of the peritoneum, the type I IFN signaling was essential for the production of CCL2, CCL7 and CCL12 and, subsequently, for the persistent CCR2-dependent recruitment of $Ly6C^{hi}$ inflammatory monocytes into the peritoneum[138].

All these studies support the hypothesis that in $RAG2^{-/-}/\gamma c^{-/-}$ and $RAG\text{-}2^{-/-}$ mice, the absence of lymphoid cell-derived monocyte-recruiting chemokines leads to the lack of inflammatory monocytes recruitment to the liver and strengthens the conclusion that monocytes are the major cell population contributing to the high induction of Viperin mRNA expression observed in WT mice.

Collectively, our results add to a growing body of research revealing the features of the *Plasmodium*-elicited innate immune response in the liver. Importantly, new light has been shed into a cell population, the ILCs, potentially responsible for the observed ISG signature at 84 hours post-*P.berghei* infection. Furthermore, whereas previous studies had identified Viperin as an antiviral ISG in numerous viral infections, we established for the first time a role for this protein in parasitic infections and uncovered the possible involvement of Viperin-positive monocytes in the inhibition of reinfection or in an yet undefined biological relevant phenomenon occurring in the late liver stage of the *Plasmodium* life cycle.

# 6. Future work

A number of questions for future research are raised:

**- What is the role of type I and type II IFNs, as well as of their potential crosstalk, in the induction of the assessed ISGs in the liver of *P. berghei*-infected WT mice throughout the course of the infection?** This question could be tackled through the analysis of the impact of type I and type II IFNs ablation in the ISG signature observed in the time course of *P. berghei* infection. The simultaneous assessment of ISGs' expression levels in WT and *Ifnar1*$^{-/-}$ mice treated with an IFNγ-neutralizing antibody should allow us to obtain an answer for the role of type II IFNs in ISGs' induction. An IFNGR1-blockade antibody should also serve the purpose or be employed in a complementary manner.

**- What is the identity and/or temporal window of induction of the IFNs responsible for the ISGs' expression in the RAG2$^{-/-}$/γc$^{-/-}$ and RAG-2$^{-/-}$ mice?** To obtain the answer to this question, we should aim at analysing the expression of both types of IFNs in previously unanalysed time points of infection, for instance, 12, 24 and 36 hpi, as well as the mRNA expression of other types of IFNs such as the type III IFN (IFN-λ), which could contribute to the ISGs' expression in nonhematopoietic cells such as the hepatocytes. In fact, Zhou *et al.* (2007) demonstrated, through gene expression array analysis, that type I and type III IFNs induce a similar subset of genes[139]. Interestingly, the same study revealed that a group of genes induced by IFN-α were also induced by IFN-λ, although to a lower level, in HepG2 cells stimulated with both cytokines[139].

**- What is the impact of the depletion of ILCs in the profile of ISGs' expression observed in WT mice, especially at 84 hours post- *P. berghei* infection?** This question could be tackled by analysing the mRNA expression levels of the ISGs' panel in *Nfil3*$^{-/-}$ mice.

**- What is the impact of ILCs' ablation on *Plasmodium* liver infection and reinfection?** In order to pursue this question, we should analyse the liver infection load in *Nfil3*$^{-/-}$ mice at 42 hpi and perform the reinfection model assay in the same knockout mouse model in order to assess the role of ILCs, activated and/or recruited by a primary *P. berghei* liver-stage infection in the context of the type I IFN response, in the impairment of a second sporozoite infection.

**- What are the detailed dynamics of myeloid cells populations in the liver following *P. berghei* sporozoite infection throughout the time course?** The infection of WT C57BL/6J with *P. berghei* sporozoites and, at each time point, the isolation and purification of the liver leukocytes followed by the analysis of the proportion of each myeloid cell type through FACS analysis should fulfil this aim.

**- Does Viperin exhibit an antiparasitic effect *in vitro*?** The observation of an anti-*Plasmodium* role for Viperin *in vivo* warranted further investigation of this matter *in vitro*. To tackle this, a comparison of

the infection load between a control cell line, which expresses Viperin, and a Viperin-knockout cell line, which exhibits Viperin deficiency, infected with *P. berghei* sporozoites should be performed. In a complementary manner, overexpression of Viperin through the transfection of Huh-7 cells with a Viperin-expressing plasmid should also be considered. In fact, a polyclonal Huh-7 cell line stably expressing a short-hairpin RNA (shRNA) targeting Viperin mRNA (known as ShRNA#5)[76] as well as an mCherry N-terminally tagged Viperin-WT[82] were already kindly provided by Dr. Michael Beard from the University of Adelaide, Australia. Preliminary results obtained from *P. berghei* infection of Huh-7 cells previously stimulated with IFN-α for 24 hours already hint that Viperin may also exhibit an anti-*Plasmodium* effect *in vitro* (Fig.6.1.).

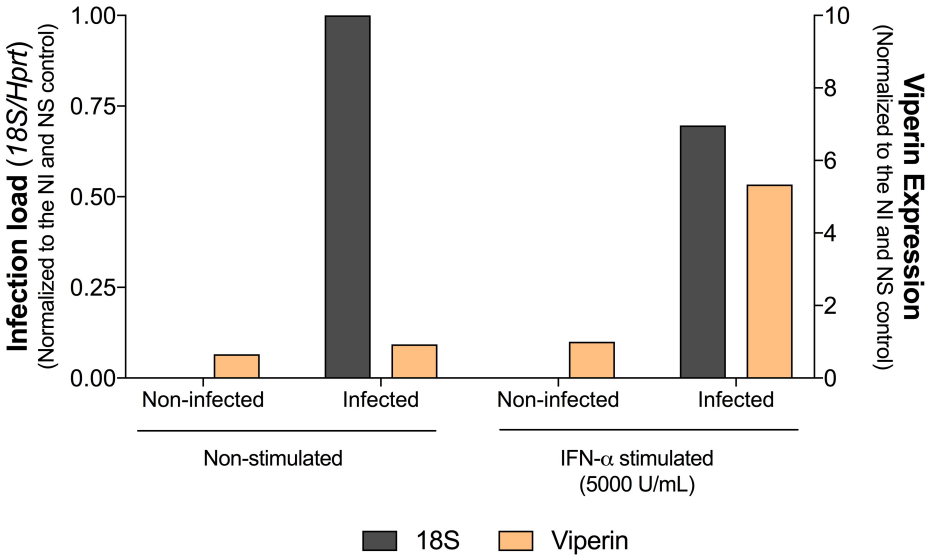


**Figure 6.1. Viperin exhibits anti-*Plasmodium* activity *in vitro* after IFN-α stimulation of Huh-7 cells.** Parasite load and Viperin mRNA expression in Huh-7 cells stimulated with 5000 U/mL of IFN-α for 24 hours prior to infection with $3\times10^4$ *P. berghei* ANKA spz and collect at 42 hpi. The relative 18S and Viperin expression were analysed through qRT-PCR. Non-infected Huh-7 cells were used as controls. Data are expressed as fold induction relative to the non-infected and non-stimulated control for infection load and relative to the non-infected and non-stimulated control for Viperin mRNA expression of the results of one preliminary experiment.

**- What is the effect of *Plasmodium* infection on the intracellular distribution of Viperin?** Physiologically, Viperin is localized in a diffuse cytoplasmic pattern consistent with ER and/or LDs distribution[80]. However, Viperin has been found to relocalize in response to some viral infections [72,83,103]. The analysis of Viperin localization relative to the parasite and to cellular structures can be performed through immunofluorescence microscopy using the mCherry N-terminally tagged Viperin WT, avoiding misleading signals given by cross-reactivity between antibodies, the anti-UIS4 antibody which stains the PV and other antibodies to stain the ER, mitochondria and the Golgi apparatus[103,140]. Viperin distribution to LD can be evaluated using Bodipy lipid probes or the oil-red O solution[77]. Preliminary results obtained from *P. berghei* infection of Huh-7 cells followed by fixation at 42 hpi and staining for the *Pb*UIS4 and Viperin suggests a potential colocalization between the two structures *in vitro* (Fig.6.2.).

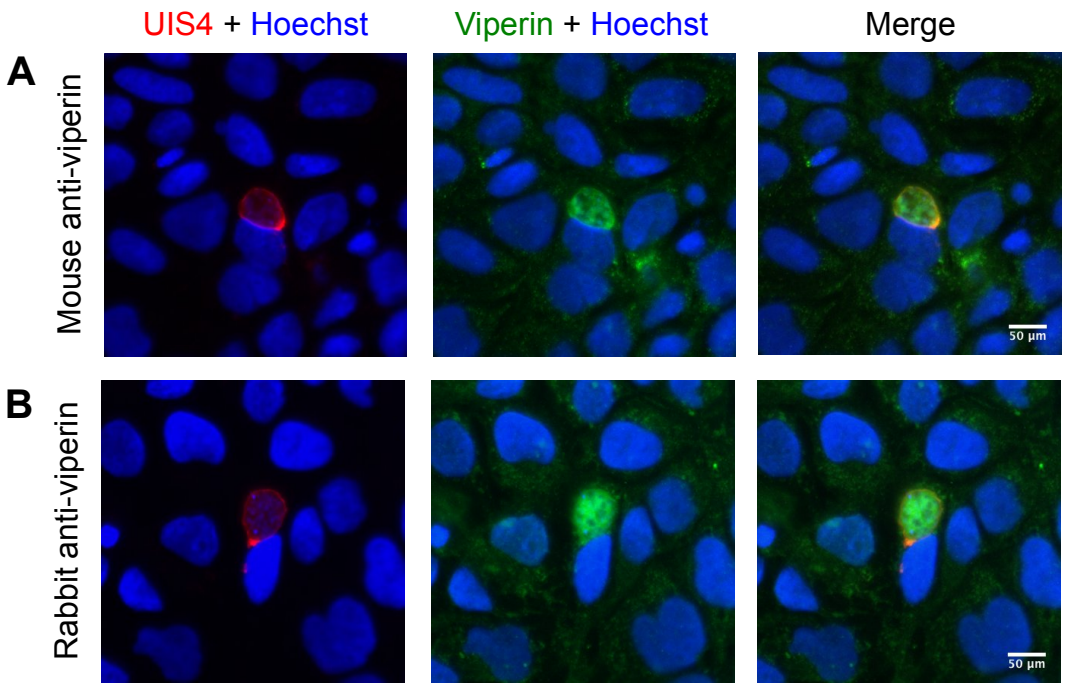


**Figure 6.2. *In vitro* Viperin protein localization relative to *P. berghei* parasites in *P. berghei*-infected Huh-7 cells.** Immunofluorescence of Huh-7 cells infected with $3\times10^4$ *P. berghei* ANKA spz and 4% PFA fixed at 42 hpi. Huh-7 cells were immunostained for *Pb*UIS4 and Viperin, with detection of stained structures with anti-goat 594 (red) and **(A)** anti-mouse 488 (green) or **(B)** anti-rabbit 488 (green), respectively. Nuclei were stained with Hoechst (blue) and representative images were acquired by widefield microscopy. Scale bars: 50 µm.

**- What are the Viperin domains involved in the antiparasitic effects?** The employment of Viperin constructs lacking each one of the protein's three domains may elucidate an important link between the structure of the protein and its involvement in the anti-*Plasmodium* activity. A panel of four Viperin mutants kindly provided by Dr. Michael Beard from the University of Adelaide, Australia, will allow us to analyse the impact of the truncation of the N-terminal (Viperin 5'Δ50), C-terminal (Viperin 3'Δ4) and the SAM domain (Viperin SAM1 and Viperin SAM1+2) on the potential antiparasitic effect of Viperin.

**- Does Viperin deficiency contribute to enhanced liver damage?** Apart from a direct impact on *Plasmodium* replication, through an yet undefined mechanism, Viperin deficiency can also have an impact on the histopathological status of the liver[90]. Thus, the histopathological analysis of the liver of *P. berghei*-infected *Viperin*$^{-/-}$ mice at each time point should provide an answer to this question.

**- Does the absence of Viperin influence the dynamics of the immune cell populations during the time course of infection?** The infection of *Viperin*$^{-/-}$ mice with *P. berghei* sporozoites and, at each time point, the isolation and purification of the liver leukocytes followed by the analysis of the proportion of each cell type through FACS analysis should uncover information capable of fulfil this aim.

**- What is the relative proportion of monocytes in the RAG2$^{-/-}$/γc$^{-/-}$ and RAG-2$^{-/-}$ mice at 84 hours post-*P. berghei* infection?** The infection of the RAG2$^{-/-}$/γc$^{-/-}$ and RAG-2$^{-/-}$ mice infected with *P.*

*berghei* sporozoites and, at each time point, the isolation and purification of the liver leukocytes followed by the analysis of the proportion of $CD11b^+$ $Ly6C^+$ monocytes through FACS analysis should fulfil this aim and provide data for an accurate correlation analysis between Viperin mRNA expression and proportion of these myeloid cells.

**- What is the impact of the depletion of monocytes on the profile of ISGs' expression observed in WT mice, especially at 84 hours post-*P. berghei* infection?** This question could be tackled by analysing the mRNA expression levels of the ISGs' panel in mice with an impaired recuitment of monocytes via anti-CCR2 antibody.

**- What is the impact of monocytes' ablation on *Plasmodium* liver reinfection?** In order to pursue this question, we should perform the reinfection model assay in monocytes-depleted mice in order to assess the role of these myeloid cells and, specifically of the Viperin-positive monocytes, activated and/or recruited by a primary *P. berghei*-liver stage infection in the context of the type I IFN response, in the impairment of a second sporozoite infection.

# 7. References


1. Dolby, K. *et al.* Malaria 1990–2009. *Portf. Rev.* 8 (2012).
2. World Health Organization (WHO). *World Malaria Report 2017* (2017).
3. White, N. J. Malaria. *Manson's Trop. Infect. Dis.* 532–600 (2014).
4. Brasil, P. *et al.* Outbreak of human malaria caused by Plasmodium simium in the Atlantic Forest in Rio de Janeiro: A molecular epidemiological investigation. *Lancet Glob. Heal.* (2017).
5. Key Facts | About Malaria | RBM. Available at: https://endmalaria.org/about-malaria/key-facts. (Accessed: 21st August 2018)
6. Prudêncio, M., Rodriguez, A. & Mota, M. M. The silent path to thousands of merozoites: The Plasmodium liver stage. *Nat. Rev. Microbiol.* **4,** 849–856 (2006).
7. Cowman, A. F., Healer, J., Marapana, D. & Marsh, K. Malaria: Biology and Disease. *Cell* **167,** 610–624 (2016).
8. Coppi, A. *et al.* Heparan sulfate proteoglycans provide a signal to Plasmodium sporozoites to stop migrating and productively invade host cells. *Cell Host Microbe* **2,** 316–327 (2007).
9. Zhao, J., Bhanot, P., Hu, J. & Wang, Q. A comprehensive analysis of Plasmodium circumsporozoite protein binding to hepatocytes. *PLoS One* **11,** 1–13 (2016).
10. Vaughan, A. M. & Kappe, S. H. I. Malaria Parasite Liver Infection and Exoerythrocytic Biology. *Cold Spring Harb Perspect Med*. 7:a025486 (2017).
11. Antinori, S., Galimberti, L., Milazzo, L. & Corbellino, M. Biology of human malaria plasmodia including Plasmodium knowlesi. *Mediterr. J. Hematol. Infect. Dis.* **4,** (2012).
12. Lindner, S. E., Miller, J. L. & Kappe, S. H. Malaria parasite pre-erythrocytic infection: preparation meets opportunity. *Cell Microbiol* **14,** 316–324 (2012).
13. Frischknecht, F. & Matuschewski, K. Plasmodium sporozoite biology. *Cold Spring Harb. Perspect. Med.* **7,** (2017).
14. Fonager, J. *et al.* Reduced CD36-dependent tissue sequestration of Plasmodium-infected erythrocytes is detrimental to malaria parasite growth in vivo. *J. Exp. Med.* **209,** 93–107 (2012).
15. Bannister, L. & Mitchell, G. The ins, outs and roundabouts of malaria. *Trends Parasitol.* **19,** 209–213 (2003).
16. Cowman, A. F. & Crabb, B. S. Invasion of red blood cells by malaria parasites. *Cell* **124,** 755–766 (2006).
17. McRobert, L. *et al.* Gametogenesis in malaria parasites is mediated by the cGMP-dependent protein kinase. *PLoS Biol.* **6,** 1243–1252 (2008).
18. Aly, A. S. I., Vaughan, A. M. & Kappe, S. H. I. Malaria parasite development in the mosquito and infection of the mammalian host. *Annu. Rev. Microbiol.* **63,** 195–221 (2009).
19. Alemu, A., Shiferaw, Y., Addis, Z., Mathewos, B. & Birhan, W. Effect of malaria on HIV/AIDS transmission and progression. *Parasites and Vectors* **6,** 1 (2013).
20. Snounou, G. Rapid, sensitive and cheap molecular diagnosis of malaria: is microscopy on the way out? *Future Microbiol.* **2,** 477–480 (2007).

21. Mouatcho, J. C. & Dean Goldring, J. P. Malaria rapid diagnostic tests: Challenges and prospects. *J. Med. Microbiol.* **62,** 1491–1505 (2013).
22. Snounou, G., Viriyakosol, S., Jarra, W., Thaithong, S. & Brown, K. N. Identification of the four human malaria parasite species in field samples by the polymerase chain reaction and detection of a high prevalence of mixed infections. *Mol. Biochem. Parasitol.* **58,** 283–92 (1993).
23. Brian De Souza, J., Hafalla, J. C. R., Riley, E. M. & Couper, K. N. Cerebral malaria: Why experimental murine models are required to understand the pathogenesis of disease. *Parasitology* **137,** 755–772 (2010).
24. Urquhart, A. D. Putative pathophysiological interactions of cytokines and phagocytic cells in severe human falciparum malaria. *Clin. Infect. Dis.* **19,** 117–131 (1994).
25. Mackintosh, C. L., Beeson, J. G. & Marsh, K. Clinical features and pathogenesis of severe malaria. *Trends Parasitol* **20,** 597–603 (2004).
26. Julius, M., Rebecca, W., Francis, K., Viviene, M. & Muregi, F. W. Cytokine levels associated with experimental malaria pathology during Plasmodium berghei ANKA infection in a mouse model. *J. Clin. Immunol. Immunopathol. Res.* **5,** 1–8 (2013).
27. Gun, S. Y. *et al.* Interferon Regulatory Factor 1 is essential for pathogenic CD8+ T cell migration and retention in the brain during experimental cerebral malaria. *Cell. Microbiol.* e12819 (2017).
28. Berendt, A. R., Simmons, D. L., Tansey, J., Newbold, C. I. & Marsh, K. Intercellular adhesion molecule-1 is an endothelial cell adhesion receptor for Plasmodium falciparum. *Nature* **341,** 57–59 (1989).
29. White, N. J. Primaquine to prevent transmission of falciparum malaria. *Lancet Infect Dis* **13,** 175–181 (2013).
30. White, N. J. *et al.* Assessment of therapeutic responses to gametocytocidal drugs in Plasmodium falciparum malaria. *Malar. J.* **13,** 483 (2014).
31. Langhorne, J., Ndungu, F. M., Sponaas, A.-M. & Marsh, K. Immunity to malaria: more questions than answers. *Nat. Immunol.* **9,** 725–32 (2008).
32. Khan, Z. M. & Vanderberg, J. P. Eosinophil-rich, granulomatous inflammatory response to Plasmodium berghei hepatic schizonts in nonimmunized rats is age-related. *Am. J. Trop. Med. Hyg.* **45,** 190–201 (1991).
33. Khan, Z. M. & Vanderberg, J. P. Specific inflammatory cell infiltration of hepatic schizonts in BALB/c mice immunized with attenuated plasmodium yoelii sporozoites. *Int. Immunol.* **4,** 711–718 (1992).
34. Isaacs, A. & Lindenmann, J. Virus Interference: I. The Interferon. *CA. Cancer J. Clin.* **38,** 280–290 (1988).
35. Ivashkiv, L. B. & Donlin, L. T. Regulation of type I interferon responses. *Nat. Rev. Immunol.* **14,** 36–49 (2015).
36. Mogensen, T. H. Pathogen recognition and inflammatory signaling in innate immune defenses. *Clin. Microbiol. Rev.* **22,** 240–273 (2009).

37. Majoros, A. *et al.* Canonical and non-canonical aspects of JAK-STAT signaling: Lessons from interferons for cytokine responses. *Front. Immunol.* **8,** (2017).
38. King, T. & Lamb, T. Interferon-γ: The Jekyll and Hyde of Malaria. *PLoS Pathog.* **11,** 8–13 (2015).
39. Jahiel, R. I., Vilcek, J. & Nussenzweig, R. S. Exogenous interferon protects mice against Plasmodium berghei malaria. *Nature* **227,** 1350–1351 (1970).
40. Portugal, S. *et al.* Host-mediated regulation of superinfection in malaria. *Nat Med* **17,** 732–737 (2011).
41. Liehl, P. *et al.* Host-cell sensors for Plasmodium activate innate immunity against liver-stage infection. *Nat. Med.* **20,** 47–53 (2014).
42. Miller, J. L., Sack, B. K., Baldwin, M., Vaughan, A. M. & Kappe, S. H. I. Interferon-Mediated Innate Immune Responses against Malaria Parasite Liver Stages. *Cell Rep.* **7,** 436–447 (2014).
43. Liehl, P. *et al.* Innate immunity induced by Plasmodium liver infection inhibits malaria reinfections. *Infect. Immun.* **83,** 1172–1180 (2015).
44. Tavares, J. *et al.* Role of host cell traversal by the malaria sporozoite during liver infection. *J Exp Med* **210,** 905–915 (2013).
45. Bongfen, S. E., Torgler, R., Romero, J. F., Renia, L. & Corradin, G. Plasmodium berghei-infected primary hepatocytes process and present the circumsporozoite protein to specific CD8+ T cells in vitro. *J. Immunol.* **178,** 7054–7063 (2007).
46. Scheller, L. F., Green, S. J. & Azad, A. F. Inhibition of nitric oxide interrupts the accumulation of CD8+ T cells surrounding Plasmodium berghei-infected hepatocytes. *Infect. Immun.* **65,** 3882–3888 (1997).
47. Sun, P. *et al.* Protective Immunity induced with malaria vaccine, RTS,S, is linked to Plasmodium falciparum Circumsporozoite Protein-specific CD4+ and CD8+ T cells producing IFN-gamma. *J. Immunol.* (2012).
48. Tsuji, M. & Zavala, F. T cells as mediators of protective immunity against liver stages of Plasmodium. *Trends Parasitol.* **19,** 88–93 (2003).
49. Rodrigues, M., Nussenzweig, R. S. & Zavala, F. The relative contribution of antibodies, CD4+ and CD8+ T cells to sporozoite-induced protection against malaria. *Immunology* **80,** 1–5 (1993).
50. Tsuji, M. *et al.* γδ T cells contribute to immunity against the liver stages of malaria in αβ T-cell-deficient mice. *Proc. Natl. Acad. Sci. U. S. A.* **91,** 345–349 (1994).
51. McKenna, K. C. *et al.* γδ T cells are a component of early immunity against preerythrocytic malaria parasites. *Infect. Immun.* **68,** 2224–2230 (2000).
52. Godfrey, D. I., MacDonald, H. R., Kronenberg, M., Smyth, M. J. & Van Kaer, L. NKT cells: What's in a name? *Nat. Rev. Immunol.* **4,** 231–237 (2004).
53. Gonzalez-Aseguinolaza, G. *et al.* α-galactosylceramide-activated Vα 14 natural killer T cells mediate protection against murine malaria. *Proc. Natl. Acad. Sci. U. S. A.* **97,** 8461–8466 (2000).

54. Artavanis-Tsakonas, K., Tongren, J. E. & Riley, E. M. The war between the malaria parasite and the immune system: Immunity, immunoregulation and immunopathology. *Clin. Exp. Immunol.* **133,** 145–152 (2003).
55. Hahn, W. O., Gale, M. J., Stetson, D., Liles, W. C. & Pepper, M. The role of Type I and Type II Interferon in the adaptive response to blood stage malaria infection. *J. Immunol.* **196,** 131.19 LP-131.19 (2016).
56. Gazzinelli, R. T., Kalantari, P., Fitzgerald, K. A. & Golenbock, D. T. Innate sensing of malaria parasites. *Nat. Rev. Immunol.* **14,** 744–757 (2014).
57. Sharma, S. *et al.* Innate Immune Recognition of an AT-Rich Stem-Loop DNA Motif in the Plasmodium falciparum Genome. *Immunity* **35,** 194–207 (2011).
58. Yu, X. *et al.* Cross-Regulation of Two Type I Interferon Signaling Pathways in Plasmacytoid Dendritic Cells Controls Anti-malaria Immunity and Host Mortality. *Immunity* **45,** 1093–1107 (2016).
59. Spaulding, E. *et al.* STING-Licensed Macrophages Prime Type I IFN Production by Plasmacytoid Dendritic Cells in the Bone Marrow during Severe Plasmodium yoelii Malaria. *PLoS Pathog.* **12,** 1–29 (2016).
60. Haque, A. *et al.* ._Type I IFN signaling in CD8˙ DCs impairs Th1-depedent malaria immunity. *J Clin Invest.* **124,** 1–14 (2014).
61. Beiting, D. P. Protozoan parasites and type I interferons: A cold case reopened. *Trends Parasitol.* **30,** 491–498 (2014).
62. Vigário, A. M. *et al.* Inhibition of Plasmodium yoelii blood-stage malaria by interferon α through the inhibition of the production of its target cell, the reticulocyte. *Blood* **97,** 3966–3971 (2001).
63. Vigário, A. M. *et al.* Recombinant Human IFN-α Inhibits Cerebral Malaria and Reduces Parasite Burden in Mice. *J. Immunol.* **178,** 6416–6425 (2007).
64. Voisine, C., Mastelic, B., Sponaas, A. M. & Langhorne, J. Classical CD11c+ dendritic cells, not plasmacytoid dendritic cells, induce T cell responses to Plasmodium chabaudi malaria. *Int. J. Parasitol.* **40,** 711–719 (2010).
65. Sebina, I. *et al.* IFNAR1-Signalling Obstructs ICOS-mediated Humoral Immunity during Non-lethal Blood-Stage Plasmodium Infection. *PLoS Pathog.* **12,** 1–26 (2016).
66. Zander, R. A. *et al.* Type I Interferons Induce T Regulatory 1 Responses and Restrict Humoral Immunity during Experimental Malaria. *PLoS Pathog.* **12,** 1–23 (2016).
67. Wu, J. *et al.* Strain-specific innate immune signaling pathways determine malaria parasitemia dynamics and host mortality. *Proc. Natl. Acad. Sci. U. S. A.* **111,** E511-20 (2014).
68. Palomo, J. *et al.* Type I interferons contribute to experimental cerebral malaria development in response to sporozoite or blood-stage Plasmodium berghei ANKA. *Eur. J. Immunol.* **43,** 2683–2695 (2013).
69. Aucan, C. *et al.* Interferon-alpha receptor-1 (IFNAR1) variants are associated with protection against cerebral malaria in The Gambia. *Genes Immun.* **4,** 275–282 (2003).
70. Haque, A. *et al.* Type I interferons suppress CD4 + T-cell-dependent parasite control during blood-stage Plasmodium infection. *Eur. J. Immunol.* **41,** 2688–2698 (2011).

71. Ball, E. A. *et al.* IFNAR1 Controls Progression to Cerebral Malaria in Children and CD8+ T Cell Brain Pathology in Plasmodium berghei-Infected Mice. *J. Immunol.* **190,** 5118–5127 (2013).
72. Chin, K.-C. & Cresswell, P. Viperin (cig5), an IFN-inducible antiviral protein directly induced by human cytomegalovirus. *Proc. Natl. Acad. Sci.* **98,** 15125–15130 (2001).
73. Duschene, K. S. & Broderick, J. B. The antiviral protein viperin is a radical SAM enzyme. *FEBS Lett.* **584,** 1263–1267 (2010).
74. Shaveta, G., Shi, J., Chow, V. T. K. & Song, J. Structural characterization reveals that viperin is a radical S-adenosyl-l-methionine (SAM) enzyme. *Biochem. Biophys. Res. Commun.* **391,** 1390–1395 (2010).
75. Fenwick, M. K., Li, Y., Cresswell, P., Modis, Y. & Ealick, S. E. Structural studies of viperin, an antiviral radical SAM enzyme. *Proc. Natl. Acad. Sci.* 201705402 (2017).
76. Helbig, K. J. *et al.* The antiviral protein viperin inhibits hepatitis C virus replication via interaction with nonstructural protein 5A. *Hepatology* **54,** 1506–1517 (2011).
77. Hinson, E. R. & Cresswell, P. The antiviral protein, viperin, localizes to lipid droplets via its N-terminal amphipathic alpha-helix. *Proc. Natl. Acad. Sci. U. S. A.* **106,** 20452–7 (2009).
78. Upadhyay, A. S. *et al.* Viperin is an iron-sulfur protein that inhibits genome synthesis of tick-borne encephalitis virus via radical SAM domain activity. *Cell. Microbiol.* **16,** 834–848 (2014).
79. Teng, T. *et al.* Viperin restricts chikungunya virus replication and pathology. *J. Clin. Invest.* **122,** (2012).
80. Helbig, K. J., Lau, D. T. Y., Semendric, L., Harley, H. A. J. & Beard, M. R. Analysis of ISG expression in chronic hepatitis C identifies viperin as a potential antiviral effector. *Hepatology* **42,** 702–710 (2005).
81. Van Der Hoek, K. H. *et al.* Viperin is an important host restriction factor in control of Zika virus infection. *Sci. Rep.* **7,** 1–14 (2017).
82. Helbig, K. J. *et al.* Viperin is induced following dengue virus type-2 (DENV-2) infection and has anti-viral actions requiring the C-terminal end of viperin. *PLoS Negl. Trop. Dis.* **7,** e2178 (2013).
83. Nasr, N. *et al.* HIV-1 infection of human macrophages directly induces viperin which inhibits viral production. *Blood*, **120,** 778–788 (2012).
84. Helbig, K. J. & Beard, M. R. The role of viperin in the innate antiviral response. *J. Mol. Biol.* **426,** 1210–1219 (2014).
85. Fitzgerald, K. a. The interferon inducible gene: Viperin. *J. Interferon Cytokine Res.* **31,** 131–5 (2011).
86. Severa, M., Coccia, E. M. & Fitzgerald, K. A. Toll-like receptor-dependent and -independent Viperin gene expression and counter-regulation by PRDI-binding factor-1/BLIMP1. *J. Biol. Chem.* **281,** 26188–26195 (2006).
87. Chan, Y.-L., Chang, T.-H., Liao, C.-L. & Lin, Y.-L. The Cellular Antiviral Protein Viperin Is Attenuated by Proteasome-Mediated Protein Degradation in Japanese Encephalitis Virus-Infected Cells. *J. Virol.* **82,** 10455–10464 (2008).
88. Seo, J.-Y., Yaneva, R. & Cresswell, P. Viperin: a multifunctional, interferon-inducible protein

that regulates virus replication. *Cell Host Microbe* **10,** 534–9 (2011).

89. Wang, S. *et al.* Viperin inhibits hepatitis C virus replication by interfering with binding of NS5A to host protein hVAP-33. *J. Gen. Virol.* **93,** 83–92 (2012).
90. Tan, K. Sen *et al.* In vivo and in vitro studies on the antiviral activities of viperin against influenza H1N1 virus infection. *J. Gen. Virol.* **93,** 1269–1277 (2012).
91. Wang, X., Hinson, E. R. & Cresswell, P. The interferon-inducible protein viperin inhibits influenza virus release by perturbing lipid rafts. *Cell Host Microbe* **2,** 96–105 (2007).
92. Szretter, K. J. *et al.* The Interferon-Inducible Gene viperin Restricts West Nile Virus Pathogenesis. *J. Virol.* **85,** 11557–11566 (2011).
93. Jumat, M. R. *et al.* Viperin protein expression inhibits the late stage of respiratory syncytial virus morphogenesis. *Antiviral Res.* **114,** 11–20 (2015).
94. McGillivary, G., Jordan, Z. B., Peeples, M. E. & Bakaletz, L. O. Replication of respiratory syncytial virus is inhibited by the host defense molecule viperin. *J. Innate Immun.* **5,** 60–71 (2013).
95. Khanlari, Z., Sabahi, F., Hosseini, S. Y. & Ghaderi, M. HCV NS3 blocking effect on IFN induced ISGs like viperin and IL28 with and without NS4A. *Hepat. Mon.* **14,** (2014).
96. Nasir, I. A., Yakubu, S. & Mustapha, J. O. Epidemiology and Synergistic Hepatopathology of Malaria and Hepatitis C Virus Coinfection. *Virol. Res. Treat.* **8,** (2017).
97. Gizzi, A. S. *et al.* A naturally occurring antiviral ribonucleotide encoded by the human genome. *Nature* (2018).
98. Qiu, L., Cresswell, P. & Chin, K. Viperin is required for optimal Th2 responses and T-cell receptor – mediated activation of NF- B and AP-1. *Response* **113,** 3520–3529 (2009).
99. Murphy, K. & Weaver, C. *Janeway's Immunobiology 9th Edition*. (2016).
100. Walker, J. A. & McKenzie, A. N. J. TH2 cell development and function. *Nat. Rev. Immunol.* **2,** (2017).
101. Saitoh, T. *et al.* Antiviral protein Viperin promotes Toll-like receptor 7- and Toll-like receptor 9-mediated type I interferon production in plasmacytoid dendritic cells. *Immunity* **34,** 352–63 (2011).
102. Siegal, F. P. The Nature of the Principal Type 1 Interferon-Producing Cells in Human Blood. *Science.* **284,** 1835–1837 (1999).
103. Seo, J.-Y., Cresswell, P., Hinson, E. R. & Yaneva, R. Human Cytomegalovirus directly induces the antiviral protein viperin to enhance infectivity. *Science.* **1093,** 1093–7 (2012).
104. Seo, J.-Y. & Cresswell, P. Viperin regulates cellular lipid metabolism during human cytomegalovirus infection. *PLoS Pathog.* **9,** e1003497 (2013).
105. Jiang, X. & Chen, Z. J. Viperin links Lipid bodies to immune defense. *Immunity* **34,** 285–287 (2011).
106. Albuquerque, S. S. *et al.* Host cell transcriptional profiling during malaria liver stage infection reveals a coordinated and sequential set of biological events. *BMC Genomics* **10,** (2009).
107. Deschermeier, C. *et al.* Mitochondrial lipoic acid scavenging is essential for Plasmodium berghei liver stage development. *Cell. Microbiol.* **14,** 416–30 (2012).

108. Itoe, M. A. *et al.* Host cell phosphatidylcholine is a key mediator of malaria parasite survival during liver stage infection. *Cell Host Microbe* **16,** 778–786 (2014).
109. Douradinha, B. G. *et al.* Visualisation and quantitative analysis of the rodent malaria liver stage by real time imaging. *PLoS One* **4,** e7881 (2009).
110. Miller, J. L. *et al.* Quantitative bioluminescent imaging of pre-erythrocytic malaria parasite infection using luciferase-expressing Plasmodium yoelii. *PLoS One* **8,** e60820 (2013).
111. Zuzarte-Luis, V., Sales-Dias, J. & Mota, M. M. Simple, sensitive and quantitative bioluminescence assay for determination of malaria pre-patent period. *Malar. J.* **13,** 15 (2014).
112. Schmittgen, T. D. & Livak, K. J. Analyzing real-time PCR data by the comparative CT method. *Nat. Protoc.* **3,** 1101–1108 (2008).
113. Schofield, L., Ferreira, A., Altszuler, R., Nussenzweig, V. & Nussenzweig, R. S. Interferon-gamma inhibits the intrahepatocytic development of malaria parasites in vitro. *J. Immunol.* **139,** 2020–2025 (1987).
114. Bogdanos, D. P., Gao, B. & Gershwin, M. E. Liver immunology. *Compr. Physiol.* **3,** 567–598 (2013).
115. Mazurier, F. *et al.* A Novel Immunodeficient Mouse Model-RAG2 gamma Cytokine Receptor Chain Double Mutants-Requiring Exogenous Cytokine Administration for Human Hematopoietic Stem Cell Engraftment Common. *J. Interf. Cytokine Res.* **19,** 533–541 (1999).
116. Shinkai, Y. *et al.* RAG-2-deficient mice lack mature lymphocytes owing to inability to initiate V(D)J rearrangement. *Cell* **68,** 855–867 (1992).
117. Belizário, J. E. Immunodeficient Mouse Models: An Overview. *Open Immunol. J.* **2,** 79–85 (2009).
118. Tanaka, T. *et al.* A novel monoclonal antibody against murine IL-2 receptor beta-chain. Characterization of receptor expression in normal lymphoid cells and EL-4 cells. *J. Immunol.* **147,** 2222–2228 (1991).
119. Schoenborn, J. R. & Wilson, C. B. Regulation of interferon-gamma during innate and adaptive immune responses. *Adv. Immunol.* **96,** 41–101 (2007).
120. Mills, C. D. M1 and M2 Macrophages: Oracles of Health and Disease. *Crit. Rev. Immunol.* **32,** 463–488 (2012).
121. Prudencio, M., Mota, M. M. & Mendes, A. M. A toolbox to study liver stage malaria. *Trends Parasitol* **27,** 565–574 (2011).
122. Itohara, S. *et al.* T cell receptor delta gene mutant mice: independent generation of alpha beta T cells and programmed rearrangements of gamma delta TCR genes. *Cell* **72,** 337–348 (1993).
123. Hinson, E. R. *et al.* Viperin Is Highly Induced in Neutrophils and Macrophages during Acute and Chronic Lymphocytic Choriomeningitis Virus Infection. *J. Immunol.* **184,** 5723–5731 (2010).
124. Holness, C. L. & Simmons, D. L. Molecular cloning of CD68, a human macrophage marker related to lysosomal glycoproteins. *Blood* **81,** 1607–13 (1993).
125. Gough, D. J. *et al.* Functional crosstalk between type I and II interferon through the regulated

expression of STAT1. *PLoS Biol.* **8,** (2010).

126. Besnard, A.-G. *et al.* IL-33-Mediated Protection against Experimental Cerebral Malaria Is Linked to Induction of Type 2 Innate Lymphoid Cells, M2 Macrophages and Regulatory T Cells. *PLOS Pathog.* **11,** 1–21 (2015).
127. Sheel, M. & Engwerda, C. R. The diverse roles of monocytes in inflammation caused by protozoan parasitic diseases. *Trends Parasitol.* **28,** 408–416 (2012).
128. Cohen, S. B. *et al.* CXCR3-Dependent CD4+T Cells Are Required to Activate Inflammatory Monocytes for Defense against Intestinal Infection. *PLoS Pathog.* **9,** (2013).
129. Fujimura, N. *et al.* CCR2 inhibition sequesters multiple subsets of leukocytes in the bone marrow. *Sci. Rep.* **5,** 11664 (2015).
130. Dunay, I. R. *et al.* Gr1+Inflammatory Monocytes Are Required for Mucosal Resistance to the Pathogen Toxoplasma gondii. *Immunity* **29,** 306–317 (2008).
131. Goncalves, R., Zhang, X., Cohen, H., Debrabant, A. & Mosser, D. M. Platelet activation attracts a subpopulation of effector monocytes to sites of *Leishmania major* infection. *J. Exp. Med.* **208,** 1253–1265 (2011).
132. Sponaas, A. *et al.* Migrating monocytes recruited to the spleen play an important role in control of blood stage malaria. *Blood,* **114,** 5522–5531 (2014).
133. Bosschaerts, T. *et al.* Tip-DC development during parasitic infection is regulated by IL-10 and requires CCL2/CCR2, IFN-γ and MyD88 signaling. *PLoS Pathog.* **6,** 35–36 (2010).
134. Palomino, D. C. T. & Marti, L. C. Chemokines and immunity. *Einstein (São Paulo)* **13,** 469–473 (2015).
135. Shi, C. & Pamer, E. G. Monocyte Recruitment During Infection and Inflammation. *Nat Rev Immunol* **11,** 762–774 (2014).
136. Zouggari, Y. & Mallat, Z. B Lymphoctes trigger monocyte mobilization and impair heart function after acute myocardial infarction. *Nat. Med.* **19,** 1273–1280 (2014).
137. Schulthess, J. *et al.* Interleukin-15-Dependent NKp46+Innate Lymphoid Cells Control Intestinal Inflammation by Recruiting Inflammatory Monocytes. *Immunity* **37,** 108–121 (2012).
138. Lee, P. Y. *et al.* Type I interferon modulates monocyte recruitment and maturation in chronic inflammation. *Am. J. Pathol.* **175,** 2023–2033 (2009).
139. Zhou, Z. *et al.* Type III Interferon (IFN) Induces a Type I IFN-Like Response in a Restricted Subset of Cells through Signaling Pathways Involving both the Jak-STAT Pathway and the Mitogen-Activated Protein Kinases. *J. Virol.* **81,** 7749–7758 (2007).
140. Hinson, E. R. & Cresswell, P. The N-terminal amphipathic α-helix of viperin mediates localization to the cytosolic face of the endoplasmic reticulum and inhibits protein secretion. *J. Biol. Chem.* **284,** 4705–4712 (2009).

# 8. Appendices

**Supplementary Table 1.** *P*-values and number (*n*) of animals used for each condition according to each figure.

| **Fig.4.1A** | | IFN-α | **Fig.4.1B** | | IFN-β | **Fig.4.1C** | | IFN-γ |
|---|---|---|---|---|---|---|---|---|
| wt | NI (n=10) | 0.0180 * | wt | NI (n=10) | 0.0393 * | wt | NI (n=10) | 0.7425 ns |
| | 42h (n=6) | | | 42h (n=6) | | | 42h (n=6) | |
| | NI (n=10) | 0.0041 ** | | NI (n=10) | 0.0138 * | | NI (n=10) | 0.8379 ns |
| | 48h (n=6) | | | 48h (n=6) | | | 48h (n=6) | |
| | NI (n=10) | 0.0002 *** | | NI (n=10) | 0.0004 *** | | NI (n=10) | 0.0237 * |
| | 60h (n=6) | | | 60h (n=6) | | | 60h (n=6) | |
| | NI (n=10) | 0.0026 ** | | NI (n=10) | 0.0035 ** | | NI (n=10) | 0.0005 *** |
| | 72h (n=6) | | | 72h (n=6) | | | 72h (n=6) | |
| | NI (n=10) | 0.0041 ** | | NI (n=10) | 0.0059 ** | | NI (n=10) | <0.0001 **** |
| | 84h n=6) | | | 84h n=6) | | | 84h n=6) | |
| | NI (n=10) | 0.066 ** | | NI (n=10) | 0.0090 ** | | NI (n=10) | <0.0001 **** |
| | 96h (n=6) | | | 96h (n=6) | | | 96h (n=6) | |
| **Fig.4.1D** | | Ifit-1 | Ifi44 | Usp18 | Ifit3 | Irf7 | Viperin | |
| wt | NI (n=10) | 0.0006 *** | <0.0001 **** | 0.0017 ** | 0.2124 ns | 0.0192 * | 0.0007 *** | |
| | 42h (n=6) | | | | | | | |
| | NI (n=10) | 0.0046 ** | 0.0007 *** | 0.3039 ns | 0.0311 * | 0.0018 ** | 0.7098 ns | |
| | 48h (n=6) | | | | | | | |
| | NI (n=10) | 0.0459 * | 0.0069 ** | 0.6130 ns | 0.0430 * | 0.0078** | 0.0841 ns | |
| | 60h (n=6) | | | | | | | |
| | NI (n=10) | 0.0019 ** | 0.0004 *** | 0.0044 ** | <0.0001 **** | <0.0001 **** | 0.0133 * | |
| | 72h (n=6) | | | | | | | |
| | NI (n=10) | <.0.0001 **** | <0.0001 **** | <0.0001 **** | <0.0001 **** | 0.0004 *** | <0.0001 **** | |
| | 84h n=6) | | | | | | | |
| | NI (n=10) | 0.010 *** | 0.0010 *** | 0.0168 * | 0.008 *** | 0.0004 *** | 0.0357 * | |
| | 96h (n=6) | | | | | | | |
| **Fig.4.2A** | | IFN-α | **Fig.4.2B** | | IFN-α | **Fig.4.2C** | | IFN-α |
| wt | NI (n=10) | 0.0180 * | $Rag2^{-/-}\gamma c^{-/-}$ | NI (n=4) | 0.7000 ns | $Rag2^{-/-}$ | NI (n=6) | 0.2616 ns |
| | 42h (n=6) | | | 42h (n=3) | | | 42h (n=6) | |
| wt | NI (n=10) | 0.0041 ** | $Rag2^{-/-}\gamma c^{-/-}$ | NI (n=4) | 0.7000 ns | $Rag2^{-/-}$ | NI (n=6) | 0.4531 ns |
| | 48h (n=6) | | | 48h (n=3) | | | 48h (n=6) | |
| wt | NI (n=10) | 0.0002 *** | $Rag2^{-/-}\gamma c^{-/-}$ | NI (n=4) | 0.8000 ns | $Rag2^{-/-}$ | NI (n=6) | 0.1850 ns |
| | 60h (n=6) | | | 60h (n=2) | | | 60h (n=6) | |
| wt | NI (n=10) | 0.0026 ** | $Rag2^{-/-}\gamma c^{-/-}$ | NI (n=4) | >0.9999 ns | $Rag2^{-/-}$ | NI (n=6) | 0.2115 ns |
| | 72h (n=6) | | | 72h (n=3) | | | 72h (n=6) | |
| wt | NI (n=10) | 0.0041 ** | $Rag2^{-/-}\gamma c^{-/-}$ | NI (n=4) | 0.4000 ns | $Rag2^{-/-}$ | NI (n=6) | 0.3515 ns |
| | 84h n=6) | | | 84h n=3) | | | 84h n=6) | |
| wt | NI (n=10) | 0.066 ** | $Rag2^{-/-}\gamma c^{-/-}$ | NI (n=4) | >0.9999 ns | $Rag2^{-/-}$ | NI (n=6) | 0.3723 ns |
| | 96h (n=6) | | | 96h (n=3) | | | 96h (n=6) | |
| **Fig.4.2D** | | IFN-β | **Fig.4.2E** | | IFN-β | **Fig.4.2F** | | IFN-β |
| wt | NI (n=10) | 0.0393 * | $Rag2^{-/-}\gamma c^{-/-}$ | NI (n=4) | 0.0571 ns | $Rag2^{-/-}$ | NI (n=6) | 0.1654 ns |
| | 42h (n=6) | | | 42h (n=3) | | | 42h (n=6) | |
| | NI (n=10) | 0.0138 * | | NI (n=4) | 0.1143 ns | | NI (n=6) | 0.2522 ns |
| | 48h (n=6) | | | 48h (n=3) | | | 48h (n=6) | |
| | NI (n=10) | 0.0004 *** | | NI (n=4) | 0.2667 ns | | NI (n=6) | 0.1948 ns |
| | 60h (n=6) | | | 60h (n=2) | | | 60h (n=6) | |
| | NI (n=10) | 0.0035 ** | | NI (n=4) | 0.2286 ns | | NI (n=6) | 0.1352 ns |
| | 72h (n=6) | | | 72h (n=3) | | | 72h (n=6) | |
| | NI (n=10) | 0.0059 ** | | NI (n=4) | 0.8571 ns | | NI (n=6) | 0.1588 ns |
| | 84h n=6) | | | 84h n=3) | | | 84h n=6) | |
| | NI (n=10) | 0.0090 ** | | NI (n=4) | 0.1143 ns | | NI (n=6) | 0.2139 ns |
| | 96h (n=6) | | | 96h (n=3) | | | 96h (n=6) | |

| **Fig.4.2G** | | IFN-γ | **Fig.4.2H** | | IFN-γ | **Fig.4.2I** | | IFN-γ |
|---|---|---|---|---|---|---|---|---|
| wt | NI (n=10) | 0.7425 ns | $Rag2^{-/-}\gamma c^{-/-}$ | NI (n=4) | 0.1143 ns | $Rag2^{-/-}$ | NI (n=6) | 0.8926 ns |
| | 42h (n=6) | | | 42h (n=3) | | | 42h (n=6) | |
| | NI (n=10) | 0.8379 ns | | NI (n=4) | 0.6286 ns | | NI (n=6) | 0.1042 ns |
| | 48h (n=6) | | | 48h (n=3) | | | 48h (n=6) | |
| | NI (n=10) | 0.0237 * | | NI (n=4) | >0.9999 ns | | NI (n=6) | 0.2311 ns |
| | 60h (n=6) | | | 60h (n=2) | | | 60h (n=6) | |
| | NI (n=10) | 0.0005 *** | | NI (n=4) | 0.0571 ns | | NI (n=6) | 0.0095 ** |
| | 72h (n=6) | | | 72h (n=3) | | | 72h (n=6) | |
| | NI (n=10) | <0.0001 **** | | NI (n=4) | 0.2286 ns | | NI (n=6) | 0.1723 ns |
| | 84h n=6) | | | 84h n=3) | | | 84h n=6) | |
| | NI (n=10) | <0.0001 **** | | NI (n=4) | 0.0571 ns | | NI (n=6) | 0.6150 ns |
| | 96h (n=6) | | | 96h (n=3) | | | 96h (n=6) | |

| **Fig.4.2J** | | Ifit-1 | Ifi44 | Usp18 | Ifit3 | Irf7 | Viperin | |
|---|---|---|---|---|---|---|---|---|
| wt | NI (n=10) | 0.0006 *** | <0.0001 **** | 0.0017 ** | 0.2124 ns | 0.0192 * | 0.0007 *** | |
| | 42h (n=6) | | | | | | | |
| | NI (n=10) | 0.0046 ** | 0.0007 *** | 0.3039 ns | 0.0311 * | 0.0018 ** | 0.7098 ns | |
| | 48h (n=6) | | | | | | | |
| | NI (n=10) | 0.0459 * | 0.0069 ** | 0.6130 ns | 0.0430 * | 0.0078** | 0.0841 ns | |
| | 60h (n=6) | | | | | | | |
| | NI (n=10) | 0.0019 ** | 0.0004 *** | 0.0044 ** | <0.0001 **** | <0.0001 **** | 0.0133 * | |
| | 72h (n=6) | | | | | | | |
| | NI (n=10) | <.0.0001 **** | <0.0001 **** | <0.0001 **** | <0.0001 **** | 0.0004 *** | <0.0001 **** | |
| | 84h n=6) | | | | | | | |
| | NI (n=10) | 0.010 *** | 0.0010 *** | 0.0168 * | 0.008 *** | 0.0004 *** | 0.0357 * | |
| | 96h (n=6) | | | | | | | |

| **Fig.4.2K** | | Ifit-1 | Ifi44 | Usp18 | Ifit3 | Irf7 | Viperin | Average of all genes |
|---|---|---|---|---|---|---|---|---|
| $Rag2^{-/-}\gamma c^{-/-}$ | NI (n=4) | 0.0571 ns | 0.0571 ns | 0.0571 ns | 0.0571 ns | 0.4000 ns | 0.1143 ns | <0.0001 *** |
| | 42h (n=3) | | | | | | | |
| | NI (n=4) | 0.0571 ns | 0.0571 ns | 0.0571 ns | 0.4000 ns | 0.1143 ns | 0.6286 ns | <0.0001 *** |
| | 48h (n=3) | | | | | | | |
| | NI (n=4) | 0.1333 ns | 0.1333 ns | 0.8000 ns | 0.8000 ns | 0.8000 ns | 0.1333 ns | 0.0071 ** |
| | 60h (n=2) | | | | | | | |
| | NI (n=4) | 0.0571 ns | 0.0571 ns | 0.4000 ns | 0.0571 ns | 0.6286 ns | 0.0571 ns | <0.0001 *** |
| | 72h (n=3) | | | | | | | |
| | NI (n=4) | 0.4000 ns | 0.8571 ns | 0.4000 ns | 0.6286 ns | 0.6286 ns | 0.4000 ns | 0.0739 ns |
| | 84h n=3) | | | | | | | |
| | NI (n=4) | 0.4000 ns | >0.9999 ns | 0.8571 ns | 0.8571 ns | >0.9999 ns | 0.8571 ns | 0.9299 ns |
| | 96h (n=3) | | | | | | | |

| **Fig.4.2L** | | Ifit-1 | Ifi44 | Usp18 | Ifit3 | Irf7 | Viperin | Average of all genes |
|---|---|---|---|---|---|---|---|---|
| $Rag2^{-/-}$ | NI (n=6) | 0.0052 ** | 0.0147 * | 0.0117 * | 0.0045 ** | 0.4227 ns | 0.0045 ** | <0.0001 *** |
| | 42h (n=6) | | | | | | | |
| | NI (n=6) | 0.7967 ns | 0.1224 ns | 0.8678 ns | 0.1276 ns | 0.1643 ns | 0.1185 ns | 0.0603 ns |
| | 48h (n=6) | | | | | | | |
| | NI (n=6) | 0.1556 ns | 0.0673 ns | 0.9482 ns | 0.0941 ns | 0.7466 ns | 0.0004 *** | 0.0003 *** |
| | 60h (n=6) | | | | | | | |
| | NI (n=6) | 0.0032 ** | 0.0059 ** | 0.0019 ** | 0.0007 *** | 0.0002 *** | 0.0023 ** | <0.0001 *** |
| | 72h (n=6) | | | | | | | |
| | NI (n=6) | 0.0814 ns | 0.1121 ns | 0.0856 ns | 0.0597 ns | 0.0389 * | 0.0107 * | <0.0001 *** |
| | 84h n=6) | | | | | | | |
| | NI (n=6) | 0.1365 ns | 0.0708 ns | 0.1218 ns | 0.0943 ns | 0.0574 | 0.6087 ns | 0.0003 *** |
| | 96h (n=6) | | | | | | | |

| **Fig.4.3A** | | IFN-α | **Fig.4.3B** | | IFN-β | **Fig.4.3C** | | IFN-γ |
|---|---|---|---|---|---|---|---|---|
| NK-depleted | NI (n=3) | >0.9999 ns | NK-depleted | NI (n=3) | 0.8000 ns | NK-depleted | NI (n=3) | 0.2000 ns |
| | 42h (n=3) | | | 42h (n=3) | | | 42h (n=3) | |
| | NI (n=3) | >0.9999 ns | | NI (n=3) | >0.9999 ns | | NI (n=3) | 0.4000 ns |
| | 48h (n=3) | | | 48h (n=3) | | | 48h (n=3) | |
| | NI (n=3) | 0.8000 ns | | NI (n=3) | 0.8000 ns | | NI (n=3) | >0.9999 ns |
| | 60h (n=3) | | | 60h (n=3) | | | 60h (n=3) | |
| | NI (n=3) | 0.3333 ns | | NI (n=3) | 0.3333 ns | | NI (n=3) | 0.2000 ns |
| | 72h (n=3) | | | 72h (n=3) | | | 72h (n=3) | |
| | NI (n=3) | 0.8000 ns | | NI (n=3) | 0.8000 ns | | NI (n=3) | 0.2000 ns |
| | 84h n=3) | | | 84h n=3) | | | 84h n=3) | |
| | NI (n=3) | >0.9999 ns | | NI (n=3) | 0.8000 ns | | NI (n=3) | 0.4000 ns |
| | 96h (n=3) | | | 96h (n=3) | | | 96h (n=3) | |

| **Fig.4.3D** | | Ifit-1 | Ifi44 | Usp18 | Ifit3 | Irf7 | Viperin | Average of all genes |
|---|---|---|---|---|---|---|---|---|
| NK-depleted | NI (n=3) | 0.2000 ns | 0.2000 ns | 0.2000 ns | 0.2000 ns | 0.8000 ns | 0.4000 ns | <0.0001 **** |
| | 42h (n=3) | | | | | | | |
| | NI (n=3) | 0.8000 ns | 0.4000 ns | 0.8000 ns | >0.9999 ns | >0.9999 ns | >0.9999 ns | 0.4150 ns |
| | 48h (n=3) | | | | | | | |
| | NI (n=3) | 0.4000 ns | >0.9999 ns | 0.8000 ns | >0.9999 ns | >0.9999 ns | 0.8000 ns | 0.9171 ns |
| | 60h (n=3) | | | | | | | |
| | NI (n=3) | 0.2000 ns | 0.2000 ns | 0.2000 ns | 0.2000 ns | 0.2000 ns | 0.2000 ns | <0.0001 **** |
| | 72h (n=3) | | | | | | | |
| | NI (n=3) | 0.2000 ns | 0.2000 ns | 0.2000 ns | 0.2000 ns | 0.2000 ns | 0.2000 ns | <0.0001 **** |
| | 84h n=3) | | | | | | | |
| | NI (n=3) | 0.2000 ns | 0.2000 ns | 0.2000 ns | 0.2000 ns | 0.4000 ns | 0.4000 ns | <0.0001 **** |
| | 96h (n=3) | | | | | | | |

| **Fig.4.4A** | | Viperin | **Fig.4.4B** | | Viperin | **Fig.4.4C** | | Viperin |
|---|---|---|---|---|---|---|---|---|
| wt | NI (n=10) | 0.0007 *** | $Rag2^{-/-}\gamma c^{-/-}$ | NI (n=4) | 0.1143 ns | $Rag2^{-/-}$ | NI (n=6) | 0.0045 ** |
| | 42h (n=6) | | | 42h (n=3) | | | 42h (n=6) | |
| | NI (n=10) | 0.7098 ns | | NI (n=4) | 0.6286 ns | | NI (n=6) | 0.1185 ns |
| | 48h (n=6) | | | 48h (n=3) | | | 48h (n=6) | |
| | NI (n=10) | 0.0841 ns | | NI (n=4) | 0.1333 ns | | NI (n=6) | 0.0004 *** |
| | 60h (n=6) | | | 60h (n=2) | | | 60h (n=6) | |
| | NI (n=10) | 0.0133 * | | NI (n=4) | 0.0571 ns | | NI (n=6) | 0.0023 ** |
| | 72h (n=6) | | | 72h (n=3) | | | 72h (n=6) | |
| | NI (n=10) | <0.0001 **** | | NI (n=4) | 0.4000 ns | | NI (n=6) | 0.0107 * |
| | 84h n=6) | | | 84h n=3) | | | 84h n=6) | |
| | NI (n=10) | 0.0357 * | | NI (n=4) | 0.8571 ns | | NI (n=6) | 0.6087 ns |
| | 96h (n=6) | | | 96h (n=3) | | | 96h (n=6) | |

| **Fig.4.5B** | |
|---|---|
| *Viperin*$^{+/+}$ (n=2) | 0.3333 ns |
| *Viperin*$^{+/-}$ (n=2) | |
| *Viperin*$^{+/+}$ (n=2) | 0.3333 ns |
| *Viperin*$^{-/-}$ (n=2) | |
| **Fig.4.5C** | |
| I (n=10) | 0.1457 ns |
| Irradiation (n=8) | |
| **Fig.4.5D** | |
| I (n=8) | 0.0002 *** |
| *Ifnar*$^{-/-}$ (n=8) | |

| **Fig.4.7A** | | Viperin | **Fig.4.7B** | | Viperin | **Fig.4.7C** | | Viperin |
|---|---|---|---|---|---|---|---|---|
| wt | NI (n=10) | 0.0007 *** | NK-depleted | NI (n=3) | 0.4000 ns | $TCRd^{-/-}$ | NI (n=4) | 0.0571 ns |
| | 42h (n=6) | | | 42h (n=3) | | | 42h (n=3) | |
| | NI (n=10) | <0.0001 **** | | NI (n=3) | 0.2000 ns | | NI (n=4) | 0.0571 ns |
| | 84h (n=6) | | | 84h (n=3) | | | 84h (n=3) | |
| **Fig.4.10A** | | CD68 | **Fig.4.10B** | | CD68 | **Fig.4.10C** | | CD68 |
| wt | NI (n=3) | 0.0714 ns | $Rag2^{-/-}\gamma c^{-/-}$ | NI (n=4) | 0.2286 ns | $Rag2^{-/-}$ | NI (n=6) | 0.6594 ns |
| | 42h (n=3) | | | 42h (n=3) | | | 42h (n=6) | |
| | NI (n=3) | 0.03570 * | | NI (n=4) | 0.6286 ns | | NI (n=6) | 0.1336 ns |
| | 48h (n=3) | | | 48h (n=3) | | | 48h (n=6) | |
| | NI (n=3) | 0.03570 * | | NI (n=4) | 0.2667 ns | | NI (n=6) | 0.6170 ns |
| | 60h (n=3) | | | 60h (n=2) | | | 60h (n=6) | |
| | NI (n=3) | 0.03570 * | | NI (n=4) | 0.6286 ns | | NI (n=6) | 0.0228 * |
| | 72h (n=3) | | | 72h (n=3) | | | 72h (n=6) | |
| | NI (n=3) | 0.03570 * | | NI (n=4) | 0.0571 ns | | NI (n=6) | <0.0001 **** |
| | 84h n=3) | | | 84h n=3) | | | 84h n=6) | |
| | NI (n=3) | 0.0952 ns | | NI (n=4) | >0.9999 ns | | NI (n=6) | 0.0421 * |
| | 96h (n=3) | | | 96h (n=3) | | | 96h (n=6) | |
| **Fig.4.11A** | | % of $CD11b^{+}Ly6C^{+}$ leukocytes | **Fig.4.11B** | | % of $CD11b^{+}Ly6C^{+}$ leukocytes | | | |
| NK-depleted | NI (n=3) | 0.1000 ns | $TCRd^{-/-}$ | NI (n=3) | 0.0571 ns | | | |
| | *Pb*-infected (n=3) | | | *Pb*-infected (n=3) | | | | |

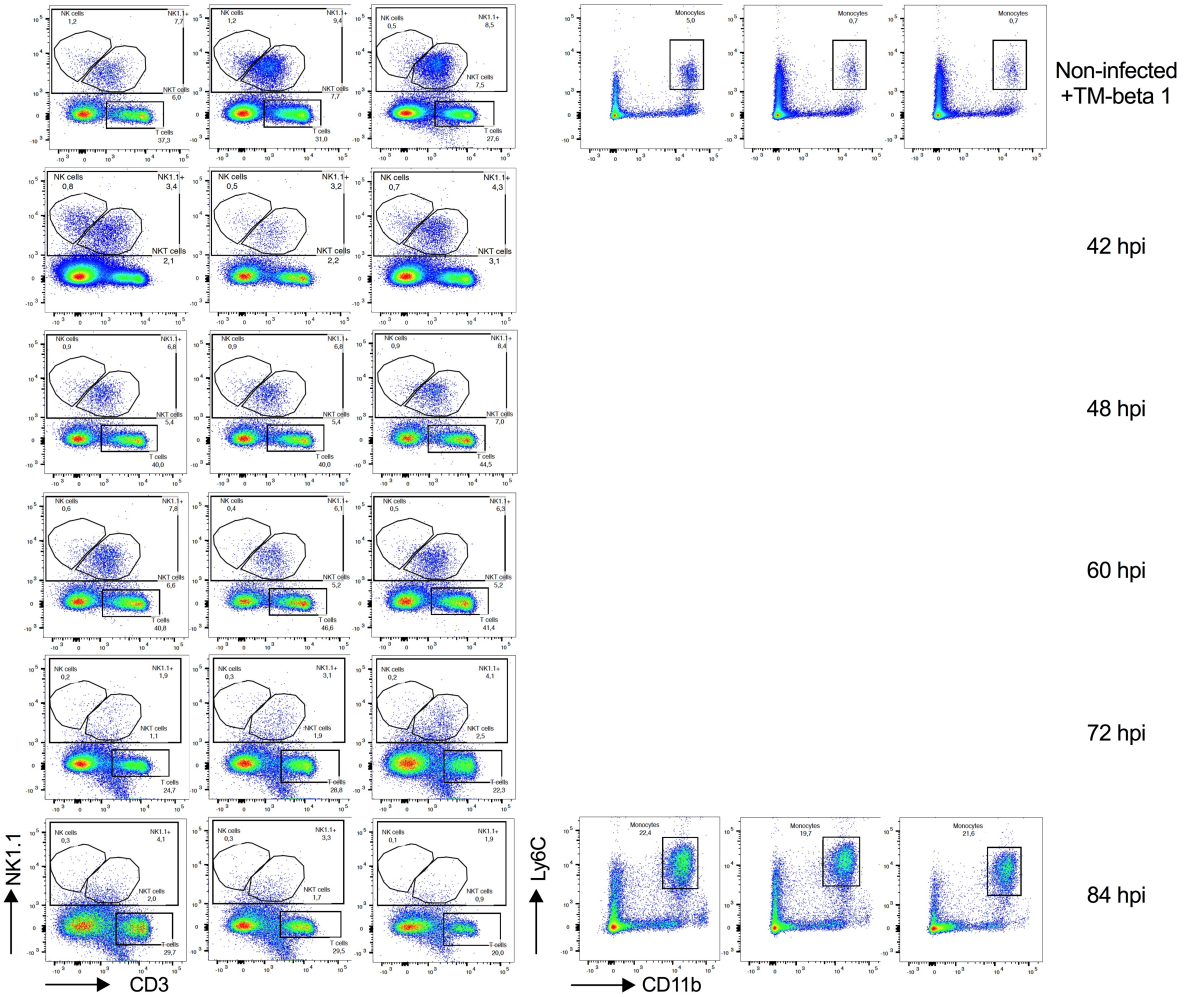


**Supplementary Figure 1. Flow cytometry analysis of the NK cell population depletion and inflammatory monocytes activated and/or recruited to the liver 84 hours post *P. berghei* infection.** Liver leukocytes were isolated at different times post-infection from *P. berghei*-infected WT mice treated with TM-beta 1 antibody. Cells were analysed for the expression of CD3 and NK1.1 as well as CD11b and Ly6C. Percentage of $NK1.1^{+}$, NK

cells ($CD3^-NK1.1^+$), NKT cells ($CD3^+NK1.1^+$), T cells ($CD3^+NK1.1^-$) and monocytes ($CD11b^+Ly6C^+$) are indicated within the respective gate. Each plot represents one individual from the indicated group on the right.

**Supplementary Table 2. Percentage of the NK cell population depletion assessed through flow cytometry.** Percentage of depletion of the NK cell population, including NK and NKT cells, assessed via flow cytometry in mice treated with TM-beta 1 antibody 2 hours post-infection with *P. berghei* ANKA spz. Non-infected mice treated with the same depleting antibody were used as controls.

| | Mouse nr. | % NK Depletion | % NKT Depletion | % (NK+NKT Depletion) |
|---|---|---|---|---|
| NI + TM-beta 1 | 1 | 84.4 | 79.6 | 77.2 |
| | 2 | 83.0 | 71.9 | 79.9 |
| | 3 | 91.7 | 54.0 | 63.4 |
| 42 hpi | 1 | 88.7 | 92.3 | 90.6 |
| | 2 | 92.0 | 92.0 | 91.2 |
| | 3 | 90.1 | 88.7 | 88.2 |
| 48 hpi | 1 | 92.9 | 88.3 | 88.4 |
| | 2 | 87.2 | 80.7 | 81.8 |
| | 3 | 84.4 | 75.2 | 77.2 |
| 60 hpi | 1 | 91.5 | 75.9 | 78.5 |
| | 2 | 94.3 | 81.0 | 83.2 |
| | 3 | 92.9 | 81.0 | 82.7 |
| 72 hpi | 1 | 96.7 | 93.3 | 91.8 |
| | 2 | 95.0 | 88.3 | 86.6 |
| | 3 | 96.7 | 84.7 | 82.3 |
| 84 hpi | 1 | 95.0 | 87.7 | 82.3 |
| | 2 | 95.0 | 89.6 | 85.8 |
| | 3 | 98.3 | 94.5 | 91.8 |

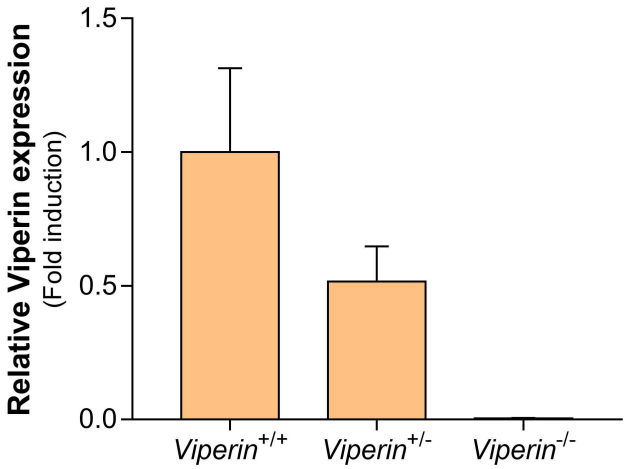


**Supplementary Figure 2. Relative Viperin mRNA expression analysed through qRT-PCR in each mouse genotype (*Viperin*$^{+/+}$, *Viperin*$^{+/-}$ and *Viperin*$^{-/-}$).** Viperin mRNA expression in whole liver extracts of *Viperin*$^{+/+}$, *Viperin*$^{+/-}$ and *Viperin*$^{-/-}$ mice infected with $3\times10^4$ *P. berghei* ANKA spz and euthanized at 42 hpi. The relative Viperin expression was analysed through qRT-PCR. Data are expressed as means ± SD of the results of two independent experiments for the WT (*n* = 2 per condition).

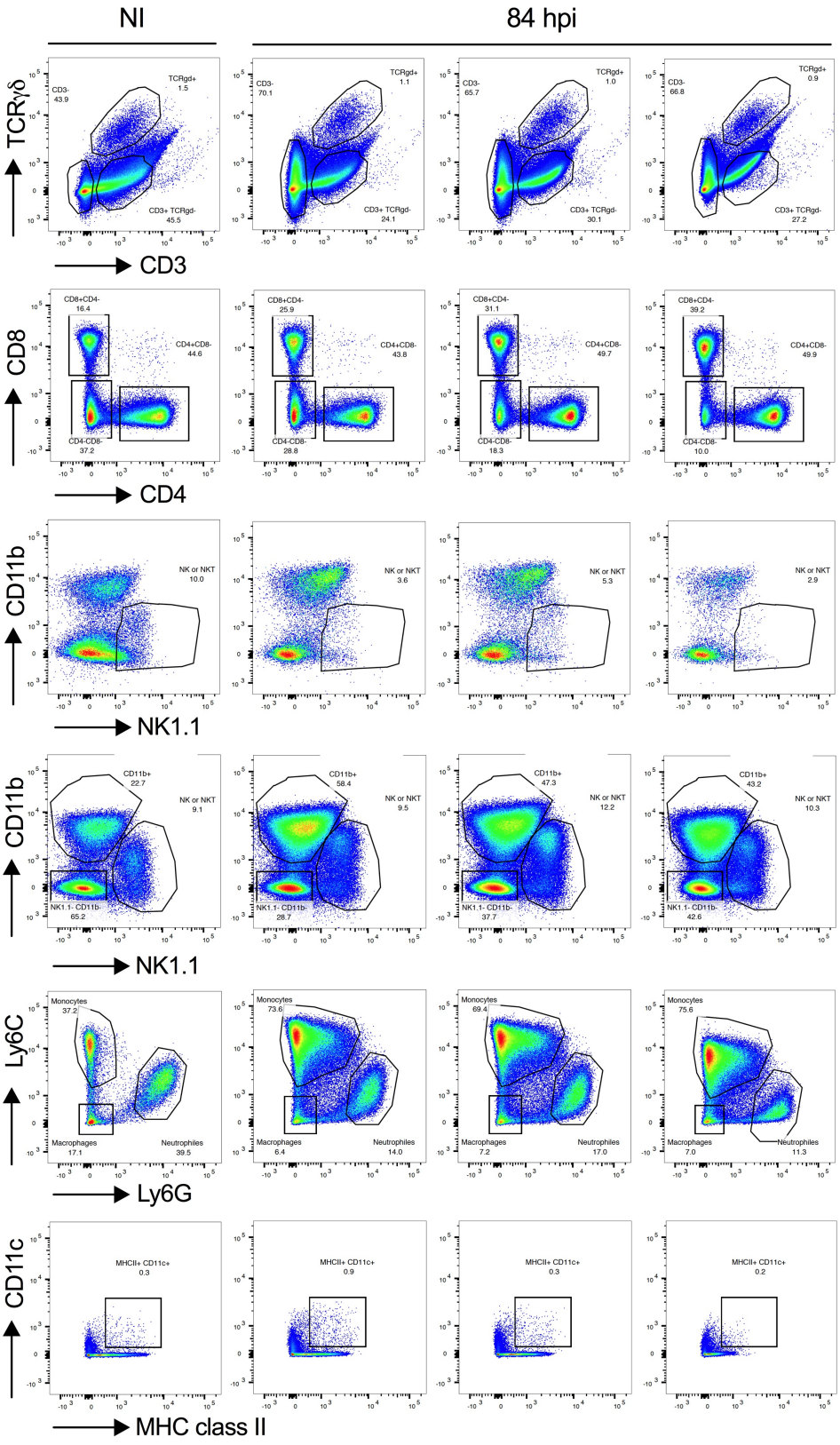


**Supplementary Figure 3. Flow cytometry analysis of liver leukocytes activated and/or recruited to the liver 84 hours post *P. berghei* infection.** Liver leukocytes were isolated from WT mice infected with $3\times10^4$ *P. berghei* ANKA spz and analysed for the identification of the following staining patterns: γδ T cells ($CD3^+TCR\ \gamma\delta^+$), CD4 helper T cells ($CD3^+TCR\ \gamma\delta^-CD4^+$), CD8 cytotoxic T cells ($CD3^+TCR\ \gamma\delta^-CD8^+$), NK cells ($CD3^-CD8^-CD4^-NK1.1^+$), NKT cells ($CD3^+NK1.1^+$), monocytes ($CD3^-CD11b^+Ly6C^+$), neutrophils ($CD3^-CD11b^+Ly6G^+$), macrophages ($CD3^-CD11b^+Ly6C^-Ly6G^-$) and DCs ($CD11c^+$MHC class $II^+$). Percentage of each cell type is indicated within the respective gate. Each column represents one individual from the indicated group on the top.

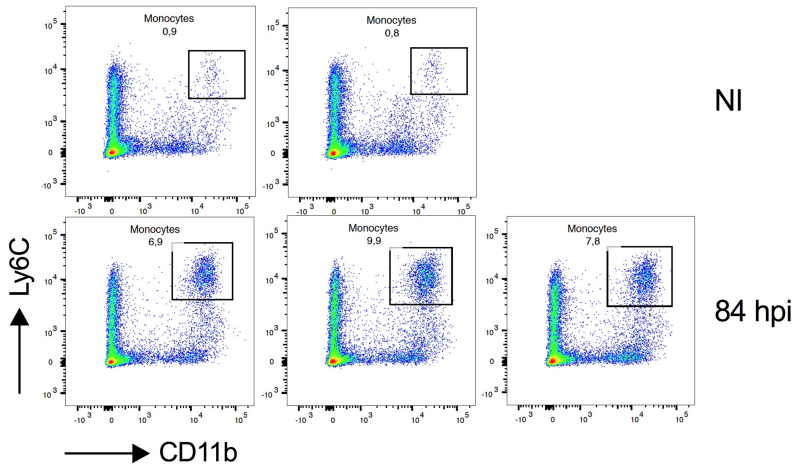


**Supplementary Figure 4. Flow cytometry analysis of inflammatory monocytes activated and/or recruited to the liver 84 hours post *P. berghei* infection of TCRd$^{-/-}$ mice.** Liver leukocytes were isolated at 84 hpi from *P. berghei*-infected TCRd$^{-/-}$ mice and analysed for the expression of CD11b and Ly6C. Percentage of CD11b$^{+}$Ly6C$^{+}$ monocytes is indicated within the respective gate. Each plot represents one individual from the indicated group on the right.

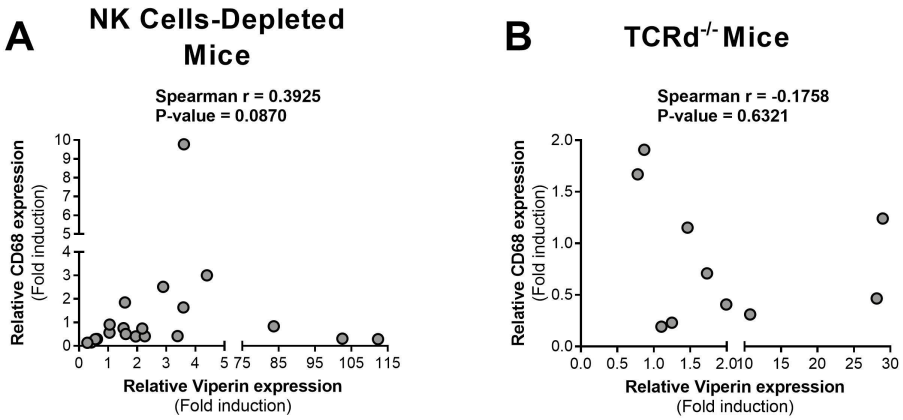


**Supplementary Figure 5. Correlation of relative Viperin and CD68 mRNA expression in the liver of different mouse models infected with *P. berghei*.** Correlation of relative Viperin and CD68 mRNA expression in the liver of NK cells-depleted **(A)** and TCRd$^{-/-}$ **(B)** mice infected with *P. berghei* ANKA spz. Spearman correlation coefficients and corresponding *p*-values are indicated. *R* greater than 0.6 was considered a strong correlation.